City of New York
Department of Environmental Protection
New York, New York

NEWTOWN CREEK WATER POLLUTION CONTROL PROJECT EAST RIVER WATER QUALITY PLAN

TASK 10.0 SYSTEM-WIDE EUTROPHICATION MODEL (SWEM)

SUBTASK 10.4 CALIBRATE SWEM WATER QUALITY

SUBTASK 10.6 VALIDATE SWEM WATER QUALITY

Prepared under subcontract to:
Greeley and Hansen
115 Broadway, Suite 13B
New York, NY 10006-1604

April 2001
Project No: GRHN0020/209

HydroQual, Inc.
Environmental Engineers and Scientists

TABLE OF CONTENTS

TABLE OF CONTENTS

LIST OF TABLES

LIST OF FIGURES

LIST OF FIGURES
(Continued)

PREFACE

The City of New York is conducting facility upgrade planning for the Newtown Creek Water Pollution Control Plant, located in Brooklyn, New York. The objective of the planning study is to develop viable management options for sewage effluent discharged from this treatment facility and other facilities discharging to the East River. As part of this planning, the City funded the development and application of two numerical models, the Harbor Eutrophication Model (HEM) and the System-wide Eutrophication Model (SWEM). The purpose of HEM was to provide a screening tool for the City of New York to evaluate the effectiveness of proposed Water Pollution Control Plant (WPCP) upgrades and other engineering alternatives to improve dissolved oxygen in receiving waters. The purpose of SWEM is to provide a more refined evaluation of proposed WPCP upgrades and other engineering alternatives and ultimately to select the best management plan for the East River.

New York City is under Consent Order to achieve secondary treatment at the Newtown Creek WPCP. In addition, the Long Island Sound Study is requiring that New York City abate the contribution of nitrogen loadings from the East River WPCPs to low dissolved oxygen levels in Western Long Island Sound. Engineering solutions to satisfy these mandates under consideration include: advanced treatment at the East River WPCPs, aggregation of East River discharges, outfall relocation, and artificial aeration techniques. The nature of the engineering solutions under consideration necessitates that HEM and SWEM include both detailed hydrodynamic and eutrophication kinetics. HEM which includes both the New York Harbor and the Western Sound was developed first and was applied to define the components of the dissolved oxygen balance and to screen approximately 20 engineering alternatives. SWEM which includes all of New York Harbor, Long Island Sound, and the New York Bight will be applied to further evaluate 20 alternatives and to formulate a management plan for the East River.

This report is a summary of work performed under Sub-tasks 10.4 and 10.6 of the Facilities Planning Project for the upgrading of the Newtown Creek Water Pollution Control Plant. The relationship of Sub-tasks 10.4 and 10.6 with other SWEM (Task 10) Sub-tasks is as follows:

Task 10: Phase II Computer Modeling - System-wide Eutrophication Model (SWEM)

- Sub-Task 10.1 - Construct the System-wide Eutrophication Model (SWEM)
- Sub-Task 10.2 - Obtain and Reduce Loading/Water Quality Data
- Sub-Task 10.3 - Calibrate SWEM for Hydrodynamics
- Sub-Task 10.4 - Calibrate SWEM for Water Quality
- Sub-Task 10.5 - Apply SWEM for Preliminary Facility Design
- Sub-Task 10.6 - Validate SWEM
- Sub-Task 10.7 - Apply SWEM for Final Facility Design

NEWTOWN CREEK WATER POLLUTION CONTROL PROJECT
EAST RIVER WATER QUALITY PLAN

TASK 10.0 - SYSTEM-WIDE EUTROPHICATION MODEL (SWEM)
SUB-TASK 10.4 CALIBRATE SWEM FOR WATER QUALITY 1994-95
SUB-TASK 10.6 VALIDATE SWEM FOR WATER QUALITY 1988-89

EXECUTIVE SUMMARY

A coupled three-dimensional time-variable hydrodynamic and water quality numerical model of eutrophication in New York Harbor, Long Island Sound and the New York Bight, System-wide Eutrophication Model (SWEM), has been developed and calibrated against observed water quality and sediment quality data for a 12 month period from October 1, 1994 through September 1995. This model has been validated with observed water quality data for a 12 month period from October 1, 1988 through September 1989.

Comparisons of the observed and computed values of the relevant water quality variables for both calibration and validation periods indicate that the model reproduces the major features of the interactions between hydrodynamic circulation, nutrient and organic carbon loadings, phytoplankton, dissolved oxygen, and nutrient fluxes over an annual cycle. While there are some discrepancies between model computations and observed data, the overall model calibration and validation to the observed data are sufficient to permit usage of the model to evaluate water quality responses to nutrient reduction scenarios and other management alternatives. On this basis, SWEM is an appropriate tool for evaluation of NYCDEP planning alternatives and development of a comprehensive East River management plan.

Based on data analysis and model results, the following conclusions may be drawn:

- Visual inspection of output from SWEM and data indicates that SWEM approximates the principal interactions between density induced circulation, nutrient inputs, and phytoplankton on an annual cycle for two distinct years. In addition, the principal components of the dissolved oxygen budget appear to have been

incorporated in the model and, in general, reproduce the observed temporal distributions of dissolved oxygen throughout the system.

- Visual inspection of model output and available data indicates that the sediment submodel reproduces the general observed features of the annual cycle of sediment oxygen demand and nutrient fluxes.

- The calibration and validation of SWEM demonstrates the model as appropriate for evaluation of NYCDEP planning alternatives and for evaluation of NYCDEP East River Plan.

- Both model calibration and validation at discrete locations are better in New York waters than New Jersey waters consistent with the goal of producing a tool for NYCDEP planning purposes. Minimal additional efforts are warranted to fine-tune local calibration and validation in New Jersey waters.

- The wholistic watershed-based nature of SWEM and overall good calibration and validation across sharp gradients in nutrients and light available to phytoplankton support consideration of SWEM as a replacement for existing models of individual system components and serve as the regional planning tool.

SECTION 1

INTRODUCTION AND MODEL DESCRIPTION

The water quality submodel of SWEM is based upon a general purpose code, row-column AESOP (RCA), developed by HydroQual, Inc., to solve a myriad of water quality problems. RCA solves general mass balance equations for water quality variables of interest. RCA was developed to take advantage of the vector and parallel processing capabilities of modern supercomputers. Parallel processing capabilities enable the mass balance equations to be solved over a finely resolved computational grid.

RCA formulates mass balance equations for each model segment for each water quality constituent, or state-variable, of interest. These mass balance equations include: 1) all horizontal, lateral and vertical components of advective flow and dispersive mixing between model segments; 2) physical, chemical, and biological transformations of the water quality variables within a model segment; and 3) point, nonpoint, fall-line and atmospheric inputs of the various water quality variables of interest. The time-variable solution of the mass balance equations involves the solution of partial differential equations.

The partial differential equations which form the water quality model, together with boundary conditions, are solved by finite difference techniques. The concentrations of the water quality variables are assumed to be centered within each water quality segment or grid cell. The finite difference equations conserve mass.

RCA was transformed into the water quality submodel of SWEM via the development of a FORTRAN subroutine which includes complex eutrophication kinetics and sediment interactions. An important criterion for the inclusion of a variable in a modeling framework is the existence of adequate field data for calibration/verification of the variable, as well as the importance of the variable in the process being considered. As a consequence of the special monitoring program conducted in New York Harbor, Long Island Sound, and the New York Bight between November 1994 and October 1995, there is an excellent data base with which to calibrate the key water quality variables required to model the eutrophication process and the effects of the management of nutrient loadings. Similarly, for 1988-89, as a consequence of the Long Island Sound Study (LISS), there is an excellent data set for validation of SWEM. The kinetic framework employed in SWEM utilizes the twenty-five state variables tabulated as Table 1-1. The numbering system in Table 1-1, S-#, will

be used subsequently in the development of kinetic equations. Other variables tracked by the model include phytoplankton chlorophyll-a , gross primary productivity, five-day biochemical oxygen demand (BOD_5), and light extinction.

The kinetic equations which will be discussed in subsequent sections incorporate the twenty-five state variables and are designed to simulate the annual cycle of phytoplankton production, its relation to the supply of nutrients, and its effect on dissolved oxygen. The simulation is based on formulating the kinetics which govern the interactions of the biota and the various nutrient forms, and the application of these kinetics to the domain of SWEM within the context of mass conservation equations.

Table 1-1 - 25 State Variables Included in SWEM

temperature	S20-ammonia nitrogen
salinity	S21-nitrate and nitrite nitrogen
winter phytoplankton carbon	S22-biogenic silica
summer phytoplankton carbon	S23-available silica
S12-refractory particulate organic phosphorus	S6-refractory particulate organic carbon
S11-labile particulate organic phosphorus	S5-labile particulate organic carbon
S14-refractory dissolved organic phosphorus	S8-refractory dissolved organic carbon
S13-labile dissolved organic phosphorus	S7-labile dissolved organic carbon
S15-dissolved inorganic phosphorus (DIP)	S9-reactive dissolved organic carbon
S17-refractory particulate organic nitrogen	S10-algal exudate dissolved organic carbon
S16-labile particulate organic nitrogen	S25-equivalents of aqueous dissolved oxygen demand
S19-refractory dissolved organic nitrogen	S24-dissolved oxygen
S18-labile dissolved organic nitrogen	

1.1 CONSERVATION OF MASS

The modeling framework used in this project and detailed in this report is based upon the principle of conservation of mass. The conservation of mass accounts for all of a material entering or leaving a body of water, transport of the material within the water body, and physical, chemical, and biological transformations of the material. For an infinitesimal volume oriented along the axis of a three-dimensional coordinate system, a mathematical formulation of the conservation of mass may be written:

$$\frac{\partial c}{\partial t} = \frac{\partial}{\partial x}\left(E_x \frac{\partial c}{\partial x}\right) + \frac{\partial}{\partial y}\left(E_y \frac{\partial c}{\partial y}\right) + \frac{\partial}{\partial z}\left(E_z \frac{\partial c}{\partial z}\right) - U_x \frac{\partial c}{\partial x} - U_y \frac{\partial c}{\partial y} - U_z \frac{\partial c}{\partial x} \qquad (1\text{-}1)$$

dispersive transport — advective transport

$\pm S(x,y,z,t)$ + $W(x,y,z,t)$

sources or sinks — external inputs

While Equation 1-1 is often taken as the "instantaneous" water quality mass balance equation, it may be interpreted as the "time-averaged over the tidal period" mass balance equation when the coefficients of the equation are chosen as follows:

- c = concentration of the water quality variable [M/L^3],
- t = time [T],
- E = dispersion (mixing) coefficient due to tides and density and velocity gradients (L^2/T),
- U = tidally-averaged net advective velocity (L/T),
- S = sources and sinks of the water quality variable, representing kinetic interactions (M/L^3-T),
- W = external inputs of the variable c (M/L^3-T),
- x,y,z = longitudinal, lateral and vertical coordinates,
- M,L,T = units of mass, length and time, respectively.

The modeling framework employed in this project is made up of three components: the transport due to density-driven currents and dispersion, the kinetic interaction between variables, and external inputs. Density-driven currents and tidally induced mixing are responsible for the movement of the water quality constituents. The hydrodynamic circulation was developed under Sub-task 10.3 and the details are presented in the Sub-task 10.3 report.

External inputs of nutrients and oxygen-demanding material are derived from municipal and industrial discharges, CSOs and natural surface runoff and direct atmospheric deposition to the water surface.

The kinetics control the rates of interactions among the water quality constituents. Ideally, in a modeling effort, they should be independent of location per se, although they may be functions of exogenous variables, such as temperature and light, which may vary with location.

Analytical solutions are not available for partial differential equations of the form of Equation 1-1 except for the simplest cases. Instead, numerical methods are utilized to solve these mass balance equations. A specific method of solution, employed in a majority of water quality modeling frameworks, is known as the finite difference technique. First, the estuary is divided into finite volumes. Then a finite difference approximation of Equation 1-1 is applied to the ith finite volume or segment, resulting in an equation of the form (see Thomann, 1972):

$$V_i \frac{dc_i}{dt} = \sum_j R_{ij}(c_j - c_i) + \sum_k Q_{ki}c_k - \sum_m Q_{im}c_i \pm S_i + W_i \qquad (1\text{-}2)$$

$$i = 1,\ 2,\ldots,\ m$$

where

V_i = volume of segment i (L^3),

c_i = concentration of the water quality variable in the ith segment (M/L^3),

R_{ij} = exchange between segment i and j resulting from dispersive mixing (L^3/T),

Q_{ki} = net advective flow entering segment i from segment k (L^3/T),

Q_{im} = net advective flow leaving segment i and going to segment m (L^3/T),

S_i = sources and sinks, in segment i representing kinetic interactions (M/T),

W_i = external inputs to segment i (M/T).

The exchange coefficients and advective flows are computed from

$$R_{ij} = \frac{E_{ij} A_{ij}}{L_{ij}} \quad (1\text{-}3a)$$

$$Q_{ij} = A_{ij} U_{ij} \quad (1\text{-}3b)$$

respectively, where E_{ij} is the dispersion coefficient, representing the overall phenomenon of mixing due to temporal variation in the tidal velocity, lateral and vertical gradients in velocity, and density differences within the water body; A_{ij} is the cross-sectional area of the ij interface; L_{ij} is the characteristic length defined as $(L_i + L_j)/2$; and U_{ij} is the net advective velocity from segment i to j. The term S_i, the sources and sinks of material in segment i, represents the kinetic interactions (physical, chemical and biological) occurring within the segment. These interactions may be functions only of the variable under consideration, for example, the first order decay of organic material. Alternately they may involve the interactions between other variables, for example, the first order feed-forward interaction between organic carbon BOD and dissolved oxygen, or the more complex interactions between phytoplankton biomass and nutrients which involve non-linear feed-forward and feedback interactions. The term W_i, the external inputs of material into segment i, includes point and nonpoint source loads, CSO loads, atmospheric loads, and inputs from the sediment bed.

Mass balance equations in the form of Equation 1-2 are formulated for each segment in the system and for each state variable included in the modeling framework. This results in n x m simultaneous finite difference equations to be solved, where n is the number of segments and m is the number of state variables.

The model kinetics are detailed in the following section.

SECTION 2

MODEL KINETICS

2.1 GENERAL STRUCTURE

Salinity and temperature are included in the water quality submodel of SWEM to verify that the transport is being imported correctly from the hydrodynamic submodel of SWEM. For salinity and temperature there are no reaction kinetics involved, i.e., they are conservative. There are no direct sources or sinks of salinity, other than via exchange with the model boundaries or via freshwater dilution resulting from WPCPs, CSOs, stormwater runoff and tributary inputs. The primary source of temperature is the input of the sun's radiant energy, while the primary sink is the radiant loss of heat to the atmosphere during the winter months. The hydrodynamic submodel of SWEM includes these sources and sinks as part of a full calculation of heat fluxes.

Figure 2-1 presents the principal kinetic interactions for the nutrient cycles and dissolved oxygen. In the phosphorus system kinetics, DIP is utilized by phytoplankton for growth. Phosphorus is returned from the phytoplankton biomass pool to the various dissolved and particulate organic phosphorus pools and to DIP through endogenous respiration and predatory grazing. The various forms of organic phosphorus are converted to DIP at a temperature-dependent rate.

The kinetics of the nitrogen species are fundamentally the same as the kinetics of the phosphorus system. Ammonia and nitrate are used by phytoplankton for growth. Ammonia is the preferred form of inorganic nitrogen for algal growth, but phytoplankton will utilize nitrate nitrogen as ammonia concentrations become depleted. Nitrogen is returned from the algal biomass and follows pathways that are similar to those of phosphorus. Organic nitrogen is converted to ammonia at a temperature-dependent rate, and ammonia is then converted to nitrate (nitrification) at a temperature- and oxygen-dependent rate. Nitrate may be converted to nitrogen gas (denitrification) in the absence of oxygen at a temperature-dependent rate.

Available silica is utilized by diatomaceous phytoplankton during growth. Silica is returned to the unavailable silica pool during respiration and predation and must undergo mineralization processes before becoming available for phytoplankton growth.

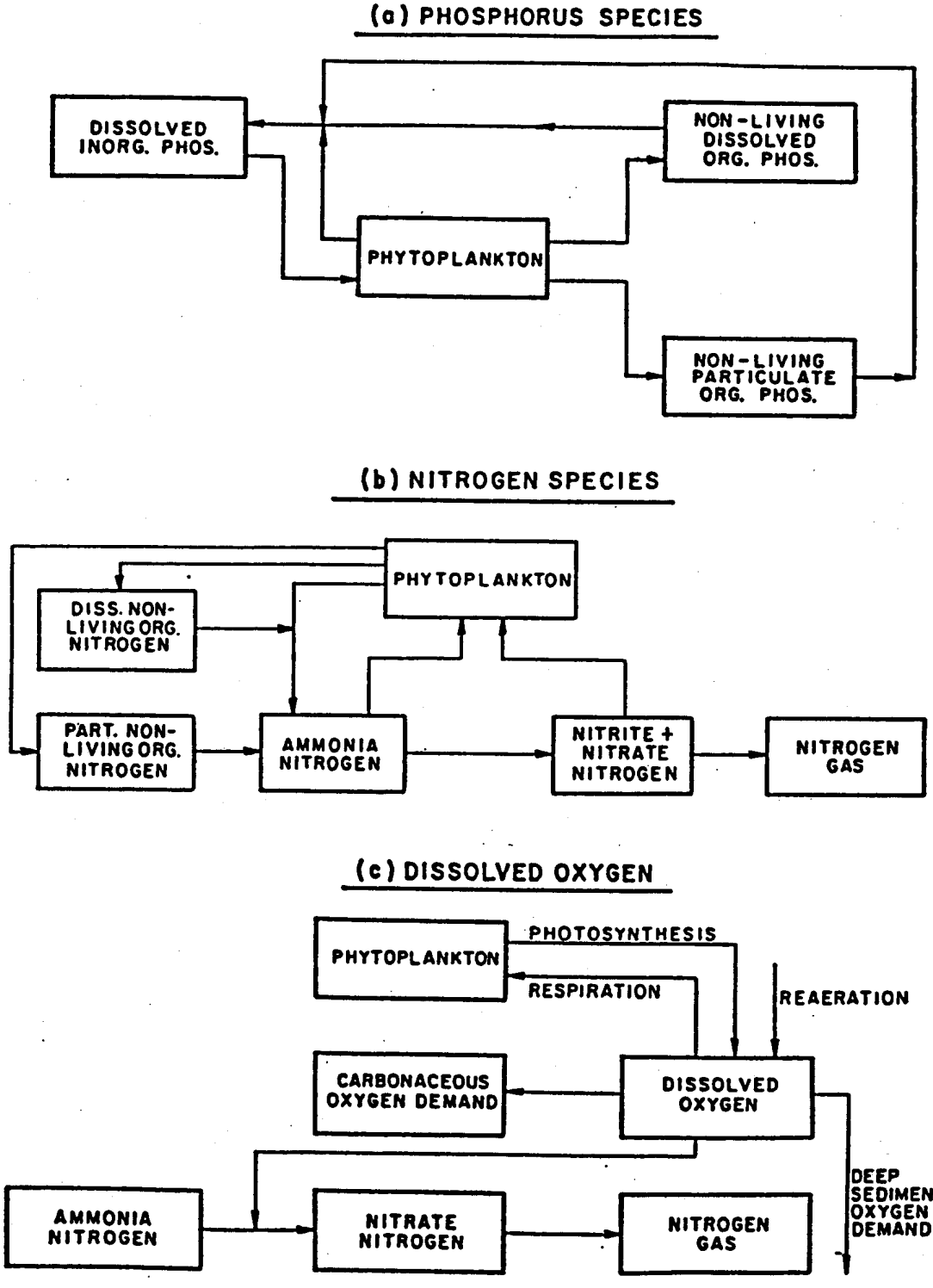

Figure 2-1. Principal Kinetic Interactions for Nutrient Cycles and Dissolved Oxygen

Dissolved oxygen is coupled to the other state variables. The sources of oxygen considered are reaeration and algal photosynthesis. The sinks of oxygen are algal respiration, oxidation of detrital carbon and carbonaceous material from wastewater treatment plant effluents and nonpoint discharges, nitrification and various sediment demands.

Organic carbon sources include anthropogenic inputs and the by-products of primary production and zooplankton grazing. The sink of organic carbon is via bacterial decomposition or oxidation. Specific details for the above reactions are presented below.

2.2 PHYTOPLANKTON GROWTH AND DEATH

The kinetic framework employed for both functional algal groups is the same, only the choice of model coefficients is different. It is convenient to express the kinetic source term for phytoplankton, S_p, as the difference between the phytoplankton growth rate, G_p, and the death rate, D_p. That is:

$$S_P = (G_P - D_P)\cdot P \qquad (2\text{-}1)$$

where P is the phytoplankton population, and where G_p and D_p have units (day^{-1}). The balance between the magnitude of the growth rate and the death rate (together with the transport and mixing) determines the rate at which phytoplankton mass is created in each volume element.

The growth rate of a population of phytoplankton in a natural environment is a complicated function of the species of phytoplankton present and their differing reactions to solar radiation, temperature, and the balance between nutrient availability and nutrient requirements. The complex and often conflicting data pertinent to this problem have been reviewed by many researchers (Rhee 1973; Hutchinson 1967; Strickland 1965; Lund 1965, and Raymont 1963). The available information is not sufficiently detailed to specify the growth kinetics for individual algal species in a natural environment. Hence, in order to construct a growth function, a simplified approach is followed. Rather than consider the problem of different species and their associated environmental and nutrient requirements, the population is characterized as a whole by a measurement of the biomass of the phytoplankton present.

For single species, the direct measure of the population size is the number of cells per unit volume. Cell counts of a single species may be obtained fairly readily in a well-controlled laboratory environment. However, in naturally occurring populations, this measure may be somewhat ambiguous. It is difficult to distinguish between viable and non-viable cells, and colonizing species tend to pose a problem because counts usually do not distinguish individual cells, and the sizes of the colonies are quite variable.

The sum of the numbers of each species, the total count, could be used to characterize biomass, but since cell size varies substantially, the picophytoplankton would dominate such an aggregation. To account for this, the total bio-volume, or wet weight of phytoplankton, assuming unit density, can be calculated using characteristic volumes for each identified species. Unfortunately, volumes can vary appreciably as a function of nutrient availability. Conversion to phytoplankton dry weight and carbon involves further species-dependent constants, which are also nutrient dependent, and therefore, are subject to variation and uncertainty. Thus, although the use of phytoplankton dry weight or carbon concentration is an appealing solution to the issue of aggregation, it suffers from some practical difficulties.

An alternative approach to this problem is to measure a parameter which is characteristic of all phytoplankton, namely, chl-a, and to use this as the aggregated variable. The principal advantages are that the measurement is direct, it integrates cell types and age, and it accounts for cell viability. The principal disadvantages are that it is a community measurement with no differentiation between functional groups (for example, diatoms or blue-green algae), and it is not necessarily a good measurement of standing crop in dry weight or carbon units, since the chlorophyll to dry weight and carbon ratios are variable, and non-active chlorophyll (phaeo-pigments) must be measured to determine viable chlorophyll concentrations.

As can be seen from the above discussion, no simple aggregate measurement is entirely satisfactory. From a practical point of view, the availability of extensive chlorophyll data essentially dictates its use as the aggregate measure of the phytoplankton population, or biomass, for calibration and verification purposes. However, SWEM uses phytoplankton carbon as a measure of algal biomass. The reasons for choosing phytoplankton carbon, rather than chl-a as the internal state variable, are twofold. The first is a desire to maintain compatibility with the modeling framework developed by HydroQual, Inc. for the Long Island Sound study, from which the basic kinetic

framework is drawn. The second reason is that the use of phytoplankton carbon greatly facilitates the model computation of oxygen-demanding material deposited to the sediment bed via settling.

With the choice of biomass units established, a growth rate which expresses the rate of production of biomass as a function of the important environmental variables, temperature, light, and nutrients, may be developed. The specific growth rate, G_p, is related to G_{Pmax}, the maximum growth rate at optimum light, temperature, and nutrients, via the following equation:

$$G_P = G_{Pmax} \cdot G_T(T) \cdot G_I(I) \cdot G_N(N) \qquad (2\text{-}2)$$

temperature light nutrients

where

$G_T(T)$ is the effect of temperature,
$G_I(I)$ is the light attenuation given by

$$G_I(I) = g(I,f,H,k_e) \qquad (2\text{-}3)$$

and

$G_N(N)$ is the nutrient limitation given by

$$G_N(N) = g(DIP,DIN\ Si) \qquad (2\text{-}4)$$

where T is the ambient water temperature; I is the incident solar radiation; f is the fraction of daylight; H is the depth of the water column; k_e is the extinction or light attenuation coefficient; and DIP, DIN, and Si are the available nutrients required for growth: dissolved inorganic phosphorus (orthophosphate), dissolved inorganic nitrogen (ammonia plus nitrite/nitrate), and available silica, respectively.

Initial estimates of G_{Pmax} were based upon previous estuarine modeling studies and were subsequently refined during the calibration process. The selected maximum growth rates are then temperature-corrected using ambient water column temperature values. The temperature-corrected growth rate is computed using the following equation, which relates G_{Pmax} (T), the growth rate at ambient temperature, T, to $G_{Pmax}(T_{opt})$, the growth rate at the optimal temperature, T_{opt}:

$$G_{Pmax}(T) = G_{Pmax}(T_{opt}) \cdot e^{-0.004 \cdot (T_{opt} - T)^2} \qquad T \leq T_{opt} \qquad (2\text{-}5a)$$

$$G_{Pmax}(T) = G_{Pmax}(T_{opt}) \cdot e^{-0.006 \cdot (T_{opt} - T)^2} \qquad T > T_{opt} \qquad (2\text{-}5b)$$

The temperature-corrected growth rate is then adjusted to reflect attenuation due to ambient light and nutrient levels.

In the natural environment, the light intensity to which the phytoplankton are exposed is not uniformly at the optimum value. At the surface and near-surface of the air-water interface, photo-inhibition can occur due to high light intensities, while at depths below the euphotic zone, light is not available for photosynthesis due to natural and algal related turbidity. The modeling framework used in this study extends from a light curve analysis formulated by Steele (1962), and accounts for both the effects of supersaturating light intensities and light attenuation through the water column. The depth-averaged light attenuated growth rate factor, $G_I(I)$, is presented in Equation 2-6 and is obtained by integrating the specific growth rate over depth:

$$G_I(I) = \frac{ef}{k_e H}\left[\exp\left(\frac{-I_o}{I_s} e^{-k_e H}\right) - \exp\left(\frac{-I_o}{I_s}\right)\right] \qquad (2\text{-}6)$$

where:

e = 2.718,
f = the photoperiod or fraction of daylight,
H = the total water column depth (m),

k_e = the total extinction coefficient, computed from the sum of the base, non-algal related, light attenuation, k_{ebase}, and the self-shading attenuation due to the ambient phytoplankton population $k_c P_{chl\text{-}a}$ (m^{-1}),

k_c = the algal related extinction coefficient per unit of chlorophyll (m^2/mg chl-a),

$P_{chl\text{-}a}$ = the ambient phytoplankton population as chlorophyll (μg chl-a/L), where $P_{chl\text{-}a} = P_c/a_{cchl}$,

P_c = the ambient phytoplankton population as carbon (mgC/L),

a_{cchl} = the ratio of algal carbon to algal chlorophyll (mgC/mg chl-a),

I_o = the total daily incident light intensity at the surface (ly/day), and

I_s = the saturating light intensity (ly/day).

The effects of various nutrient concentrations on the growth of phytoplankton have been investigated, and the results are quite complex. As a first approximation to the effect of nutrient concentration on the growth rate, it is assumed that the phytoplankton population in question follows Monod growth kinetics with respect to the important nutrients. That is, at an adequate level of substrate concentration, the growth rate proceeds at the saturated rate for the ambient temperature and light conditions. However, at low substrate concentration, the growth rate becomes linearly proportional to substrate concentration. Thus, for a nutrient with concentration Nj in the jth segment, the factor by which the saturated growth rate is reduced in the jth segment is $Nj/(K_m + Nj)$. The constant, K_m, which is called the Michaelis, or half-saturation constant, is the nutrient concentration at which the growth rate is half the saturated growth rate. Since there are three nutrients, nitrogen, phosphorus, and silica, considered in this framework, the Michaelis-Menton expression is evaluated for each nutrient and the minimum value is chosen to reduce the saturated growth rate,

$$G_N(N) = \text{Min}\left(\frac{DIN}{K_{mN} + DIN}, \frac{DIP}{K_{mP} + DIP}, \frac{Si}{K_{mSi} + Si}\right). \qquad (2\text{-}7)$$

Numerous mechanisms have been proposed which contribute to the death rate of phytoplankton: endogenous respiration, grazing by herbivorous zooplankton, sinking or settling from the water column, and parasitization (Fogg, 1965). The first three mechanisms have been included in previous models for phytoplankton dynamics, and they have been shown to be of general importance. For this study, only endogenous respiration and settling have been explicitly included in the modeling framework. The effect of zooplankton grazing is included indirectly using a time-

variable algal loss rate that was developed based upon measurements of zooplankton abundance. For the domain of SWEM, field data have shown that in certain locations, particularly the lower East River, filtration by benthic bivalves is also an important loss mechanism of phytoplankton. The effect of benthic bivalve filtration on the loss of phytoplankton is included indirectly in SWEM by increasing the deposition rate of algae to the sediment on a location specific basis.

The endogenous respiration rate of phytoplankton is the rate at which the phytoplankton oxidize their organic carbon to carbon dioxide per unit weight of phytoplankton organic carbon. Respiration is the reverse of the photosynthesis process, and as such, contributes to the death rate of the phytoplankton population. If the respiration rate of the phytoplankton as a whole is greater than the growth rate, there is a net loss of phytoplankton carbon or biomass. The endogenous respiration rate has been shown to be temperature dependent (Riley et al., 1949) and is determined via Equation 2-8,

$$k_{PR}(T) = k_{PR}(20°C)\cdot\theta_{PR}^{T-20} \qquad (2\text{-}8)$$

where k_{PR} (20°C) is the endogenous respiration rate at 20°C, and $k_{PR}(T)$ is the temperature corrected rate, and θ_{PR} is the temperature correction coefficient. The units of k_{PR} are day-1.

The sinking of phytoplankton is an important contribution to the overall mortality of the phytoplankton population, particularly in lakes and coastal oceanic waters. Published values of the sinking velocity of phytoplankton, mostly in quiescent laboratory conditions, range from 0.1 to 18.0 m/day. In some instances, however, the settling velocity is zero or negative. Actual settling rates in natural waters are a complex phenomenon, affected by vertical turbulence, density gradients, and the physiological state of the different species of phytoplankton. An important factor determining the physiological state of algae is nutrient availability. Bienfang et al. (1982) measured sinking rate response of four marine diatoms to depletion of nitrate, phosphate, and silicate. All four species showed significant increase in sinking rate under conditions of silica depletion; one species showed increased settling rate under nitrate limitation. An analysis of field experiments by Culver and Smith (1989) indicated that low concentrations of nitrate, as well as light availability, affected diatom settling rates. Although the effective settling rate of phytoplankton is greatly reduced in a relatively shallow, well-mixed river or estuary due to vertical turbulence, it still can contribute to the overall

mortality of the algal population. In addition, the settling phytoplankton can be a significant source of nutrients to the sediments and can play an important role in the generation of SOD. For these reasons, a term representing phytoplankton settling has been included in the algal mortality expression, and is determined by:

$$k_{sP} = \frac{v_{sPb}}{H} + \frac{v_{sPn}}{H} \cdot \left(1 - G_N(N)\right) \qquad (2\text{-}9)$$

where k_{sP} is the net effective algal loss rate due to settling (day^{-1}) at 20°C, v_{sPb} is the base settling velocity of phytoplankton (m/day), v_{sPn} is the nutrient dependent settling rate, (m/day), $G_N(N)$ is defined by Equation 2-7, and H is the depth of the segment, (m). A temperature correction is applied to equation 2-9.

Zooplankton grazing, depending upon time of the year and zooplankton biomass levels, may be an important loss rate for phytoplankton. Zooplankton abundance data suggest that the highest numbers of herbivorous zooplankton occur during the months March, April, and May. An attempt to convert the zooplankton abundance data to zooplankton carbon using limited available measures of zooplankton size, support this conclusion. It appears that zooplankton biomass is also highest during the late spring. The loss term used to represent zooplankton grazing, k_{grz}, has been assigned on a monthly basis in units of day^{-1} based on the data.

Filtration by benthic bivalves, depending upon time of the year and biomass levels at a particular location, may be an important loss rate for phytoplankton. Benthic bivalve abundance and biomass data suggest that benthic bivalves are present in high numbers in the lower East River and upper New York Bay. The rate of benthic filtration, or water column clearance (m/day), is assigned on a location specific basis with a temperature dependency. Water column clearance is determined from a regression equation developed for Chesapeake Bay between water column clearance rate and benthic bivalve biomass. In the kinetics, the deposition flux of algae to the sediment bed is incrememented to reflect the clearance rate. For practical purposes, the loss of algae due to benthic filtration is included in the k_{sP} term of equation 2-10.

The total loss rate for phytoplankton is the sum of the three loss rates described below:

$$D_P = k_{PR}(T) + k_{sP} + k_{grz}(T) \qquad (2\text{-}10)$$

This completes the specification of the growth and death rates for phytoplankton in terms of the physical variables: light, temperature, and available nutrients. Table 2-1 summarizes the above equations and the model coefficients used in this study. With these variables known as a function of time, it would be possible to calculate the annual cycle of phytoplankton chlorophyll. However, the nutrient concentrations are not known a priori since they depend upon the phytoplankton population which develops. Thus, these systems are interdependent and cannot be analyzed separately. It is necessary to formulate mass balances for the nutrients as well as the phytoplankton in order to calculate the chlorophyll which would develop for a given set of environmental conditions.

2.2.1 Stoichiometry and Uptake Kinetics

A principal component in the mass balance equations for the nutrient systems included in the eutrophication framework is the nutrient uptake kinetics associated with algal growth. In order to quantify the nutrient uptake, it is necessary to specify the population stoichiometry in units of nutrient uptake per mass of population synthesized. For carbon as the unit of population biomass, the relevant ratios are the mass of nitrogen, phosphorus, and silica per unit mass of carbon. Figure 2-2 illustrates the variable nitrogen stoichiometry used at key locations in this study. Figure 2-2 shows that in areas of the domain where nitrogen is plentiful, nitrogen stoichiometry remains constant. Conversely, Figure 2-2 shows that in areas of the domain where nitrogen becomes depleted, the nitrogen stoichiometry varies.

Once the stoichiometric ratios have been determined, the mass balance equations may be written for the nutrients in much the same way as for the phytoplankton biomass. The principal processes determining the distribution of nutrients among the various pools are: the uptake of

Table 2-1 - Phytoplankton Net Growth Equations

$$S_P = (G_{Pmax} \cdot G_T(T) \cdot G_I(I) \cdot G_N(N) - k_{PR}\theta_{PR}^{T-20} - k_{sP} - k_{kgrz}) \cdot P_c$$

Temperature Correction

$$G_{Pmax}(T) = G_{Pmax}(T_{opt}) \cdot e^{-0.004(T_{opt}-T)^2}$$

$$G_{Pmax}(T) = G_{Pmax}(T_{opt}) \cdot e^{-0.006(T_{opt}-T)^2}$$

Light Reduction

$$G_I(I) = \frac{ef}{K_e H}\cdot(e^{-\alpha_1} - e^{-\alpha_o})$$

$$\alpha_1 = \frac{I_o}{I_s} e^{-k_e H} \qquad \alpha_o = \frac{Io}{Is}$$

$$k_e = k_{e_{base}} + 1000 \cdot k_c \cdot P_c / a_{cchl}$$

Nutrient Uptake

$$G_N(N) = \text{Min}\left[\frac{DIN}{K_{mN} + DIN}, \frac{DIP}{K_{mP} + DIP}, \frac{Si}{K_{mSi} + Si}\right]$$

DIN = dissolved inorganic nitrogen = $NH_3 + NO_2 + NO_3$
DIP = dissolved inorganic phosphorus
Si = available silica

Algal Settling

$$k_{sP} = \frac{v_{sPb}}{H} + \frac{V_{sPn}}{H} \cdot (1 - G_N(N))$$

Table 2-1 - Phytoplankton Net Growth Equations
(Continued)

Exogenous Variables

Description	Notation
Total Extinction Coefficient	k_e
Base Extinction Coefficient	k_{ebase}
Total Daily Surface Solar Radiation	I_o
Temperature	T
Segment Depth	H
Fraction of Daylight	F

Rate Constants

Description	Notation	Winter Diatoms	Summer Assemblage	Units
Maximum Specific Growth Rate at T_{opt}	G_{pmax}	1.7	3.0	day^{-1}
Temperature Coefficient	θ_p	1.068	1.068	
Temperature Optimum	T_{opt}	6.	26.0	°C
Phytoplankton Self-Light Attenuation	K_c	0.017	0.017	m^2/mg chl-a
Half-Saturation Constant for Nitrogen	K_{mN}	10.	10.	µgN/L
Half-Saturation Constant for Phosphorus	K_{mP}	1.	1.	µgP/L
Algal Endogenous Respiration	k_{PR}	0.085	0.125	day^{-1}
Temperature Coefficient	θ_{PR}	1.068	1.068	
Base Algal Settling Rate	v_{sPb}	0.2	0.2	m/day
Nutrient Dependent Algal	v_{sPn}	0.5	0.5	m/day
Loss Due to Zooplankton Grazing	k_{grz}	0.03-0.10	0.03-0.10	day^{-1}
Carbon/Chlorophyll Ratio	a_{cchl}	50.	100.	mgC/mg chl-a

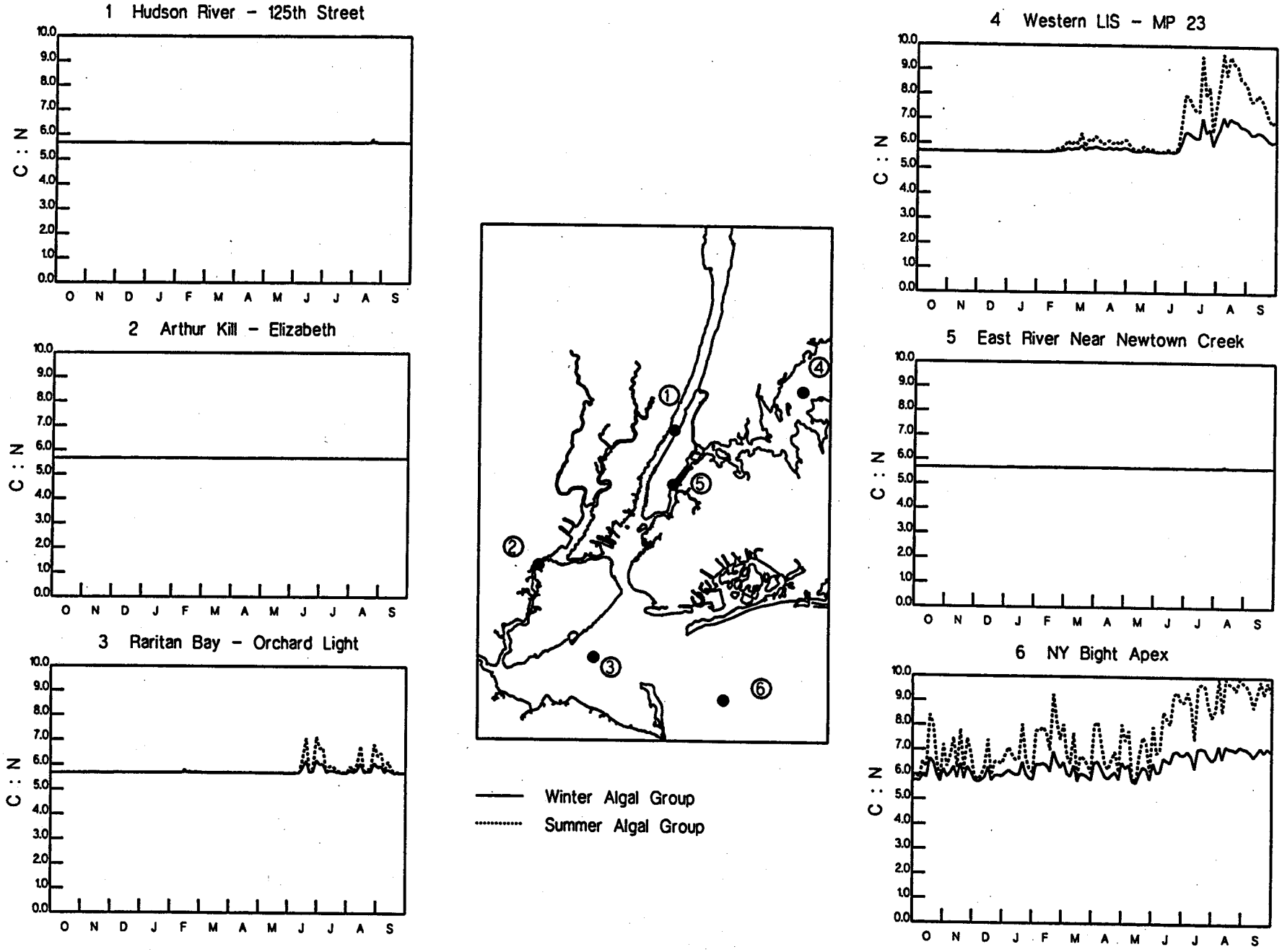

Figure 2-2. Algal Carbon to Nitrogen Ratio
SWEM 1994-95

inorganic nutrients by phytoplankton for cell growth, the release of inorganic and organic nutrients by algal respiration and predation processes, and the recycling of organic nutrients to inorganic forms via bacterial hydrolysis and mineralization.

In their work on Lake Huron and Saginaw Bay, Di Toro and Matystick (1980) proposed a nutrient recycle formulation that was a function of the localized phytoplankton population. Drawing from an analysis of available field data and citing the work of others (Hendry 1977; Lowe 1976; Henrici 1938; Menon et al., 1972; and Rao 1976) that indicated bacterial biomass increased as phytoplankton biomass increased, the mechanism chosen, saturating recycle, was a compromise. This compromise was between the conventional first-order temperature corrected mechanism and a second-order recycle mechanism, in which the recycle rate is directly proportional to the phytoplankton biomass present, as indicated in pure culture, bacteria seeded laboratory studies (Jewell and McCarty 1971). The various relationships may be written:

First-order recycle: $$k(T) = k'(20°C)\theta^{T-20} \qquad (2\text{-}11a)$$

Second-order recycle: $$k(T) = k''(20°C)\theta^{T-20} \cdot P_c \qquad (2\text{-}11b)$$

Saturating recycle: $$k(T) = k'(20°C)\theta^{T-20} \cdot \frac{P_c}{K_{mP_c} + P_c} \qquad (2\text{-}11c)$$

Saturating recycle permits second-order dependency at low phytoplankton concentrations when $P_c << K_{mPc}$, where K_{mPc} is the half saturation constant for recycle. It also permits first-order recycle when the phytoplankton greatly exceed the half saturation constant. Basically, this mechanism employs a second order recycle that slows the recycle rate if the algal population is small, but does not permit the rate to increase continuously as phytoplankton increase. The assumption is that at higher population levels, other factors are limiting the recycle kinetics so that it proceeds at its maximum first-order rate.

2.2.2 Organic Carbon

Six organic carbon state variables are considered: reactive dissolved organic (ReDOC), labile dissolved (LDOC), refractory dissolved (RDOC), labile particulate (LPOC), refractory particulate (RPOC) and dissolved algal exudate (ExDOC). Reactive, labile, and refractory distinctions are based upon the time scale of oxidation or decomposition. Reactive organic carbon decomposes on a time scale of days to a week or two; labile organic carbon decomposes on the time scale of several weeks to a month or two; refractory organic carbon decomposes on the order of months to a year. Reactive and labile organic carbon decompose primarily in the water column or else rapidly in the sediments. Refractory organic carbon decomposes much more slowly, almost entirely in the sediments.

The principal sources of organic carbon are anthropogenic inputs and natural runoff, and detrital algal carbon, which is produced as a result of predation. Zooplankton take up and redistribute algal carbon to the organic carbon pools via grazing, assimilation, respiration, and excretion. Since zooplankton are not directly included in SWEM, the redistribution of algal carbon by zooplankton is simulated by empirical distribution coefficients.

An additional term, representing the excretion of DOC by phytoplankton during photosynthesis, is included in the model. This algal exudate is very reactive and has a time constant similar to the reactive DOC.

The decomposition of organic carbon is assumed to be temperature and bacterial biomass mediated. Since bacterial biomass is not directly included within the model framework, phytoplankton biomass is used as a surrogate variable. Table 2-2 presents the reaction rate terms for each of the organic carbon pools considered in the model framework together with the model coefficient used in this study.

An additional loss mechanism of particulate organic matter is that due to filtration by benthic bivalves. This loss is handled in the model kinetics by increasing the deposition of non-algal particulate organic carbon from the water column to the sediment in a manner analogous to that described in Section 2.2 above for the loss of algal carbon.

Table 2-2 - Organic Carbon Reaction Equations
(Numbering scheme refers to Table 1-1)

Labile Particulate Organic Carbon (LPOC)

$$S_5 = f_{LPOC} \cdot k_{grz}(T) \cdot P_c - k_{5,7}\theta_{5,7}^{T-20} \cdot LPOC \cdot \frac{P_c + ReDOC + ExDOC}{K_{mP_c} + P_c + ReDOC + ExDOC} - \frac{v_5}{H} \cdot LPOC$$

Refractory Particulate Organic Carbon (RPOC)

$$S_6 = f_{RPOC} \cdot k_{grz}(T) \cdot P_c - \frac{v_6}{H} \cdot RPOC - k_{6,8}\theta_{6,8}^{T-20} \cdot RPOC \cdot \frac{P_c + ReDOC + ExDOC}{K_{mp_c} + P_c + ReDOC + ExDOC}$$

Labile Dissolved Organic Carbon (LDOC)

$$S_7 = f_{LDOC} \cdot k_{grz}(T) \cdot P_c \cdot k_{5,7}\theta_{5,7}^{T-20} \cdot LPOC \cdot \frac{P_c + ReDOC + ExDOC}{K_{mP_c} + P_c + ReDOC + ExDOC}$$
$$- k_{7,0}\theta_{7,0}^{T-20} \cdot LDOC \cdot \frac{LDOC}{K_{mLDOC} + LDOC} \cdot \frac{DO}{k_{DO} + DO} \cdot \frac{P_c + ReDOC + ExDOC}{K_{mP_c} + P_c + ReDOC + ExDOC}$$
$$- \frac{5}{4} \cdot \frac{12}{14} \cdot K_{DN}\theta_{DN} \cdot NO_x \cdot \frac{K_{NOX}}{K_{NOX} + DO} \cdot \frac{LDOC}{K_{mLDOC} + LDOC}$$

Refractory Dissolved Organic Carbon (RDOC)

$$S_8 = f_{RDOC} \cdot k_{grz}(T) \cdot P_c - k_{8.0}\theta_{8,0}^{T-20} \cdot RDOC \cdot \frac{P_c + ReDOC + ExDOC}{K_{mP_c} + P_c} \cdot \frac{DO}{K_{DO} + DO}$$
$$+ k_{6,8}\theta_{6,8}^{T-20} \cdot RPOC \cdot \frac{P_c + ReDOC + ExDOC}{K_{mP_c} + P_c + ReDOC + ExDOC}$$

Reactive Dissolved Organic Carbon (ReDOC)

$$S_9 = - k_{9,0}\theta_{9,0}^{T-20} \cdot ReDOC \cdot \frac{ReDOC}{K_{mLDOC} + ReDOC} \cdot \frac{DO}{K_{DO} + DO} \cdot \frac{P_c + ReDOC + ExDOC}{K_{mP_c} + P_c + ReDOC + ExDOC}$$

Table 2-2 - Organic Carbon Reaction Equations
(Numbering scheme refers to Table 1-1)
(Continued)

Algal Exudate Dissolved Organic Carbon (ExDOC)

$$S_{10} = f_{ExPP} \cdot G_P \cdot P_c - k_{10,0} \theta_{10,0}^{T-20} \cdot ExDOC \cdot \frac{ExDOC}{K_{mLDOC} + ExDOC} \cdot \frac{DO}{K_{DO} + DO} \cdot \frac{P_c + ReDOC + ExDOC}{K_{mP_c} + P_c + ReDOC + ExDOC}$$

Table 2-2 - Organic Carbon Reaction Equations
(Numbering scheme refers to Table 1-1)
(Continued)

Description	Notation	Value	Units
Phytoplankton Biomass	P_c	-	mgC/L
Specific Phytoplankton Growth Rate	G_P	Eq. 2-2	day^{-1}
Half Saturation Constant for Phytoplankton Limitation	K_{mP_c}	0.0	mgC/L
Half Saturation Constant for LDOC	K_{mLDOC}	0.0	mgC/L
Fraction of Grazed Organic Carbon Recycled to:			
the LPOC pool	f_{LPOC}	0.40	
the RPOC pool	f_{RPOC}	0.05	
the LDOC pool	f_{LDOC}	0.45	
the RDOC pool	f_{RDOC}	0.10	
Fraction of Primary Productivity Going to the Algal Exudate DOC pool	f_{Expp}	0.20	
Hydrolysis Rate for RPOC	$k_{6,8}$	0.01	day^{-1}
Temperature Coefficient	$\theta_{6,8}$	1.08	
Hydrolysis Rate for LPOC	$k_{5,7}$	0.20	day^{-1}
Temperature Coefficient	$\theta_{5,7}$	1.08	
Settling Rate of LPOC	v_5	1.0	m/day
Settling Rate of RPOC	v_6	1.0	m/day
Segment depth	H	-	m
Oxidation Rate of LDOC	$k_{7,0}$	0.15	day^{-1}
Temperature Coefficient	$\theta_{7,0}$	1.08	
Oxidation Rate of RDOC	$k_{8,0}$	0.008	day^{-1}
Temperature Coefficient	$\theta_{8,0}$	1.08	
Oxidation Rate of ReDOC	$k_{9,0}$	0.3	day^{-1}
Temperature Coefficient	$\theta_{9,0}$	1.047	
Oxidation Rate of ExDOC	$k_{10,0}$	0.1	day^{-1}

Table 2-2 - Organic Carbon Reaction Equations
(Numbering scheme refers to Table 1-1)
(Continued)

Description	Notation	Value	Units
Temperature Coefficient	$\theta_{10,0}$	1.08	
Half Saturation for Oxygen Limitation	K_{DO}	0.2	mgO_2/L
Dissolved Oxygen	DO	-	mgO_2/L
Denitrification Rate	K_{DN}	0.05	day^{-1}
Temperature Coefficient	θ_{DN}	1.045	
Nitrate + Nitrite	NOX	-	mgN/L
Half Saturation Constant for Denitrification	K_{NOX}	0.10	mgO_2/L

2.2.3 Phosphorus

The SWEM eutrophication model includes five principal phosphorus forms: labile and refractory dissolved organic (LDOP and RDOP, respectively), labile and refractory particulate organic (LPOP and RPOP, respectively), and DIP. Inorganic phosphorus is utilized by phytoplankton for growth and is returned to the various organic and inorganic forms via respiration and predation. A fraction of the phosphorus released during phytoplankton respiration and predation is in the inorganic form and readily available for uptake by other viable algal cells. The remaining fraction released is in the dissolved and particulate organic forms. The organic phosphorus must undergo a mineralization or bacterial decomposition into inorganic phosphorus before it can be used by phytoplankton. Table 2-3 presents the reaction rate terms and coefficients for each of the five phosphorus forms.

2.2.4 Nitrogen

The kinetic structure for nitrogen is similar to that for the phosphorus system. Table 2-4 summarizes the terms used for the nitrogen system kinetics. During algal respiration and death, a fraction of the cellular nitrogen is returned to the inorganic pool in the form of NH_3. The remaining fraction is recycled to the dissolved and particulate organic nitrogen pools. Organic nitrogen undergoes a bacterial decomposition, the end-product of which is NH_3. Ammonia nitrogen, in the presence of nitrifying bacteria and oxygen, is converted to nitrite nitrogen and subsequently nitrate nitrogen (nitrification). Both ammonia and nitrate are available for uptake and use in cell growth by phytoplankton; however, for physiological reasons, the preferred form is NH_3. The ammonia preference term takes the following form:

$$\alpha_{NH_3} = NH_3 \cdot \frac{NO_2+NO_3}{(K_{mN}+NH_3)(K_{mN}+NO_2+NO_3)} \qquad (2\text{-}12)$$

$$+ NH_3 \cdot \frac{K_{mN}}{(NH_3+NO_2+NO_3)(K_{mN}+NO_2+NO_3)}$$

Table 2-3 - Phosphorus Reaction Rates
(Numbering scheme refers to Table 1-1)

Labile Particulate Phosphorus (LPOP)

$$S_{11} = a_{PC} \cdot f_{LPOP} \cdot (k_{PR}(T) + k_{grz}(T)) \cdot P_c - k_{11,13} \theta_{11,13}^{T-20} \cdot LPOP \cdot \frac{P_c + ReDOC + ExDOC}{K_{mP_c} + P_c + ReDOC + ExDOC} - \frac{v_{s11}}{H} \cdot LPOP$$

Refractory Particulate Organic Phosphorus (RPOP)

$$S_{12} = a_{PC} \cdot f_{RPOP} \cdot (k_{PR}(T) + k_{grz}(T)) \cdot P_c - \frac{v_{s12}}{H} \cdot RPOP - k_{12,14} \theta_{12,14}^{T-20} \cdot RPOP \frac{P_c + ReDOC + ExDOC}{K_{mPC} + P_c + ReDOC + ExDOC}$$

Labile Dissolved Organic Phosphorus (LDOP)

$$S_{13} = a_{PC} \cdot f_{LDOP} \cdot (k_{PR}(T) + k_{grz}(T)) \cdot P_c + k_{11,13} \theta_{11,13}^{T-20} \cdot LPOP \cdot \frac{P_c + ReDOC + ExDOC}{K_{mP_c} + P_c + ReDOC + ExDOC} - k_{13,15} \theta_{13,15}^{T-20} \cdot LDOP \cdot \frac{P_c + ReDOC + ExDOC}{K_{mP_c} + P_c + ReDOC + ExDOC}$$

Refractory Dissolved Organic Phosphorus (RDOP)

$$S_{14} = a_{PC} \cdot f_{RDOP} \cdot (k_{PR}(T) + k_{grz}(T)) \cdot P_c + k_{12,14} \theta_{12,14}^{T-20} \cdot RPOP \cdot \frac{P_c + ReDOC + ExDOC}{K_{mP_c} + P_c + ReDOC + ExDOC} - k_{14,15} \theta_{14,15}^{T-20} \cdot RDOP \cdot \frac{P_c + ReDOC + ExDOC}{K_{mP_c} + P_c + ReDOC + ExDOC}$$

Dissolved Inorganic Phosphorus (DIP)

$$S_{15} = (k_{13,15} \theta_{13,15}^{T-20} \cdot LDOP + k_{14,15} \theta_{14,15}^{T-20} \cdot RDOP) \cdot \frac{P_c + ReDOC + ExDOC}{K_{mP_c} + P_c + ReDOC + ExDOC} - a_{PC} \cdot (1 - f_{DIP}) \cdot (K_{PR}(T) + K_{grz}(T)) \cdot P_c$$

Table 2-3 - Phosphorus Reaction Rates
(Numbering scheme refers to Table 1-1)
(Continued)

Description	Notation	Value	Units
Phytoplankton Biomass	P_c	-	mgC/L
Temperature Corrected Algal Respiration Rate	$k_{PR}(T)$	Eq. 2-8	day^{-1}
Temperature Corrected Grazing Rate	$k_{grz}(T)$	0.03 - 0.10	day^{-1}
Specific Phytoplankton Growth Rate	G_P	Eq. 2-2	day^{-1}
Phosphorus to Carbon Ratio	a_{PC}	-	mgP/mgC
Fraction of Respired and Grazed Algal Phosphorus Recycled to:			
the LPOP pool	f_{LPOP}	0.25	
the RPOP pool	f_{RPOP}	0.10	
the LDOP pool	f_{LDOP}	0.10	
the RDOP pool	f_{RDOP}	0.10	
the DIP pool	f_{DIP}	0.45	
LPOP Hydrolysis Rate at 20°C	$k_{11,13}$	0.085	day^{-1}
Temperature Coefficient	$\theta_{11,13}$	1.08	
RPOP Hydrolysis Rate at 20°C	$k_{12,14}$	0.01	day^{-1}
Temperature Coefficient	$\theta_{12,14}$	1.08	
LPOP Settling Rate	v_{s11}	1.0	m/day
RPOP Settling Rate	v_{s12}	1.0	m/day
LDOP Mineralization Rate at 20°C	$k_{13,15}$	0.10	day^{-1}
Temperature Coefficient	$\theta_{13,15}$	1.08	
RDOP Mineralization Rate at 20°C	$k_{14,15}$	0.01	day^{-1}
Temperature Coefficient	$\theta_{14,15}$	1.08	

Table 2-4 - Nitrogen Reaction Rates
(Numbering scheme refers to Table 1-1)

Labile Particulate Organic Nitrogen (LPON)

$$S_{16} = a_{NC} \cdot f_{LPON} \cdot (k_{PR}(T) + k_{grz}(T)) \cdot P_c - k_{16,18} \theta_{16,18}^{T-20} \cdot LPON \cdot \frac{P_c + ReDOC + ExDOC}{K_{mP_c} + P_c + ReDOC + ExDOC} - \frac{v_{s16}}{H} \cdot LPON$$

Refractory Particulate Organic Nitrogen (RPON)

$$S_{17} = a_{NC} \cdot f_{RPON} \cdot (k_{PR}(T) + k_{grz}(T)) \cdot P_c - \frac{v_{s17}}{H} \cdot RPON - K_{17,19} \theta_{17,19}^{T-20} \cdot RPON \cdot \frac{P_c + ReDOC + ExDOC}{k_{mP_c} + P_c + ReDOC + ExDOC}$$

Labile Dissolved Oxygen Nitrogen (LDON)

$$S_{18} = a_{NC} \cdot f_{LDON} \cdot (k_{PR}(T) + k_{grz}(T)) \cdot P_c \cdot k_{16,18} \theta_{16,18}^{T-20} \cdot LPON \cdot \frac{P_c + ReDOC + ExDOC}{K_{mP_c} + P_c + ReDOC + ExDOC} - k_{18,20} \theta_{18,20}^{T-20} \cdot LDON \cdot \frac{P_c + ReDOC + ExDOC}{K_{mP_c} + P_c + ReDOC + ExDOC}$$

Refractory Dissolved Oxygen Nitrogen (RDON)

$$S_{19} = a_{NC} \cdot f_{RDON} \cdot (k_{PR}(T) + k_{grz}(T)) \cdot P_c \cdot k_{17,19} \theta_{17,19}^{T-20} \cdot LPON \cdot \frac{P_c + ReDOC + ExDOC}{K_{mP_c} + P_c + ReDOC + ExDOC} - k_{19,20} \theta_{19,20}^{T-20} \cdot RDON \cdot \frac{P_c + ReDOC + ExDOC}{K_{MP_c} + P_c + ReDOC + ExDOC}$$

Table 2-4 - Nitrogen Reaction Rates
(Numbering scheme refers to Table 1-1)
(Continued)

Ammonia Nitrogen (NH_3)

$$S_{20} = (k_{18,20}\theta_{18,20}^{T-20}\cdot LDON + k_{19,20}\theta_{19,20}^{T-20}\cdot RDON)\cdot\frac{P_c + ReDOC + ExDOC}{K_{mP_c} + P_c + ReDOC + ExDOC}$$
$$- k_{20,21}\theta_{20,21}^{T-20}\cdot NH_3\cdot\frac{DO}{K_{nitr} + DO}$$
$$+ a_{NC}\cdot(1-\alpha_{NH_3})\cdot(1-f_{ExPP})\cdot G_p\cdot P_c - a_{NC}\cdot(1-f_{NH_3})\cdot(k_{PR}(T) + k_{grz}(T))\cdot P_c$$

Nitrite + Nitrate Nitrogen ($NO_2 + NO_3$)

$$S_{21} = k_{20,21}\theta_{20,21}^{T-20}\cdot NH_3\cdot\frac{DO}{K_{nitr} + DO} - a_{NC}\cdot(1-\alpha_{NH_3})\cdot(1-f_{ExPP})\cdot G_p\cdot P_c$$
$$- k_{21,0}\theta_{21,0}^{T-20}\cdot(NO_2 + NO_3)\cdot\frac{K_{NO_3}}{K_{NO_3} + DO}\cdot\frac{LDOC}{K_{mLDOC} + LDOC}$$

Table 2-4 - Nitrogen Reaction Rates
(Numbering scheme refers to Table 1-1)
(Continued)

Description	Notation	Value	Units
Phytoplankton Biomass	P_c	-	mgC/L
Temperature Corrected Algal Respiration Rate	$k_{PR}(T)$	Eq. 2-8	day^{-1}
Temperature Corrected Grazing Rate	$k_{grz}(T)$	0.03 - 0.10	day^{-1}
Specific Phytoplankton Growth Rate	G_P	Eq. 2-2	day^{-1}
Nitrogen to Carbon Ratio	a_{NC}	-	mgN/mgC
Fraction of Primary Producivity Going to the Algal Exudate DOC Pool	f_{ExPP}	0.2	
Fraction of Respired and Grazed Algal Nitrogen Recycled to:			
the LPON pool	f_{LPON}	0.3	
the RPON pool	f_{RPON}	0.1	
the LDON pool	f_{LDON}	0.125	
the RDON pool	f_{RDON}	0.125	
the NH_3 pool	f_{NH_3}	0.350	
LPON Hydrolysis Rate at 20°C	$k_{16,18}$	0.05	day^{-1}
Temperature Coefficient	$\theta_{16,18}$	1.08	
RPON Hydrolysis Rate at 20°C	$k_{17,19}$	0.008	day^{-1}
Temperature Coefficient	$\theta_{17,19}$	1.08	
LPON Settling Rate	v_{s16}	1.0	m/day
RPON Settling Eate	v_{s17}	1.0	m/day
LDON Mineralization Rate at 20°C	$k_{18,20}$	0.085	day^{-1}
Temperature Coefficient	$\theta_{18,20}$	1.08	
RDON Mineralization Rate at 20°C	$k_{19,20}$	0.008	day^{-1}
Temperature Coefficient	$\theta_{19,20}$	1.08	
Nitrification Rate at 20°C	$k_{20,21}$	0.05	day^{-1}
Temperature Coefficient	$\theta_{20,21}$	1.08	
Half Saturation Constant for Oxygen Limitation	K_{nitr}	1.0	MgO_2/L
Denirification Rate at 20°C	$k_{21,0}$	0.05	day^{-1}
Temperature Coefficient	$\theta_{21,0}$	1.045	
Michaelis Constant for Denitrification	K_{NO_3}	0.1	MgO_2/L

The behavior of this equation, for a Michaelis value, K_{mN}, of 10 μgN/L, is illustrated on Figure 2-3. The behavior of Equation 2-12 is most sensitive at low values of ammonia or nitrate. For a given concentration of ammonia, as the available nitrate increases above approximately the Michaelis limitation, the preference for ammonia reaches a plateau. Also, as the concentration of available ammonia increases, the plateau occurs at values closer to unity, that is, total preference for ammonia.

The process of nitrification in natural waters is carried out by aerobic autotrophs, *Nitrosomonas* and *Nitrobacter,* in particular. It is a two-step process with *Nitrosomonas* bacteria responsible for the conversion of ammonia to nitrite (NO_2) and *Nitrobacter* responsible for the subsequent conversion of nitrite to nitrate (NO_3). Essential to this reaction process are aerobic conditions. In order to reduce the number of state variables required in the modeling framework, it was decided to incorporate nitrite and nitrate together as a single state variable. Therefore, the process of nitrification is assumed to be approximated by a first-order reaction rate that is a function of the water column dissolved oxygen concentration and ambient temperature.

Denitrification refers to the reduction of NO_3 (or NO_2) to N_2 and other gaseous products such as N_2O and NO. This process is carried out by a large number of heterotrophic, facultative anaerobes. Under normal aerobic conditions found in the water column, these organisms utilize oxygen to oxidize organic material. However, under the anaerobic conditions found in the sediment bed or during extremely low oxygen conditions in the water column, these organisms are able to use NO_3 as the electron acceptor. The process of denitrification is included in the modeling framework simply as a sink of nitrate. This can always occur in the anaerobic sediment layer. In the water column, however, denitrification should only occur under extremely low dissolved oxygen conditions. This is accomplished computationally by modifying the linear first-order denitrification rate by the expression $K_{NO3}/(K_{NO3} + DO)$. This expression is similar to the Michaelis-Menton expression; for concentrations of dissolved oxygen greater than 1 mg/L, the expression reduces denitrification to near zero, whereas for dissolved oxygen levels less than 0.1 mg/L, this expression permits denitrification to occur.

2.2.5 Silica

Two silica state-variables are considered: available silica (Si) and unavailable or particulate biogenic silica (SiU). Available silica is dissolved and is utilized by diatoms during growth for their

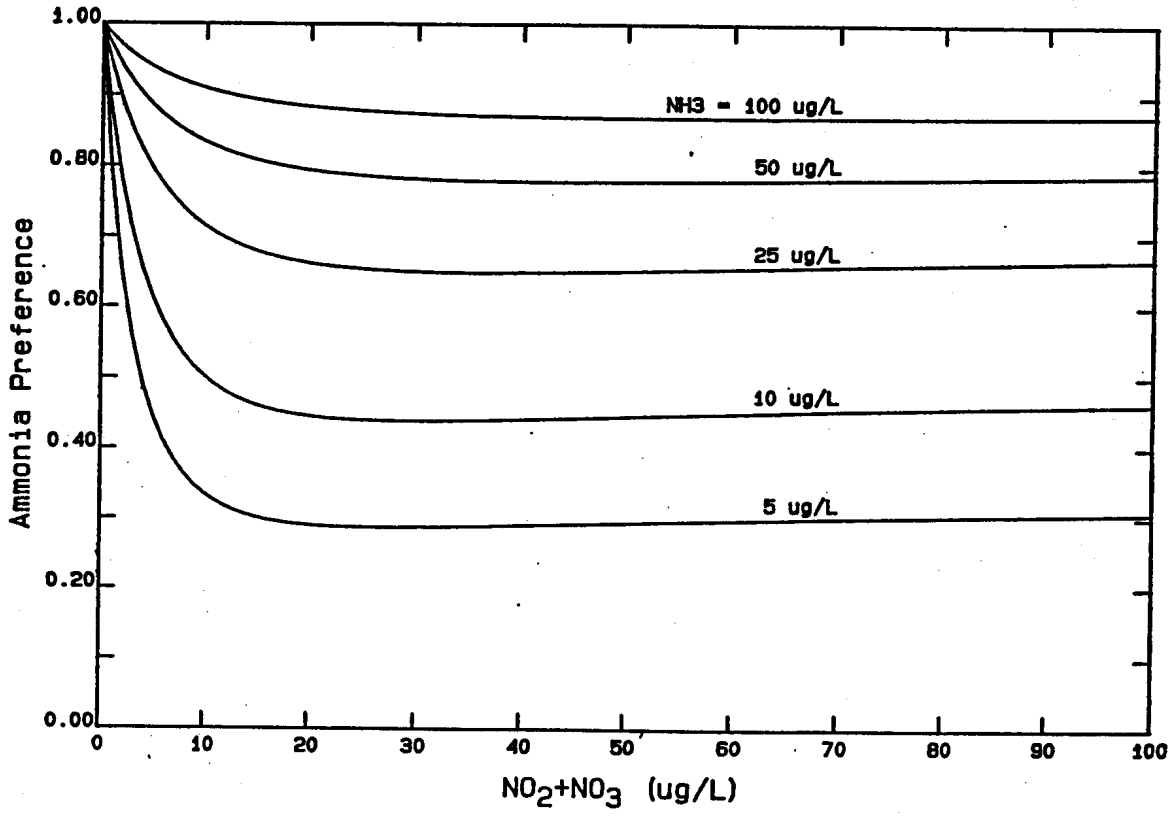

Figure 2-3. Behavior of the Ammonia Preference Structure for Various Concentrations of NH_3 and NO_2 + NO_3

cell structure. Unavailable or particulate biogenic silica is produced from diatom respiration and diatom grazing by zooplankton. Particulate biogenic silica undergoes mineralization to available silica or settles to the sediment from the water column. Table 2-5 presents the kinetic terms of the state-variable equations for the two silica forms utilized in the model framework.

2.2.6 Dissolved Oxygen

A by-product of photosynthetic carbon fixation is the production of dissolved oxygen. The rate of oxygen production and nutrient uptake is proportional to the growth rate of the phytoplankton, since its stoichiometry is fixed. An additional source of oxygen from algal growth occurs when the available ammonia nutrient source is exhausted and the phytoplankton begin to utilize the available nitrate. This additional oxygen source can be seen by comparing equations 2-13a and 2-13b (Morel 1983).

$$106\ CO_2 + 16\ NH_4^+ + H_2PO_4^- + 106\ H_2O \qquad \text{(2-13a)}$$

$$\Rightarrow \text{Protoplasm} + 106\ O_2 + 15H^+$$

$$106\ CO_2 + 16\ NO_3^- + H_2PO_4^- + 122\ H_2O + 17\ H^+ \qquad \text{(2-13b)}$$

$$\Rightarrow \text{Protoplasm} + 138\ O_2$$

The above equations present the stoichiometric description of the photosynthetic process assuming ammonium (Equation 2-13a) or nitrate (Equation 2-13b) as the nitrogen source and assuming algal biomass to have Redfield stoichiometry:

$$\text{Biomass} = C_{106}\ H_{263}\ O_{110}\ N_{16}\ P_1 \qquad \text{(2-14)}$$

Oxygen-deficient or under-saturated waters are replenished via atmospheric reaeration. The reaeration coefficient is a function of the average tidal velocity, wind, and temperature, and is computed using Equations 2-15a and 2-15b:

Table 2-5 - Silica Reaction Equations

Unavailable or Biogenic Silica (Bsi)

$$S_{22} = (k_{PR}(T)+K_{grz}(T))\cdot P_c - k_{22,23}\theta_{22,23}^{T-20}\cdot BSi\cdot\frac{P_c+ReDOC+ExDOC}{K_{mP_c}+P_c+reDOC+ExDOC} - \frac{v_{22}}{H}\cdot BSi$$

Available Silica (Si)

$$S_{23} = K_{22,23}\theta_{22,23}^{T-20}\cdot BSi\cdot\frac{P_c+ReDOC+ExDO}{K_{mP_c}+P_c+ReDOC+ExI}$$

Description	Notation	Value	Units
Phytoplankton Biomass	P_c	-	mgC/L
Temperature Corrected Algal Respiration Rate	$k_{PR}(T)$	Eq. 2-8	day^{-1}
Temperature Corrected Grazing Rate	$k_{grz}(T)$	0.03 - 0.10	day^{-1}
Specific Phytoplankton Growth Rate	G_P	Eq. 2-2	day^{-1}
Silica to Carbon Ratio	a_{SC}	-	mgSi/mgC
Mineralization Rate of Biogenic Silica	$k_{22,23}$	0.08	day^{-1}
Temperature Coefficient	$\theta_{22,23}$	1.08	
S_iU Settling Rate	v_{22}	1.0	m/day

$$k_a\ (20^oC) = k_L/H \qquad (2\text{-}15a)$$

wind

$$k_a(T) = k_a(20^oC)\theta_a^{\,T-20} \qquad (2\text{-}15b)$$

temperature

where

k_a = reaeration coefficient (day^{-1})
k_L = the surface mass transfer coefficient (m/day),
H = depth (m),

and

θ_a = temperature coefficient.

Dissolved oxygen saturation is a function of both temperature and salinity and is determined via Equation 2-16 (Hyer et al., 1971):

$$DO_{sat} = 14.6244 - 0.367134 \cdot T + 0.0044972 \cdot T^2 - 0.0966 \cdot S + 0.00205 \cdot S \cdot T + 0.0002739 \cdot S^2 \qquad (2\text{-}16)$$

where S is the salinity in ppt.

Dissolved oxygen is diminished in the water column as a result of algal respiration, which is the reverse process of photosynthesis, as a result of nitrification:

$$NH_4^+ + 2O_2 \Rightarrow NO_3^- + H_2O + 2H^+ \quad (2\text{-}17)$$

as a result of the oxidation of carbonaceous material (including detrital phytoplankton):

$$CH_2O + O_2 \Rightarrow CO_2 + H_2O \quad (2\text{-}18)$$

and, if dissolved oxygen concentrations are sufficiently low, as a result of denitrification:

$$5CH_2O + 4NO_3^- + 4H^+ \Rightarrow 5CO_2 + 2N_2 + 7H_2O \quad (2\text{-}19)$$

Table 2-6 presents a summary of the kinetic terms in the dissolved oxygen mass balance equation and the associated coefficients used in this study.

2.2.7 Secondary Variables

There are a number of secondary variables that can be computed along with the model's primary state-variables for which calibration data exist. The most obvious of these are gross primary productivity, BOD_5 and extinction coefficient. Gross primary productivity, an indirect measure of the depth integrated algal growth rate, was obtained by deploying a series of bottles containing surface water at various depths in the water column and measuring dissolved oxygen production. An internal model variable, which can be used to compare against gross primary productivity, is formulated via the following equation:

$$PP_{gross} = a_{OC} \cdot \alpha_{NH_3} G_P + \left(a_{OC} + 2 \cdot a_{ON} \cdot a_{NC}\right)\left(1 - \alpha_{NH_3}\right) \cdot G_P \quad (2\text{-}20)$$

where the first term in the equation represents algal oxygen production when using NH_3 as the substrate, and the second term represents algal oxygen production using nitrate as the substrate (Equations 2-13a and 2-13b), and where:

Table 2-6 - Dissolved Oxygen and O_2^* Reaction Equations

Dissolved Oxygen (DO)

$$
\begin{aligned}
S_{24} &= a_{OC}\cdot\alpha_{NH_3}\cdot G_P\cdot P_c + (a_{NO_3}c)\cdot(1-\alpha_{NH_3})\cdot G_P\cdot P_c \\
&+ k_a\theta_a^{T-20}\cdot(DO_{sat}-DO) - a_{OC}\cdot k_{PR}\theta_{PR}^{T-20}\cdot P_c \\
&- 2\cdot a_{ON}\cdot k_{20,21}\theta_{20,21}^{T-20}\cdot NH_3\cdot\frac{DO}{K_{nitr}+DO} \\
&- a_{oc}\cdot\left[k_{7,0}\theta_{7,0}^{T-20}\cdot LDOC\cdot\frac{LDOC}{K_{mLDOC}+LDOC} + k_{8,0}\theta_{8,0}^{T-20}\cdot RDOC + k_{9,0}\theta_{9,0}^{T-20}\right. \\
&\left.\cdot\, ReDOC\cdot\frac{ReDOC}{K_{mLDOC}+ReDOC} + k_{10,0}\theta_{10,0}^{T-20}\cdot ExDOC\cdot\frac{ExDOC}{K_{mLDOC}+ExDOC}\right] \\
&\cdot\frac{P_c+ReDOC+ExDOC}{K_{mP_c}+P_c+ReDOC+ExDOC}\cdot\frac{DO}{K_{DO}+DO} \\
&- \left[K_{O_2^*}\cdot\theta_{O_2^*}^{T-20}\cdot O_2^*\cdot\frac{P_c+ReDOC+ExDOC}{K_{mP_c}+P_c+ReDOC+ExDOC}\cdot\frac{DO}{K_{DOQ}+DO}\right]
\end{aligned}
$$

Sulfide Oxygen Equivalent (O_2^*)

$$
S_{25} = k_{O_2^*}\theta_{O_2^*}^{T-20}\cdot O_2^*\cdot\frac{DO}{K_{DOQ}+DO}\cdot\frac{P_c+ReDOC+ExDOC}{K_{mP_c}+P_c+ReDOC+ExDOC}
$$

Table 2-6 - Dissolved Oxygen and o_2^* Reaction Equations (Continued)

Description	Notation	Value	Units
Oxygen to Carbon Ratio	a_{OC}	32/12	$mgO_2/mg\ C$
Oxygen to Nitrogen Ratio	a_{ON}	32/14	$mgO_2/mg\ N$
Oxygen to Carbon Ratio for Nitrogen Uptake	$a_{No_3}c$	$a_{OC}+a_{ON}\cdot 2a_{NC}$	$mgO_2/mg\ C$
Reaeration Rate at 20°C	k_a	Eq. 2.15a	day^{-1}
Temperature Coefficient	θ_a	1.024	none
Oxygen Transfer Coefficient	k_L	-	m^{-1}
Dissolved Oxygen Saturation	DO_{sat}	Eq. 2.16	mgO_2/L
Oxidation Rates and Temperature Coefficients:			
for LDOC	$k_{7,0}$	0.15	day^{-1}
	$\theta_{7,0}$	1.08	
for RDOC	$k_{8,0}$	0.008	day^{-1}
	$\theta_{8,0}$	1.08	
for ReDOC	$k_{9,0}$	0.3	day^{-1}
	$\theta_{9,0}$	1.047	
for ExDOC	$k_{10,0}$	0.1	day^{-1}
	$\theta_{10,0}$	1.08	
Oxidation Rate of Dissolved Sulfide	$k_{O_2^*}$	0.15	day^{-1}
Temperature Coefficient	$\theta_{O_2^*}$	1.08	day^{-1}
Half Saturation Constant for $\theta_{O_2^*}$	K_{DOQ}	0.100	mgO_2/L

PP_{gross} = the gross primary productivity (μg O_2/L-day),
G_P = the temperature-corrected, light-corrected, nutrient-corrected algal growth rate, (Equations 2-2 through 2-7, (day-1)),
a_{OC} = the oxygen to carbon ratio (32 mgO_2/12 mgC),
a_{ON} = the oxygen to nitrogen ratio (32 mgO_2/14 mgN),
a_{NC} = the nitrogen to carbon ratio (variable),
α_{NH_3} = the preference for ammonia (Equation 2-12).

In a similar manner, an internal variable may be formulated and used to compare to the BOD_5 data. The bottle BOD_5 is a measurement of community respiration, since it includes algal respiration, the bacterial decomposition of both detrital algal material and non-algal carbonaceous matter, and the effects of nitrification. The model estimate of the bottle BOD_5 can be expressed as follows:

$$BOD_5 = 2.67\cdot\left[RDOC\cdot(1-e^{-5k_{RC}})+LDOC\cdot(1-e^{-5k_{LC}})+ReDOC\cdot(1-e^{-5k_{ReC}})\right.$$

$$\left.+ExDOC\ (1-e^{-5k_{ExC}})\right] + 0_2^*\cdot(1-e^{-5k_{0_2^*}}) + P_c\cdot(1-e^{-5k_{PR}}) + 4.57\cdot NH_3\cdot(1-e^{-5k_{nitr}}) \quad (2\text{-}21)$$

where

BOD_5 = the 5-day bottle BOD (mg O_2/L),
k_{RC} = the oxidation rate of refractory dissolved organic material (day^{-1}),
k_{LC} = the oxidation rate of labile dissolved organic material (day^{-1}),
k_{ReC} = the oxidation rate of reactive dissolved organic material (day^{-1}),
k_{ExC} = the oxidation rate of algal exudate dissolved organic material (day^{-1}),
0_2^* = oxygen equivalent of sulfide (mg O_2^*/L),
$k_{0_2^*}$ = the oxidation rate of sulfide (day^{-1}),
k_{PR} = the algal respiration rate (day^{-1}),
k_{nitr} = nitrification rate (day^{-1}).

The final internal variable which may be computed is the total water column extinction coefficient (Equation 2-22):

$$k_{e_{obs}} = k_{e_{base}} + 1000 \cdot k_c \cdot P_c / a_{cchl} \quad (2\text{-}22)$$

where

$k_{e_{obs}}$ = the observed water column extinction coefficient (m^{-1}),
$k_{e_{base}}$ = the base or background extinction coefficient related to non-algal turbidity (m^{-1}),
k_c = the extinction coefficient per unit of phytoplankton chlorophyll-a (m^2/mg chl-a),
P_c = the phytoplankton biomass (mgC/L)
a_{cchl} = the carbon to chlorophyll ratio (mgC/mg chl-a).

2.3 SEDIMENT SUBMODEL

An important component of the water column nutrient and dissolved oxygen mass balance equations is the interaction with the sediments. In historical eutrophication models, the SOD and nutrient fluxes were input as distributed loads. However, there was generally no effort to ensure that the SOD and nutrient fluxes bore any relationship to the delivery of organic material to the sediment. The present sediment submodel corrects that historical modeling deficiency and effectively closes the mass balance between the water column and the sediment.

The sediment submodel incorporated as part of the water quality model used in this study utilizes the same framework as employed in the Chesapeake Bay study, conducted for the U.S. EPA Chesapeake Bay Program. The sediment submodel can be conceived of as having three parts: the deposition of particulate organic matter (POM) to the sediment from the water column; the decay or diagenesis of the POM in the sediment; and the flux of the resulting end-products to the overlying water column.

The delivery of POM to the sediments of New York Harbor is a spatially varying phenomenon. Once delivered to the sediment, POM is mineralized in the anaerobic layer. Diffusion and particle mixing transfer the dissolved and particulate reduced species to the aerobic layer where they can react. Finally, particulate and dissolved species can be buried via sedimentation.

2.3.1 Sediment Model Framework

The sediment submodel is based on the principle of mass balance. A mass balance equation is written for POM in sediment segments that lie under each bottom water column segment of the water quality model. The mass balance equations account for changes in POM in the sediment due to deposition from the overlying water column, sedimentation, and decay or diagenesis.

The decay of POM is assumed to follow first-order kinetics as described by Berner (1964, 1974). Thus, POM is assumed to decompose at an overall rate directly proportional to its own concentration. This can be expressed as:

$$\frac{dG}{dt} = - kG \qquad (2\text{-}23)$$

where:

G = concentration of metabolizable organic material (mg/L),
k = first-order decay constant for decomposition (day^{-1}).

Berner (1980) expanded the simple G model into a multi-G model, which more realistically recognizes that the pool of decomposable, sedimentary organic material is actually composed of various groups of compounds that have different reactivities with regard to decomposition. The present model framework assumes a 3-G model structure; that is, POM is assumed to be comprised of a labile component, a refractory component and a slow refractory component. Each of these components is assumed to decay following different first-order reaction rates. It is further assumed, as with any biological process, that the reactions rates are temperature dependent.

2.3.2 Sediment Submodel Mass Balance Equations

Since temperature is considered to be a conservative variable, it will be presented first. A temperature balance is written for each of the two sediment layers as follows:

Layer 1:

$$\frac{dT_1}{dt} = \frac{D}{H_1}\left(T_{owc} - T_1\right) + \frac{D}{H_1}\left(T_2 - T_1\right) \qquad (2\text{-}24A)$$

Layer 2:

$$\frac{dT_2}{dt} = \frac{D}{H_2}\left(T_1 - T_2\right) \qquad (2\text{-}24B)$$

where:

T_1 = temperature in Layer 1(°C),
D = thermal diffusion coefficient (cm^2/sec),
T_{owc} = temperature of the overlying water column (°C),
H_1 = depth of Layer 1 (cm),
T_2 = temperature in Layer 2 (°C),
H_2 = depth of Layer 2 (cm).

Using a continuous solution analytical model for temperature diffusion in the sediment, Matisoff, 1978 estimated D to vary between 1.32×10^{-3} cm^2/sec to 1.86×10^{-3} cm^2/sec based on an analysis of two sediment cores. Using a discrete form of the same model, Matisoff found D to range between 1.08×10^{-3} to 1.77×10^{-3} cm^2/sec for the same two cores. A value of 1.80×10^{-3} cm^2/sec was used in this study.

A mass balance equation can be written for each of the 3-G components of POM in each sediment layer. The following mass balance equation is written for the ith component of particulate organic nitrogen (PON):

Layer 1:

$$\frac{dPON_{i_1}}{dt} = \frac{v_{dep}}{H_1}\cdot\left(f_{p1_i}\cdot ncrb_1 P_{c_1} + f_{p2_i}\cdot ncrb_2\cdot P_{c_2} + f_{pon_i}\cdot PON_{owc}\right) \quad (2\text{-}25a)$$

$$- \frac{v_{sed}}{H_1}\cdot PON_{i_1} - k_{diag_i}(T_1)\cdot PON_{i_1}$$

Layer 2:

$$\frac{dPON_{i_2}}{dt} = \frac{v_{sed}}{H_2}\cdot PON_{i_1} - \frac{v_{sed}}{H_2}\cdot PON_{i_2} - k_{diag_i}(T_2)\cdot PON_{i_2} \quad (2\text{-}25b)$$

where:

PON_{i_1}	=	the concentration of the ith-G component of PON in Layer 1(gm/m^3),
v_{dep}	=	deposition velocity of PON from the overlying water column to the sediment (cm/day),
H_1	=	depth of sediment Layer 1 (cm),
f_{p1_i}	=	fraction of phytoplankton functional group 1 that is comprised of G_i,
$ncrb_1$	=	nitrogen to carbon ratio for phytoplankton group 1 (mgN/mgC),
P_{c_1}	=	concentration of phytoplankton group 1 (mg C/L),
f_{p2_i}	=	fraction of phytoplankton functional group 2 that is comprised of G_i,
$ncrb_2$	=	nitrogen to carbon ratio for phytoplankton group 2 (mgN/mgC),
P_{c_2}	=	concentration of phytoplankton group 2 (mgC/L),
PON_{owc}	=	concentration of PON in the overlying water column (mgN/L),
f_{pon_i}	=	fraction of overlying water column PON that is comprised of G_i,
v_{sed}	=	sedimentation velocity (cm/day),
$k_{diag_i}(T)$	=	temperature corrected diagenetic decay coefficient for G_i (day^{-1}),
T_1	=	temperature in Layer 1 (°C),
PON_{i_2}	=	the concentration of the ith-G component of PON in Layer 2 (gm/m^3),
H_2	=	depth of sediment Layer 2 (cm),
T_2	=	temperature in Layer 2 (°C).

Similar equations can be written for POC, particulate organic phosphorus (POP) and particulate biogenic silica (BSi), utilizing the appropriate phosphorus to carbon and silica to carbon ratios.

The resultant end-products of the diagenesis or decay of the particulate organic matter include ammonia nitrogen, dissolved inorganic phosphorus and dissolved inorganic silica. These end products can also undergo additional biological, chemical and physical processing within the sediment layer. For example, ammonia nitrogen can in the oxic layer undergo nitrification; inorganic phosphorus can sorb to the solids present in the sediment; all dissolved inorganic nutrients can exchange with the overlying water column. A more complete development of the sediment model theory, as extracted from HydroQual's final report to the U.S. Army Corps of Engineers and the USEPA Chesapeake Bay Program (DiToro and Fitzpatrick 1993) is presented in Appendix A. Table 2-7 presents the 16 state-variables in the sediment submodel and Table 2-8 presents values of key coefficients and reactivity fraction distributions.

Table 2-7. Sediment Submodel State-Variables

State Variable
1. Temperature
2. Labile POP
3. Refractory POP
4. Slow Refractory POP
5. Labile PON
6. Refractory PON
7. Slow Refractory PON
8. Labile POC
9. Refractory POC
10. Slow Refractory POC
11. Biogenic Silica
12. Ammonia Nitrogen
13. Nitrate Nitrogen
14. Inorganic Phosphorus
15. Dissolved Silica
16. Hydrogen Sulfide

Table 2-8 - Sediment Submodel Model Coefficients

Description	Notation	Value	Units
Physical Related			
Water column-sediment layer temperature diffusion coefficient	D	0.0156	cm^2/sec
depth of active sediment layer	H_2	10.	cm
deposition velocity at 20°C for:	v_{dep}		
phytoplankton		[0.2-1.0]• (eq. 2-9)	m/day
non-phytoplankton POM		0.1-1.0	m/day
sedimentation velocity	v_{sed}	0.25	cm/yr
Diagenesis Related			
G1 diagenesis decay rate at 20°C	k_{diag1}	0.035	day^{-1}
temperature correction coefficient	θ_1	1.10	
G2 diagenesis decay rate at 20°C	k_{diag2}	0.0018	day^{-1}
temperature correction coefficient	θ_2	1.15	
G3 diagenesis decay rate at 20°C	k_{diag3}	0.000001	day^{-1}
temperature correction coefficient	θ_3	1.17	

	Labile	Refractory	Slow Refractory
G-Model Fraction Splits			
Phosphorus			
phytoplankton group 1	0.65	0.20	0.15
phytoplankton group 2	0.65	0.20	0.15
non-phytoplankton POM	0.65	0.20	0.15
Nitrogen			
phytoplankton group 1	0.65	0.25	0.10
phytoplankton group 2	0.65	0.25	0.10
non-phytoplankton POM	0.65	0.25	0.10
Carbon			
phytoplankton group 1	0.65	0.20	0.15
phytoplankton group 2	0.65	0.20	0.15
non-phytoplankton POM	0.65	0.20	0.15

SECTION 3

MODEL CALIBRATION

3.1 INTRODUCTION

The overall objective is to calibrate the water quality model to the observed data, utilizing a set of model coefficients and parameters that are consistent with the observed data and field studies and are within the general ranges of values reported in the literature and accepted by the modeling community. Coincident with this objective is the goal to utilize a set of model coefficients that are consistent across spatial segments and consistent in time.

The general procedure followed is to perform a series of iterative runs of the model using estimates of the various coefficients and parameters. Comparisons are made between model output and observed data, using computer generated plots in order to make a qualitative assessment of the model's goodness of fit. This process continues through the adjustment or tuning of the model parameters until a reasonable reproduction of the observed data is attained or no further improvement is possible.

This section provides the details of the calibration effort and presents model versus data comparisons for the final calibration run.

The detailed discussions of the previous section presents the kinetic structure of the SWEM water quality submodel. This section will present the details of the implementation of the modeling framework together with results of the calibration effort. Included are rationales leading up to the final choices used in the modeling effort, together with the assumptions and compromises that were necessary.

The final calibration is the result of multiple model runs which were made to obtain a consistent set of model coefficients that are reasonable and reproduce the observed data for all state variables considered. With the exception of exogenous variables such as flow, temperature, solar radiation, and extinction coefficients, all model coefficients were consistent for the 12 month calibration period. The method employed in determining the values of the model coefficients is essentially one of trial and error. The starting point was a set of rate constants and parameter values

which were used in the Long Island Sound modeling effort (i.e., LIS 3.0) and which were used in the eutrophication and sediment modeling effort for the Chesapeake Bay system.

3.2 MODEL INPUTS

A number of exogenous variables incorporated in the SWEM modeling framework, such as freshwater flow and solar radiation, were either temporally or spatially variable or both. Since data were available to define many of these variables on a daily basis, they were approximated by a series of piecewise linear functions. These piecewise linear functions consist of a series of daily-averaged values of the exogenous variables and associated Julian dates. This is consistent with the available data and the time scale of the model framework.

Model calibration patterns are imported directly from the hydrodynamic submodel. The hydrodynamic model is calibrated and validated to physical measurements of tidal stage, velocities, temperature, and salinity. The calibration and validation of the hydrodynamic model are presented separately as part of Sub-tasks 10.3 and 10.6.

All loads to the SWEM domain from WPCPs, industrial treatment plants, combined sewer overflows, stormwater, and atmospheric deposition are based on daily monitoring records (DMRs), 1994 Interstate Sanitation Commission sampling, and the 1994-95 SWEM field sampling program. All loads which serve as input the SWEM model are presented in the Sub-task 10.2 report.

3.2.1 Model Grid

A three-dimensional hydrodynamic submodel for SWEM, which operated independently of the water quality model, was developed under Sub-task 10.3. The model domain is comprised of 41,160 wet and dry grid cells. Quantities computed by this model include surface elevation, three-dimensional velocities and diffusivities, temperature and salinity. Details of the model theory, formulation and calibration results are presented in the report for Sub-task 10.3. The model grid information, tidal stage, velocities and diffusivities, were outputted as one-hour averages and were stored for subsequent use by the water quality submodel. The model grid is presented in Figure 3-1.

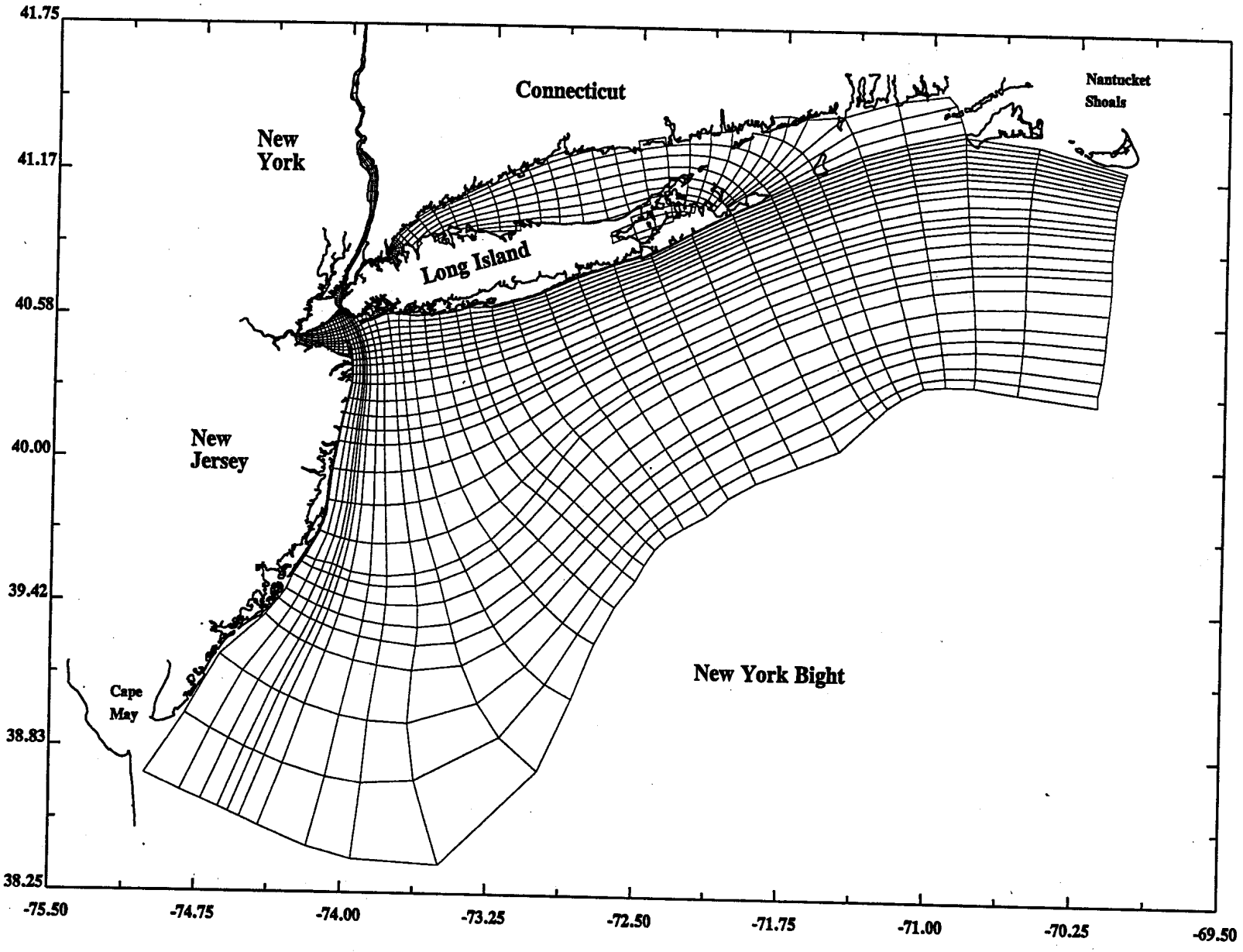

Figure 3-1. Model Grid for System Wide Eutrophication Model: Complete Model Domain

3.2.2 Boundary Conditions

Flow entering or leaving Long Island Sound or the New York Bight along the boundaries of SWEM carries with it phytoplankton, nutrients, organic carbon and dissolved oxygen. These mass fluxes may be a substantial source or sink of material to the system. This is an important consideration in terms of the total controllable load. Therefore, considerable attention was focused on the specification of the boundary concentrations. Attempts were made to correlate the concentrations of the various water quality state- variables to time of the year. Data collected during the monitoring program in support of SWEM in 1994 and 1995 were used. Figures 3-2 and 3-3 show the monitoring program stations which cover the southern and eastern reaches of the SWEM open boundary. Notice that the open boundary monitoring stations, stations 177, 178, 190, 195, 198, 201, 206, 205, and 204, are sufficiently far enough away from the Harbor and Sound to ensure that data collected near the open boundary of SWEM are not impacted by loads internal to the domain of SWEM. Values of concentrations for the various water quality constituents assigned at the boundaries are shown on the calibration diagrams (Section 3.3 and Appendix B).

3.2.3 Extinction Coefficients

Water column transparency and, therefore, extinction coefficient plays an important role in primary productivity. Phytoplankton primary productivity is greater in areas of high light penetration than in light-limited areas, given the same nutrient availability. There is considerable variability in water column transparency over the domain of SWEM. Generally, the inner Harbor has higher extinction coefficients than outer areas, due to higher suspended solids loadings. Monthly-averaged estimates of extinction coefficients were made by correcting the observed extinction coefficient data for phytoplankton chl-a, using Equation 2-22. Observed and computed extinction coefficients are shown on the calibration diagrams (Section 3.3 and Appendix B).

3.2.4 Reaeration Coefficients

Reaeration coefficients are determined internally in the water quality model, by providing estimates of K_L, the surface transfer coefficient for oxygen, and then using Equations 2-15a and 2-15b. Figure 3-4 presents the time-invariant but spatially-variable estimates of K_L. The spatial variability reflects the high tidal velocities in the East River, leading to higher values for K_L by

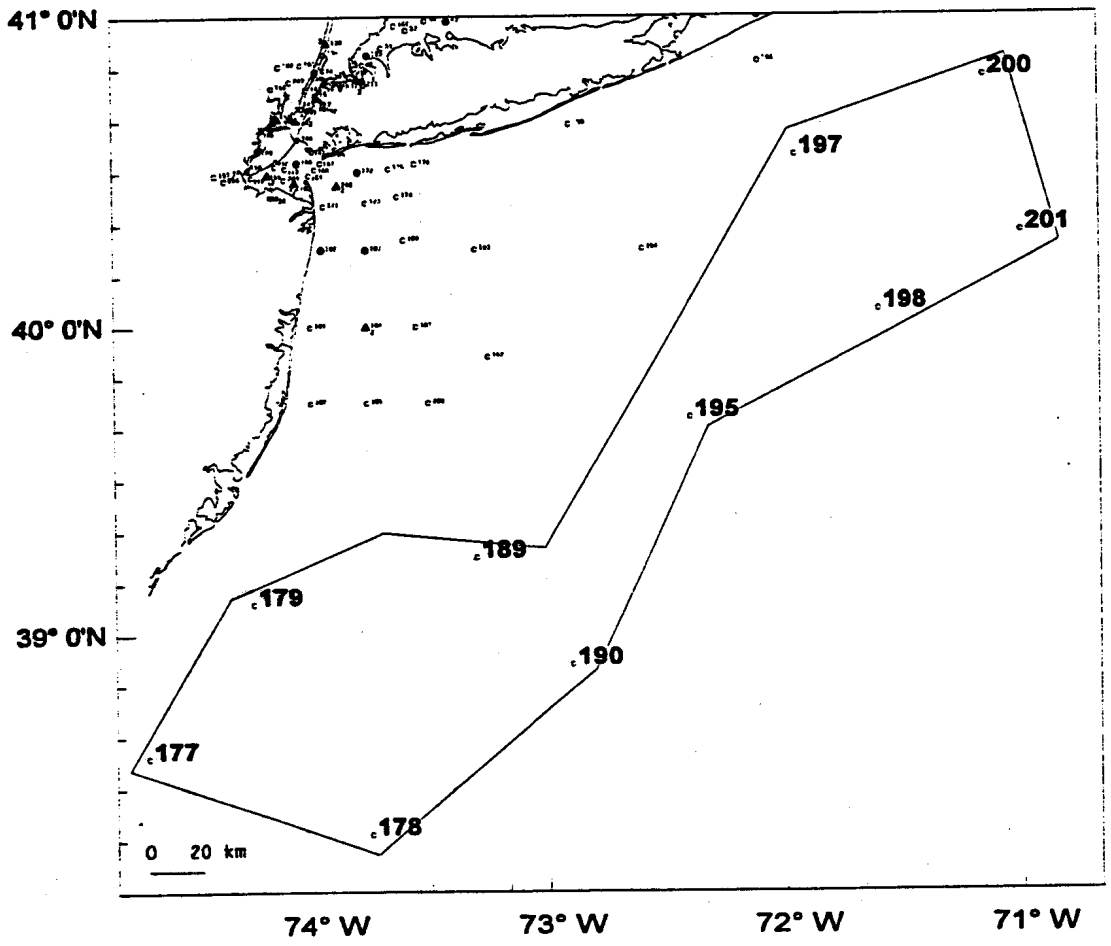

Figure 3-2. Open Boundary Monitoring Stations (Southern End)

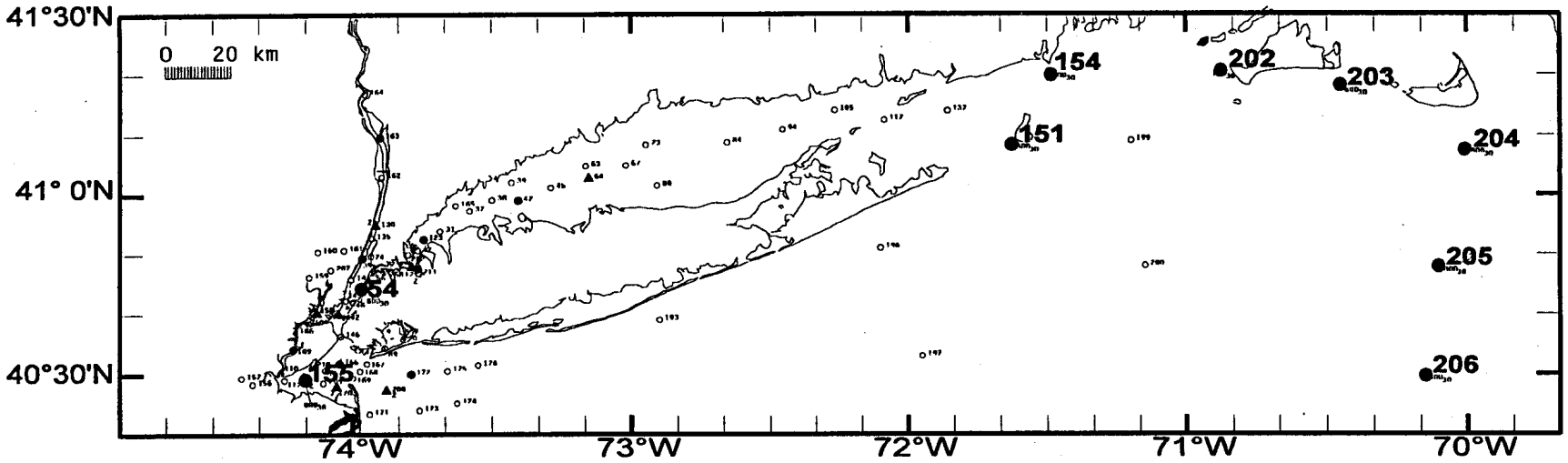

Figure 3-3. Open Boundary Monitoring Stations (Eastern End)

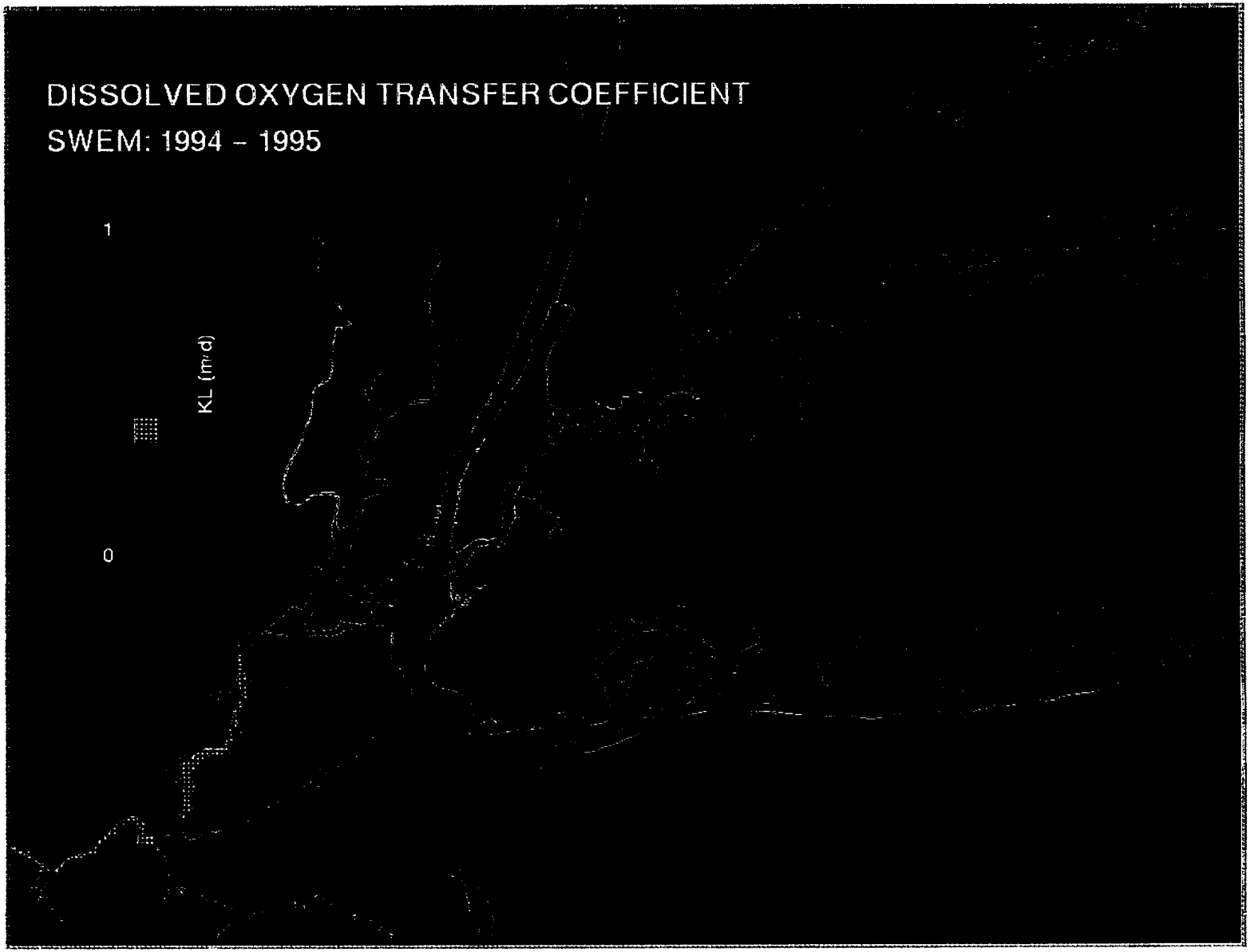

Figure 3-4. Dissolved Oxygen Transfer Coefficient

comparison to the segments located in the Narrows, and the effects of winds and tides in the eastern portion of the Sound.

3.2.5 Water Temperature

The temperature regime of the Harbor/Bight/Sound system is an important exogenous variable because it acts as a key driving force for the behavior of phytoplankton and for temperature-mediated bacterial decomposition and recycle kinetics. Temperature is also used together with salinity data to calibrate the transport structure. As such, considerable effort was made to define the annual cycle of water column temperature during the calibration of the hydrodynamic submodel of SWEM as detailed in the report for Sub-task 10.3.

3.2.6 Solar Radiation

The second principal exogenous driving force for phytoplankton growth is solar radiation. Short-wave radiation from the sun is used by phytoplankton for photosynthesis. As this radiation passes through the atmosphere, it can be absorbed and scattered by the gases in the air and by water vapor, clouds, and dust. As a result of such processes, solar radiation reaching the earth's surface is partly in the form of direct radiation and partly in the form of diffuse radiation at the water surface.

Daily incident solar radiation was estimated using hourly estimates of percent cloud cover from Central Park and the methodology of Rosati and Miyakoda (1988) which relates latitude and percent cloud cover to incident solar radiation. Figure 3-5 presents the incident solar radiation as a function of time for the calibration period.

3.2.7 Fraction of Daylight

The growth rate formulation for phytoplankton, as described in Section 2, depends on the length, or fraction, of daylight, since photosynthesis takes place only in the presence of sunlight. Daily fractions of daylight were generated using hourly incident solar radiation estimates. Fraction of daylight for each day of the calibration period was assigned as the fraction of 24 hours having non-zero incident solar radiation.

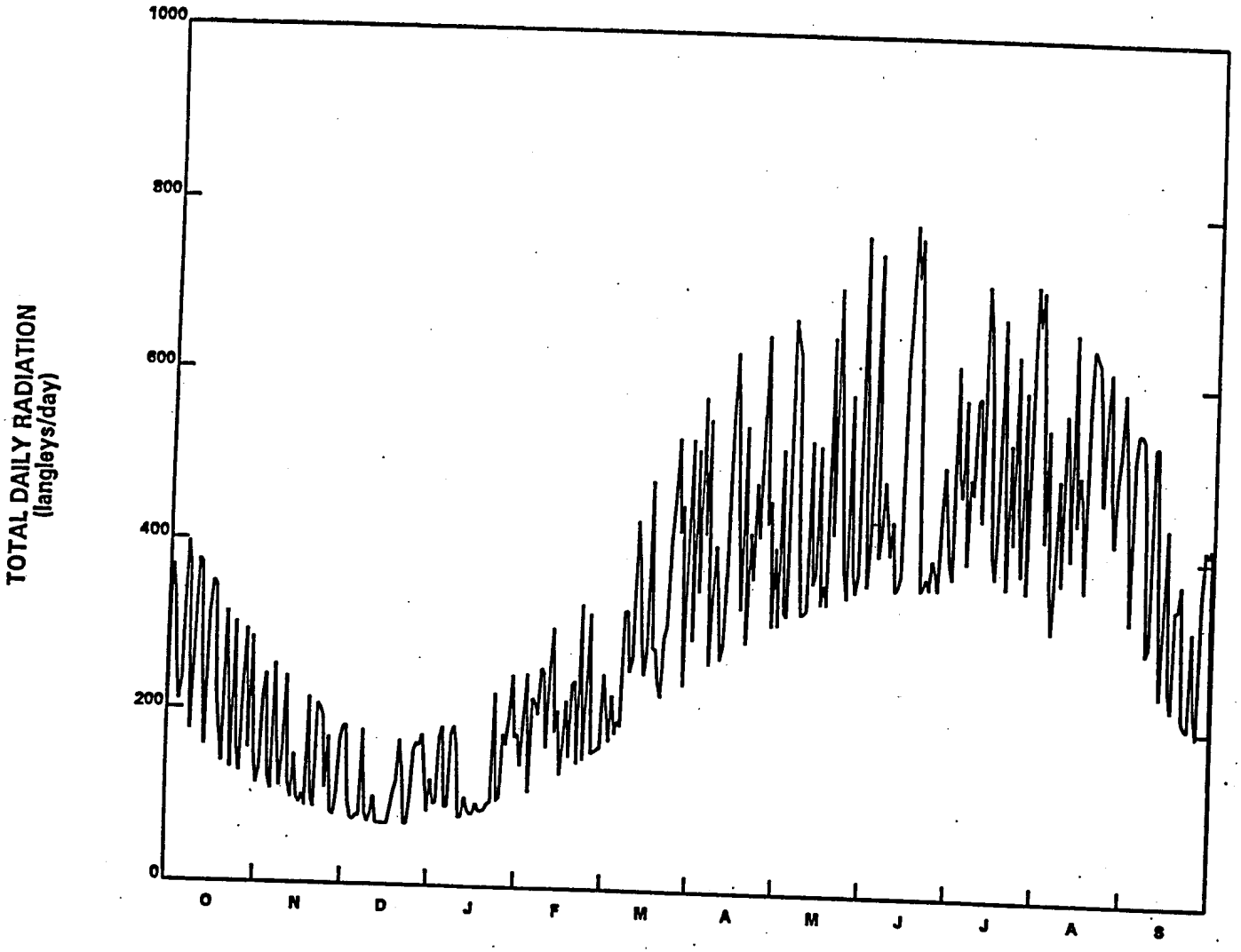

Figure 3-5. Incident Solar Radiation at Central Park

3.2.8 Particulate Organic Deposition Rates and Sedimentation Rates

An important parameter required by the sediment model is the net deposition rate of POM from the water column to the sediment. Estimates of net deposition were guided by estimates of bottom layer net non-tidal velocities as arrived at from the calibration to salinity and temperature. It is assumed that little or no net deposition would occur in regions of the system where net bottom velocities are high, due to scour and resuspension. Net deposition is also the mechanism by which the effects of benthic filtration are simulated in SWEM. Rates of net deposition were adjusted on a spatially varying basis to reflect the water column filtration of POM by benthic bivalves.

The sedimentation velocity is the rate at which material is buried in the sediment due to the deposition of fresh organic and inorganic material. No direct measurements are available for estimating sedimentation velocities for the sediment model. However, for coastal estuaries these rates are usually low, on the order of 0.1 to several cm/year. Lacking better estimates, a spatially uniform sedimentation rate of 0.25 cm/year was used in this study. The model is fairly insensitive to this rate, since at 1 cm/year and for a 10 cm thick surface sediment layer and a 100 cm thick bottom sediment layer, little or no POM is lost via burial. This is because it all decomposes, within the 110 year period required for a particle to traverse the depth of the sediment layer.

3.2.9 Variable Stoichiometry

Phytoplankton can adjust their internal stoichiometry as a nutrient becomes limiting. Therefore, it is necessary to account for this phenomenon in the model. The relationship employed in the model is described by an empirical equation (Cerco and Cole, 1993):

$$C{:}Nutr = C_{min} + (C_{max} - C_{min}) * e^{-\min(10,C_O)} \qquad (3\text{-}1)$$

where:

C:Nutr	=	carbon to nutrient ratio for algal biomass (mg C/mg Nutrient)
C_{min}	=	minimum of carbon to nutrient ratio i.e., Redfield ration, (mg C/mg Nutrient)
C_{max}	=	maximum of carbon to nutrient ratio (mg C/mg Nutrient)
C_o	=	coefficient determining the range of nutrient's limitation (L/mg Nutrient)

Hence, the behavior of the carbon to nutrient ratio of algae is a function of dissolved inorganic nutrient concentration that is available in water column. This functional form is shown on Figure 3-6 for nitrogen, phosphorus and silica, respectively. When the available dissolved inorganic nutrient becomes scarce or limited, the carbon to nutrient ratio increases gradually to a maximum value. Conversely, under nonlimiting conditions, the ratio declines to the minimum and follows the well-known Redfield ratio 40 and 5.67 for C/P and C/N, respectively. Table 3-1 presents the coefficients used in the Equation 3-1 for each of the appropriate nutrients.

Table 3-1. Values of Coefficients for Equation 3-1 Used in SWEM

Ratio	Algal Species	Cmin	Cmax	Co
C/P	Winter Diatoms	40.0	90.0	200.0
	Summer Assemblage	40.0	90.0	200.0
C/N	Winter Diatoms	5.67	7.2	10.0
	Summer Assemblage	5.67	10.0	10.0
C/Si	Winter Diatoms	2.2	8.0	12.0
	Summer Assemblage	10.0	0.0	0.0

3.3 MODEL RESULTS

The primary goal of this study is to develop a mathematical model which describes the eutrophication and hypoxia processes of the Harbor/Bight/Sound system. One method for judging the adequacy of the model in describing these processes is to compare the results of model computations to observed data. In the ideal world, there would be little or no difference between model computation and observed data. However, there is inherent variability in the measurements of concentration of the water quality variables. This variability may be due to measurement error or inadequate laboratory procedures. The variability may also be due to natural processes; for example, the effect of local cloud cover or wind mixing on phytoplankton primary productivity. There is also the spatial variability introduced when comparing the observed data from one or two randomly selected sampling locations within a model segment to the model output of a spatially well mixed segment.

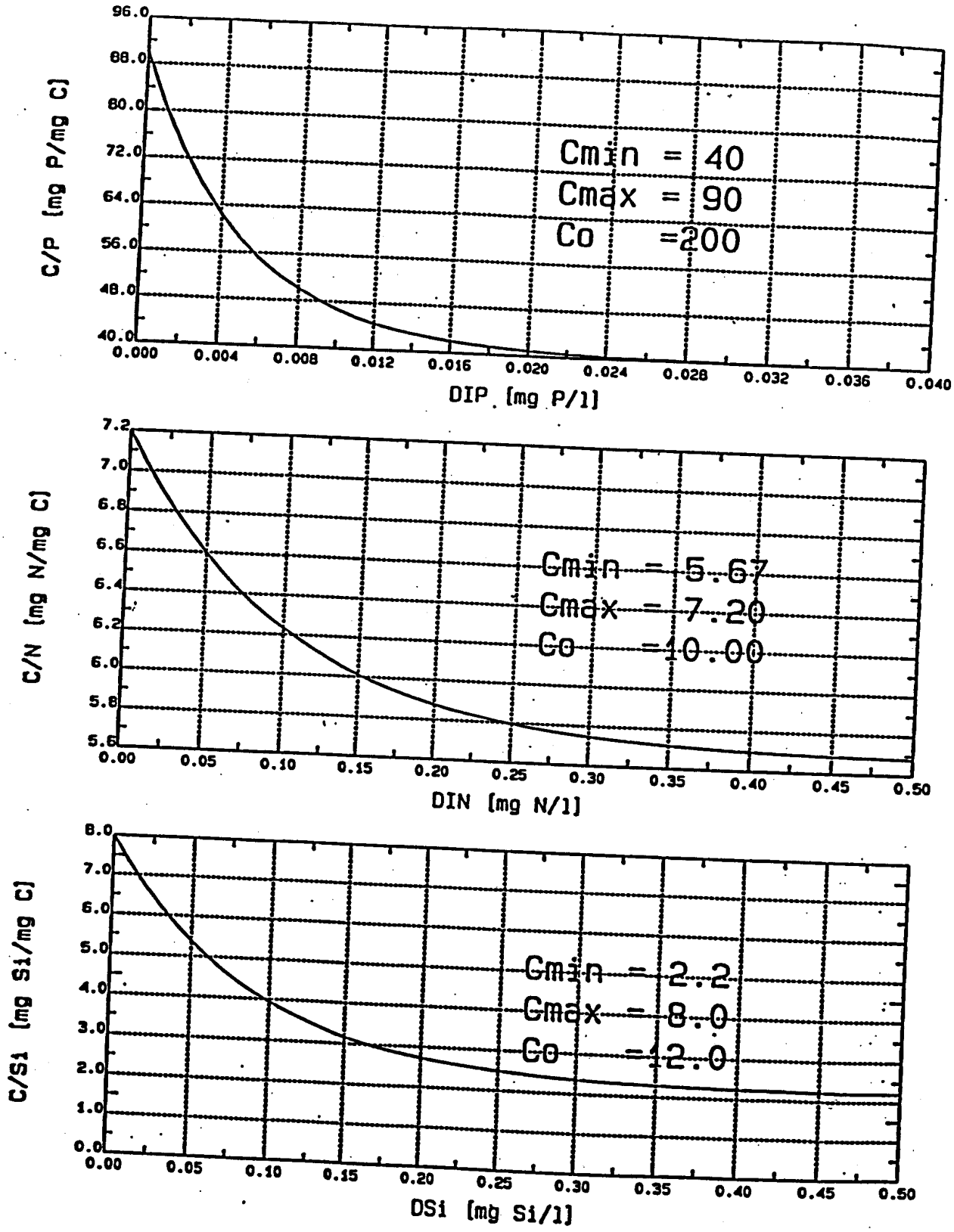

Figure 3-6. Carbon to Nutrient Ratios vs. Dissolved Nutrients for Winter Diatoms

It is required that the model reproduce the annual cycle of phytoplankton biomass, as well as primary productivity. The model should also be able to reproduce the super-saturated dissolved oxygen concentrations observed in the surface layer of the water in and near the region of peak phytoplankton biomass.

It is necessary that the water quality model compute the proper factors which limit algal productivity. For example, in the East River the model should limit algal productivity due to light and residence time limitations, rather than due to nutrient limitation. In the Central and Eastern Sound, phytoplankton growth should be limited by nutrient availability, rather than light. The model should also predict the correct limiting nutrient in regions where nutrient limitation governs algal growth. Historically, inorganic nitrogen is observed to be the limiting nutrient in Long Island Sound, although there are periods of time in the late spring when silica could limit growth.

Sediment flux data were also collected as part of the monitoring effort in support of SWEM. Since a sediment submodel has been incorporated as part of the model framework, model adequacy can also be judged by comparing the observed and computed spatial and temporal distributions of sediment nutrient and oxygen fluxes. Both the spatial and temporal sediment sampling program were more limited in scope than the water column sampling program. Hence, the comparisons of observed and computed fluxes are more limited than the water column comparisons.

3.3.1 Water Column Results

Model calibration results are presented as a series of computer- generated plots which compare model computations versus observed data. These plots are presented in two fashions for the water column: primarily, as a sequence of temporal plots and, secondly, as a sequence of spatial plots. The plots present surface and bottom computations of the concentrations of various water quality state variables, using solid lines (surface) and dashed lines (bottom) to represent the model output. Observed data are presented as discrete points, representing the average and the range of the data. In these plots, the observed data are grouped into surface and bottom layers based on the sampling locations and the bathymetric depths of their corresponding model cells. All data sampled at depths within 50 percent of the bathymetric depths below the water surface or above the bottom, are included in the surface and the bottom layers, respectively. In addition, only those data stations lying along or within one box of the model spatial transect are included in the spatial comparisons.

The temporal plots present model computations averaged over 3.5-day periods at 36 locations. Spatial plots represent 10-day averaged model output with the exception that real minimum and maximum values of chlorophyll-a and dissolved oxygen are displayed. The spatial plots include 16 spatial transects which cover major areas of the SWEM domain.

Rather than present all the time-series and monthly-averaged spatial plots at this point (2592 spatial profiles and 648 temporal profiles), examples will be presented in the main body of this report. The complete set of calibration figures is presented in Appendix B.

3.3.1.1 Temporal Comparisons

An example of temporal comparisons between model output and observed data is presented in Figure 3-7a for Western Long Island Sound and Figure 3-7b for the Hudson River at 125th Street. There are two pages associated with each position showing 18 water quality variables. The first page presents comparisons (left to right) for chl-a, POC, dissolved oxygen, DIN, DIP, dissolved inorganic silica (Diss Si), salinity (SAL), temperature (TEMP), and light extinction (Ke). The second figure presents comparisons (top to bottom) of ammonia nitrogen (NH_4-N), nitrite plus nitrate nitrogen (NO_2+NO_3), TN, BOD-5, particulate biogenic silica (Part silica), TP, DOC, POC, TOC.

Figures 3-7a and 3-7b present results for both surface and bottom layer segments versus surface and bottom layer data. The model computation for the surface is represented by a solid line; bottom layer computations are represented by a dashed line. The surface observed data are presented as an open upward pointing triangle; bottom observed data are shown using a filled downward pointing triangle. Data for these comparisons are from the 1994-95 SWEM monitoring program. In the dissolved oxygen panel, the saturation concentration of the surface layer is shown as a coarsely dashed line. The dissolved oxygen panel also displays the surface maxima and bottom minima computed by the model. Both Figure 3-7a and 3-7b show that the model reproduces the annual cycle of phytoplankton biomass, as evidenced by the POC and chlorophyll model and data comparisons, and dissolved oxygen. Highest POC concentrations are computed and observed for the months of July and August versus lower POC concentrations computed during the late spring, fall and early winter.

In the Sound dissolved oxygen concentrations are computed and observed to be above saturation for February, March and April. The model reproduces the 4 to 5 mg/L deficit observed

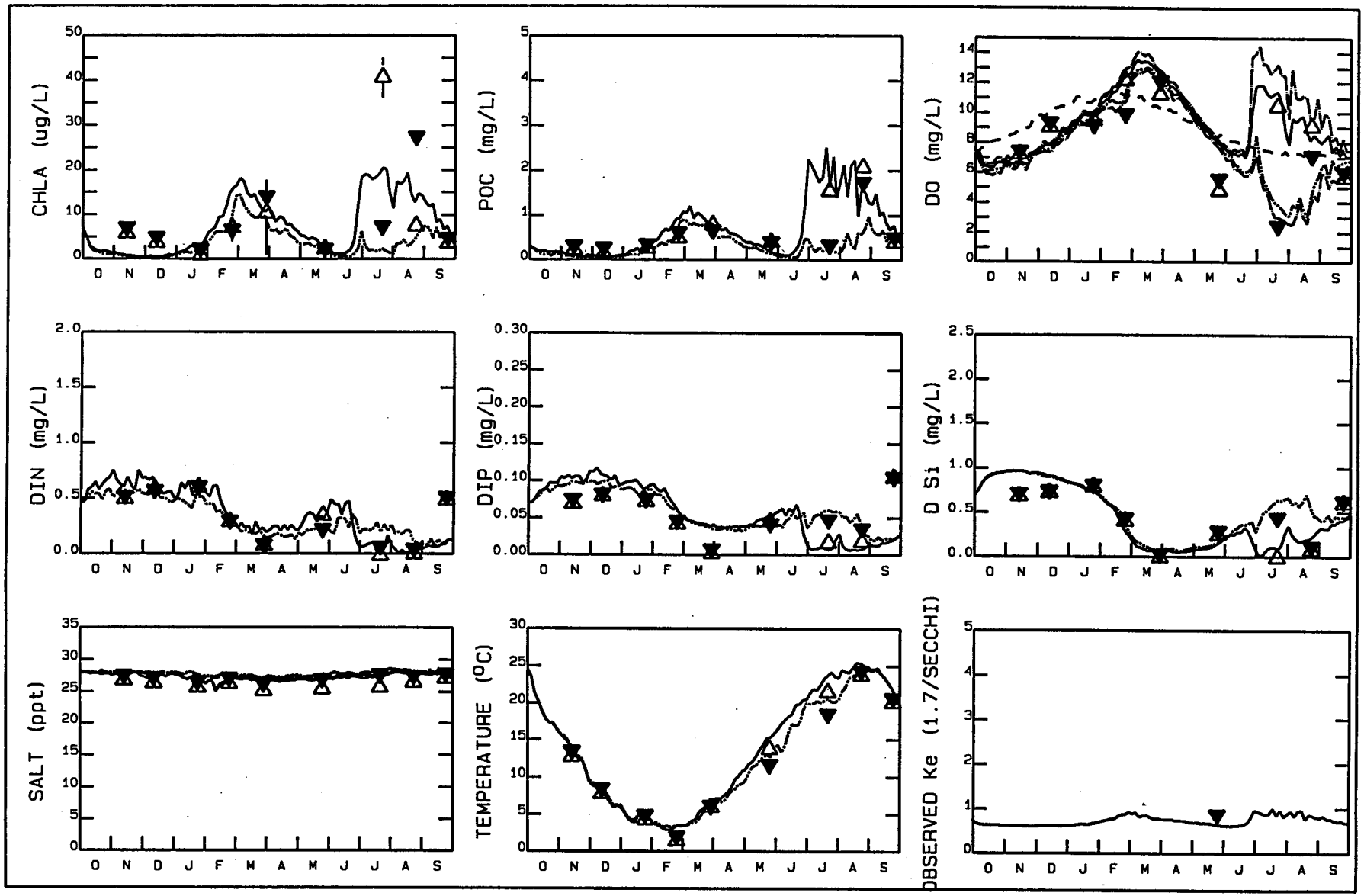

Figure 3-7a. 1994-95 SWEM Calibration, Temporal Comparisons for Western Long Island Sound, MP 23

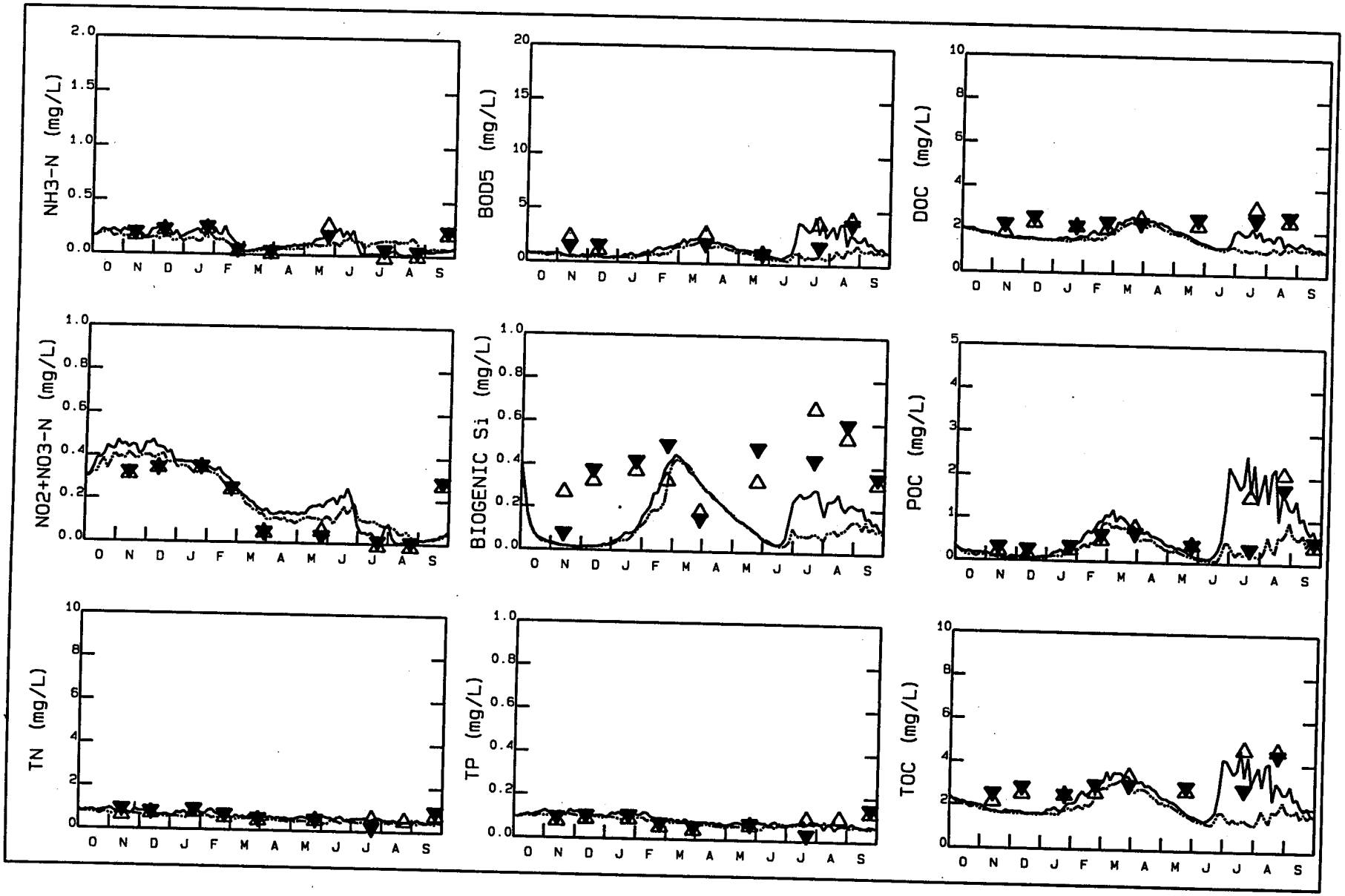

Figure 3-7a. 1994-95 SWEM Calibration, Temporal Comparisons for Western Long Island Sound, MP 23 (Continued)

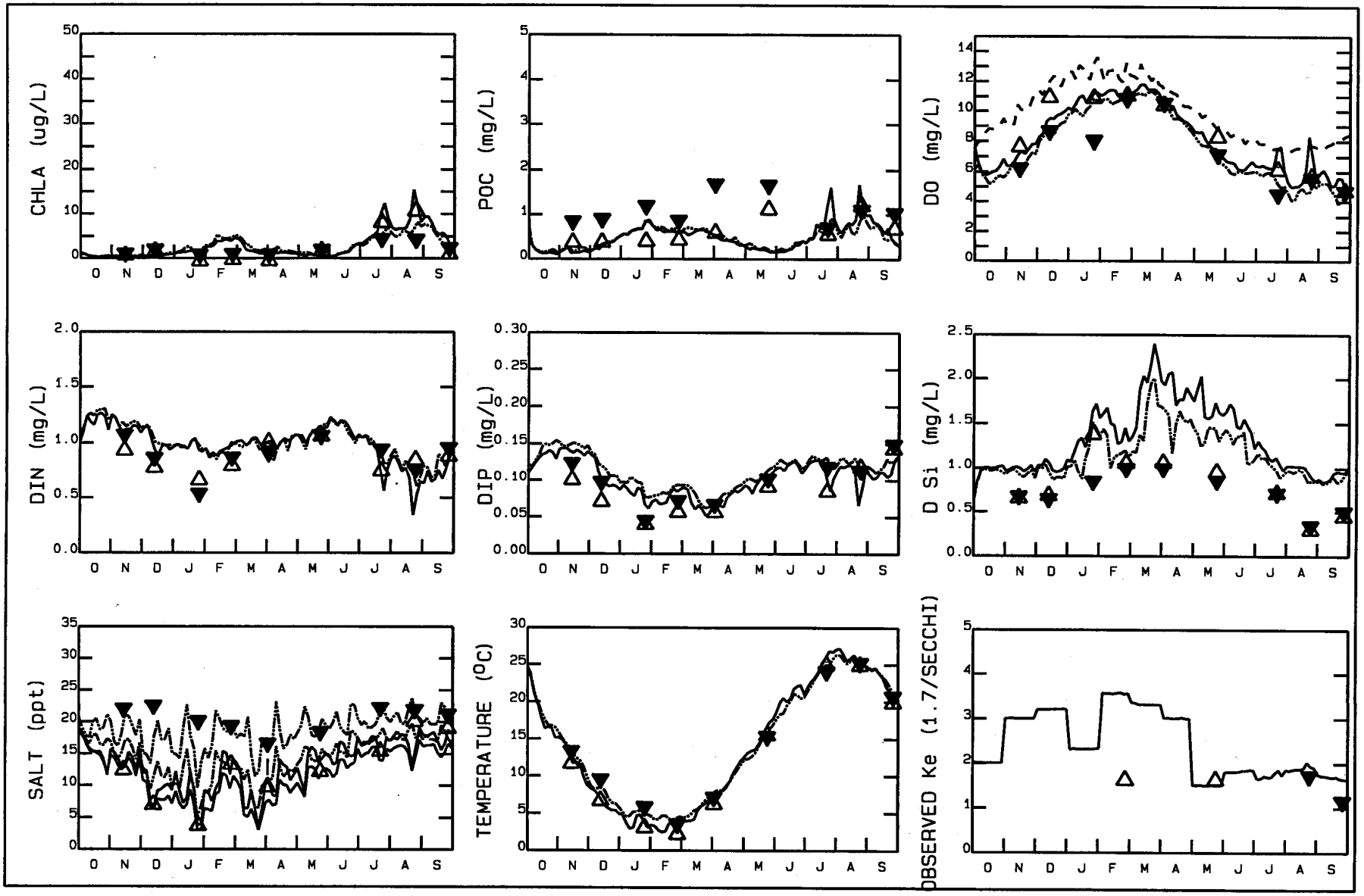

Figure 3-7b. 1994-95 SWEM Calibration, Temporal Comparisons for Hudson River, 125th Street

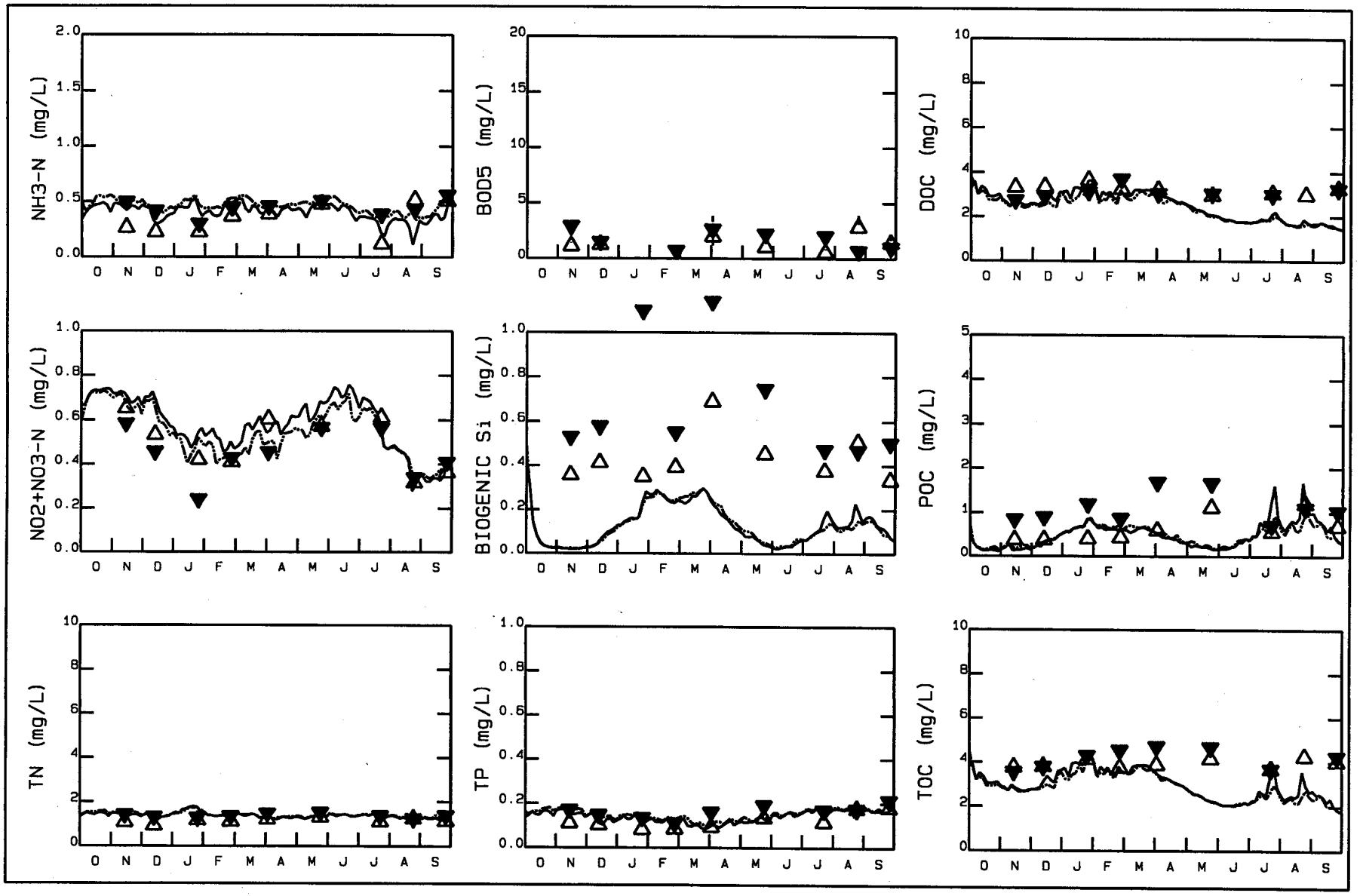

Figure 3-7b. 1994-95 SWEM Calibration, Temporal Comparisons for Hudson River, 125th Street (Continued)

for bottom waters in July as well as the observed 8 mg/L stratification in dissolved oxygen between surface and bottom waters. Also, in the Sound, nutrient limitations are observed. During March, both Si and DIP observations approach limiting levels. In July and August, a depletion of DIN is observed. The model computations of inorganic nutrients shown on Figure 3-7a reproduce the observed values and capture the limitations. Conversely, Figure 3-7b demonstrates that both model and data do not show nitrogen limitations in the Hudson River.

The comparisons for total nitrogen, total phosphorus, and total organic carbon are all good as demonstrated by Figure 3-7 for both the Western Long Island Sound and Hudson River. The model results for particulate biogenic silica are under-estimated, and is likely due to a missing load of biogenic silica. Figure 3-7a demonstrates the ability of the model to reproduce pre-bloom conditions, the development of the spring bloom, its subsequent limitation by silica and zooplankton predation; the onset of hypoxia beginning in July and the limitation of the summer bloom by inorganic nitrogen depletion.

Figures 3-8 thru 3-11 present a summary of temporal trends at several diverse positions throughout the system for the key variables DIN, Chl-a, average DO, and maxima and minima DO. Figure 3-8 shows agreement between model and data that nitrogen is plentiful in Harbor locations such as the East River, Hudson River, and Arthur Kill. Conversely, Figure 3-8 shows model and data agreement that nitrogen can approach limiting levels at certain times of the year in Western Long Island Sound, Raritan Bay, and the New York Bight Apex. Figure 3-9 shows calculated and observed profiles of chlorophyll-a. Model and data both show that during the summer, algal biomass is higher in western Long Island Sound and Raritan Bay than at other locations. Figures 3-10 and 3-11 demonstrate that the model is not only able to pick up the annual variability in dissolved oxygen at various locations throughout the system, but the observed vertical stratification as well.

3.3.1.2 Spatial Comparisons

The purpose of this section is to examine the model calibration along 16 longitudinal axes covering a substantial portion of the system. As with the temporal plots presented earlier, both surface and bottom model results and data are presented. Model calculations are shown by a solid line for surface results and a dashed line for the bottom, with dotted lines for the maxima and minima of the model computations of dissolved oxygen and phytoplankton biomass during a 10-day period. Dotted lines are included on the POC panel to show the algal fraction of the POC. Data are

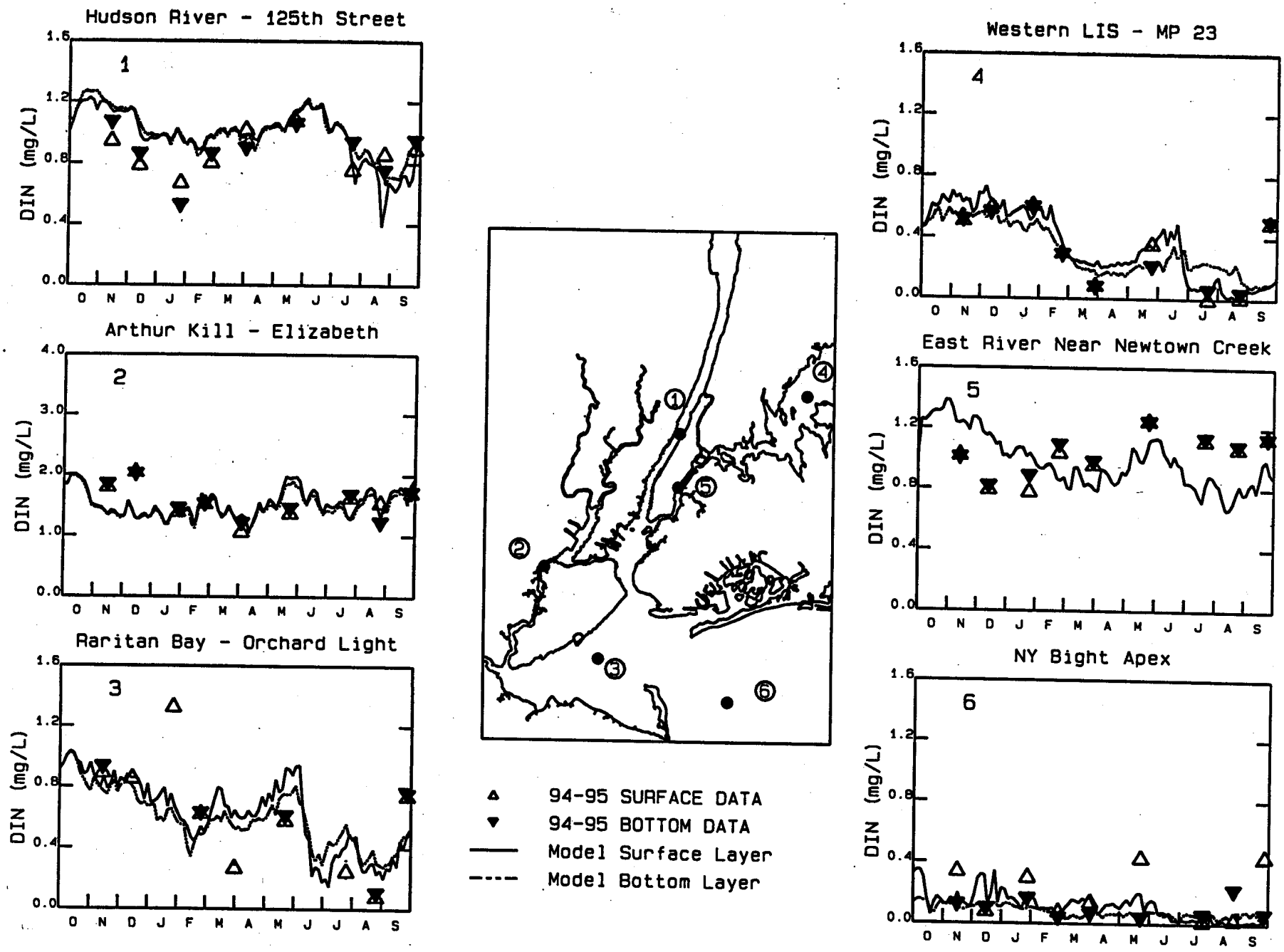

Figure 3-8. 1994-95 SWEM Calibration
Dissolved Inorganic Nitrogen Comparisons

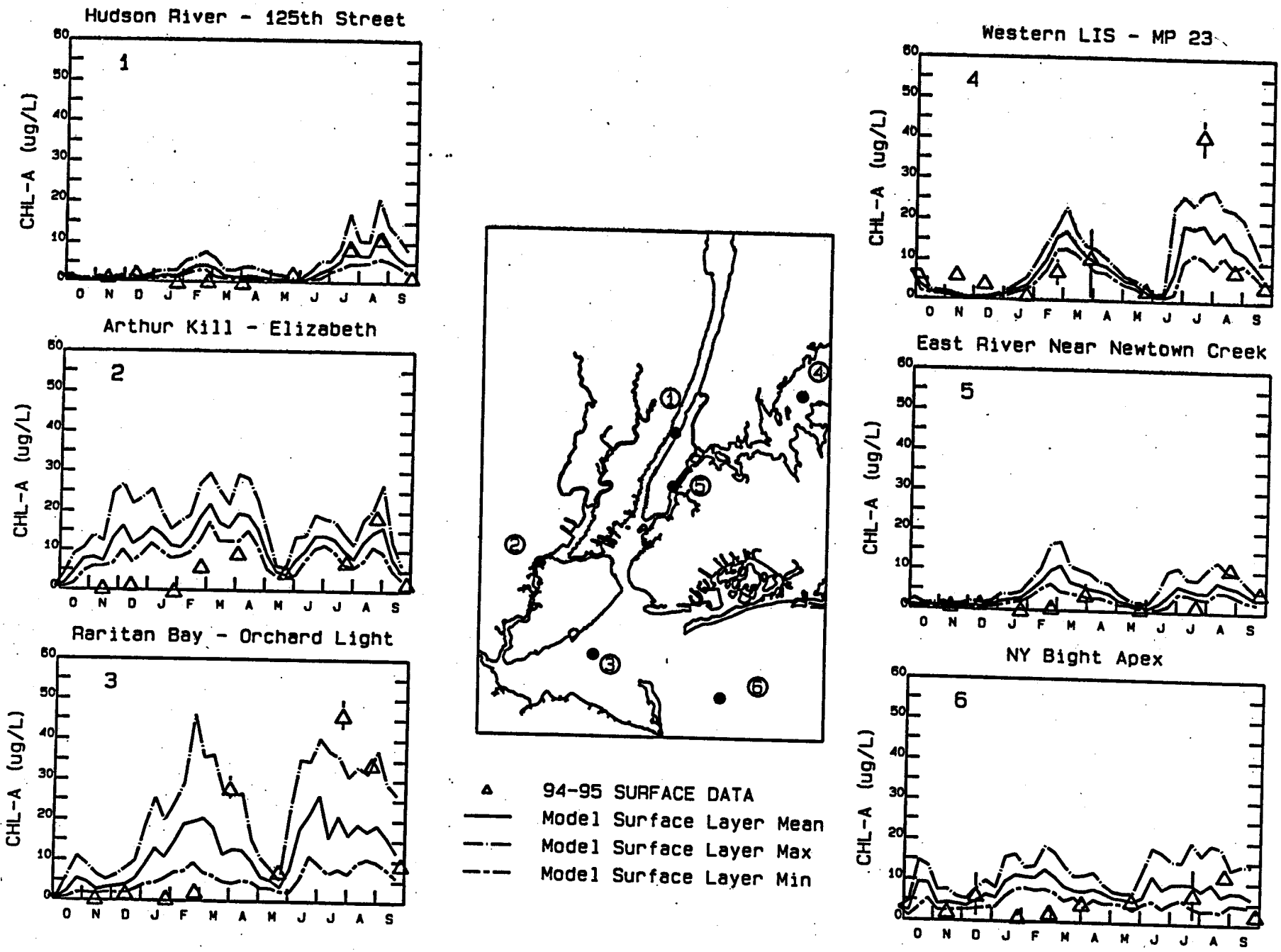

Figure 3-9. 1994-95 SWEM Calibration
Chlorophyll 'a' Comparisons

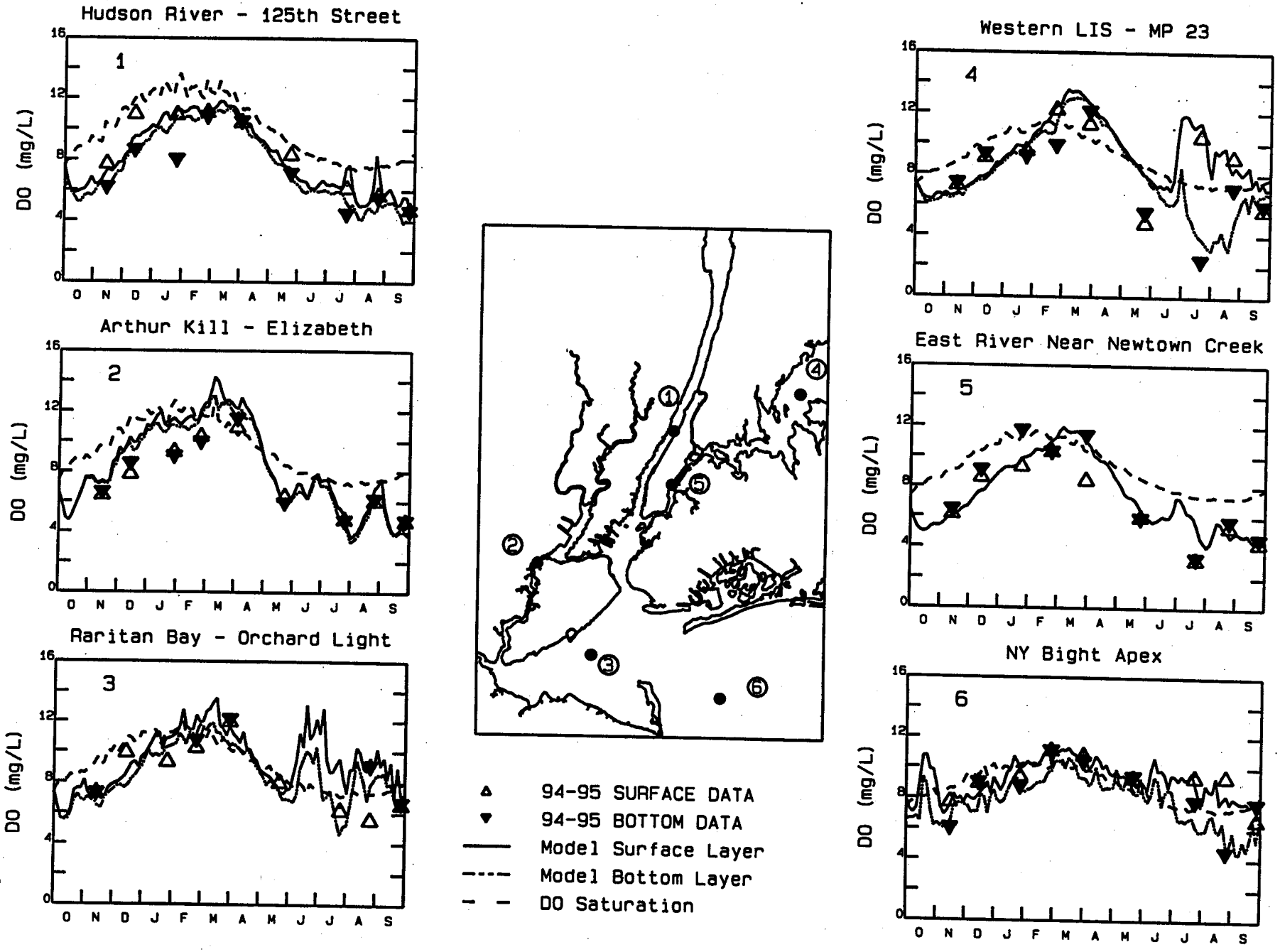

Figure 3-10. 1994-95 SWEM Calibration Mean Dissolved Oxygen Comparisons

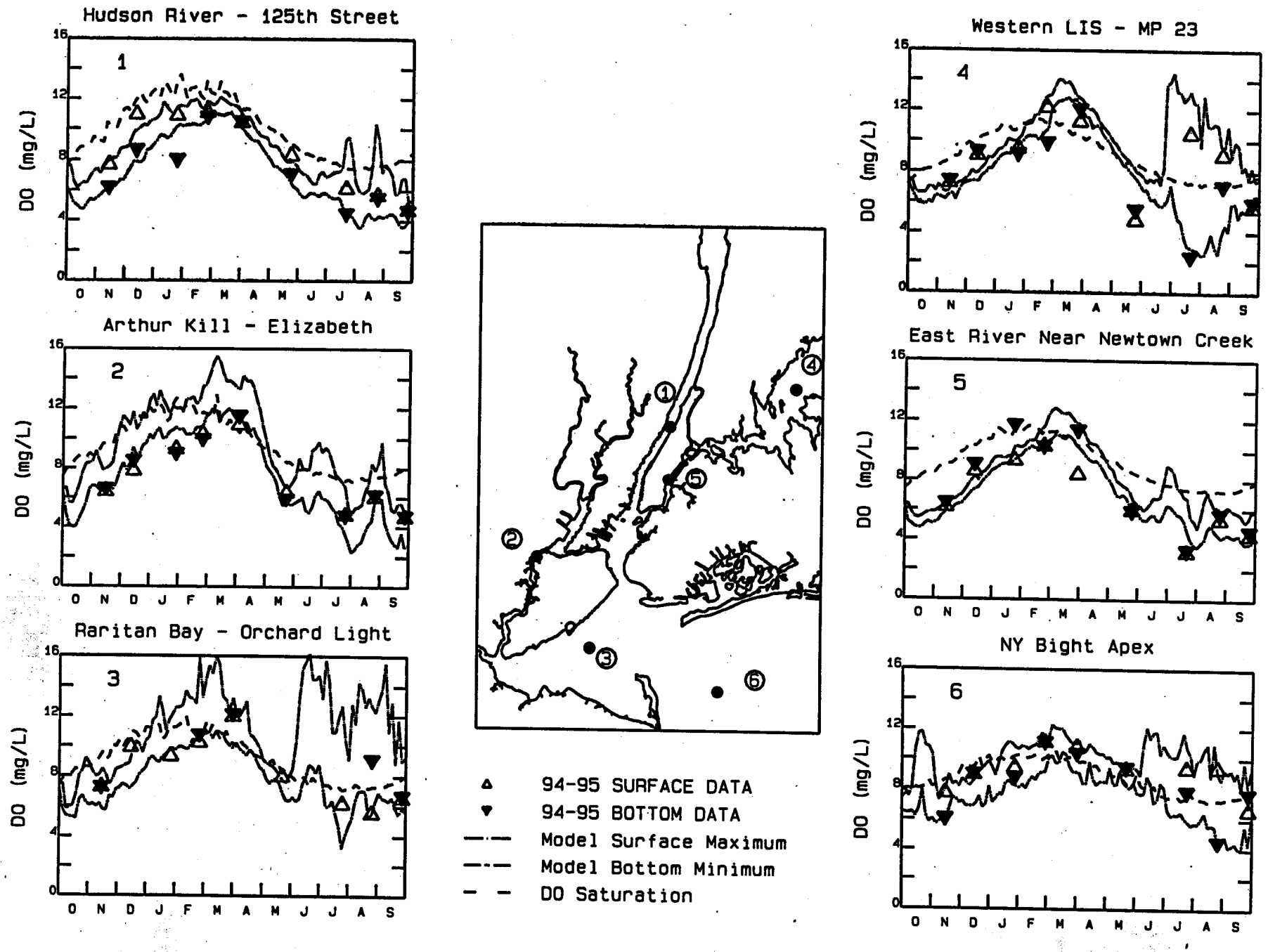

Figure 3-11. 1994-95 SWEM Calibration Minimum-Maximum Dissolved Oxygen

shown by upward pointing filled triangles and downward pointing solid triangles for the surface and bottom, respectively as noted on each figure. Two pages each containing 9 profiles are presented for each of 9 cruises for each of 16 transects. In order to reduce the number of plots presented here, all spatial profiles are included in Appendix B.

The major source of data for model-data comparisons is the 1994-95 SWEM monitoring program performed by Battelle Ocean Services. Other data sources include NYCDEP Harbor Survey, Connecticut DEP routine monitoring, Con Ed monitoring and special studies performed by HydroQual. For comparison purposes, model results of a 10-day average closest to the time period of the Battelle survey is used.

Figure 3-12a which presents model calibration results for August 1995 in the East River and Long Island Sound is an example spatial profile. As can be seen from the plots of salinity and temperature the model reproduces favorably the observed salinity and temperature. The model is able to capture the sharp salinity gradient observed between milepoints 0 and 20, and the relatively flat spatial profile observed between milepoints 20 and 80.

As also shown on Figure 3-12a, the model reproduces the spatial profile of chl-a, with peak concentrations in the Western Narrows, between milepoints 15 to 30. The model maxima, however, underestimate the absolute peak chl-a near milepoint 20, by 10 to 15 ug/L. The model-data comparison of dissolved oxygen is favorable for most of the Sound. The model captures the peak of super-saturated concentration around milepoint 20 and the low dissolved oxygen levels between milepoint 30 and 60.

Figure 3-12a page 2 presents the model calibration for DOC, POC, BOD, Biogenic Silica, Dissolved Silica, TON, NH_4, NO_2+NO_3 and TN. In general, the calibration results are satisfactory. The model reproduces peak concentrations of POC and BOD in Western Long Island Sound and also reproduces the nitrogen profiles in the East River and Long Island Sound. While the model and data comparison is favorable for dissolved inorganic silica, overall the biogenic silica results do not compare well with the observed data. It would appear that a source of biogenic silica has been underestimated or missed.

Figure 3-12b shows the model-data comparison for August 1995 in the Hudson River. Overall the model-data comparisons are very favorable. In particular, the model captures the POC

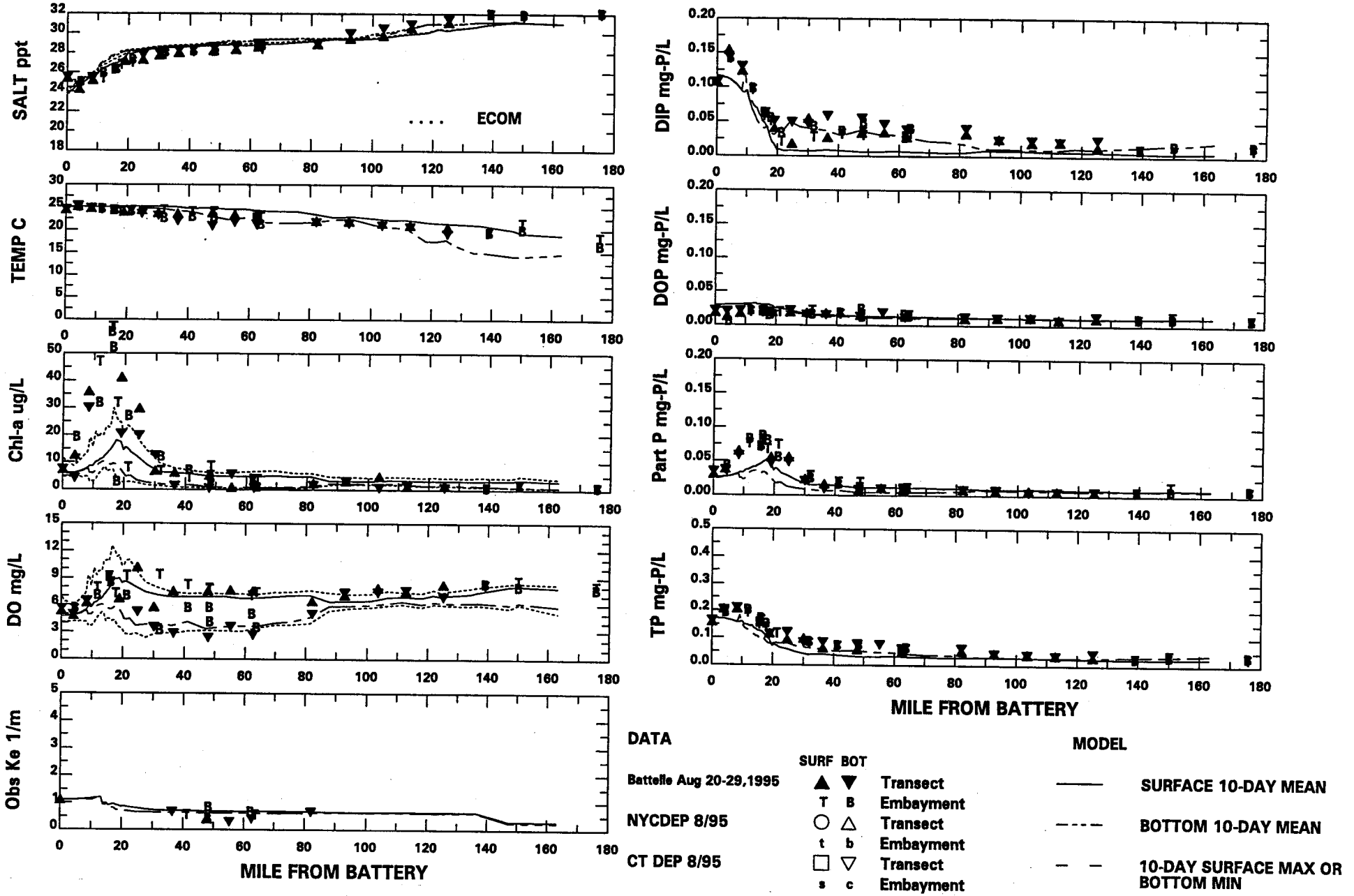

Figure 3-12a. 1994-95 SWEM Calibration, August, East River - Long Island Sound Spatial Comparison

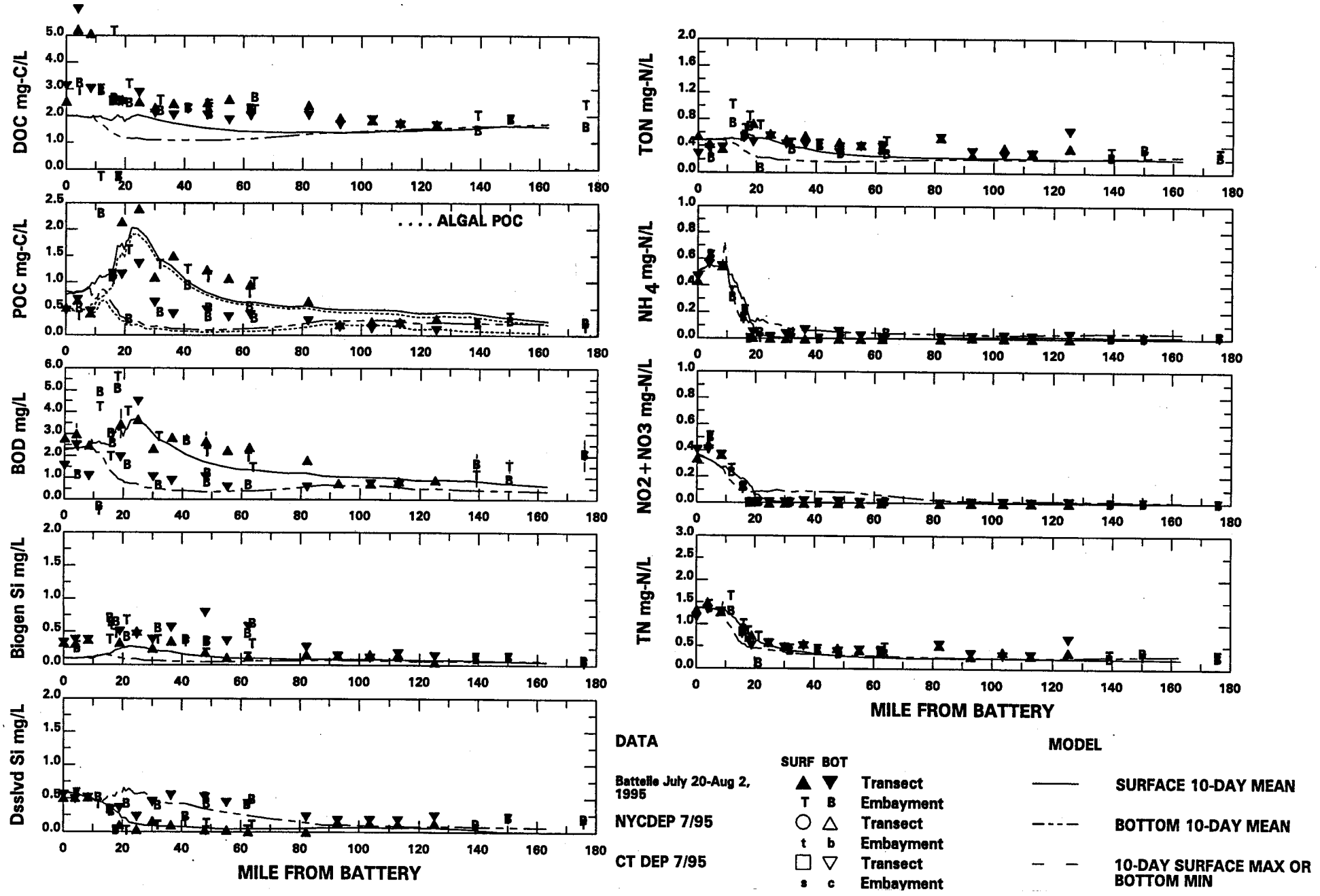

Figure 3-12a. 1994-95 SWEM Calibration, August, East River - Long Island Sound Spatial Comparison (Continued)

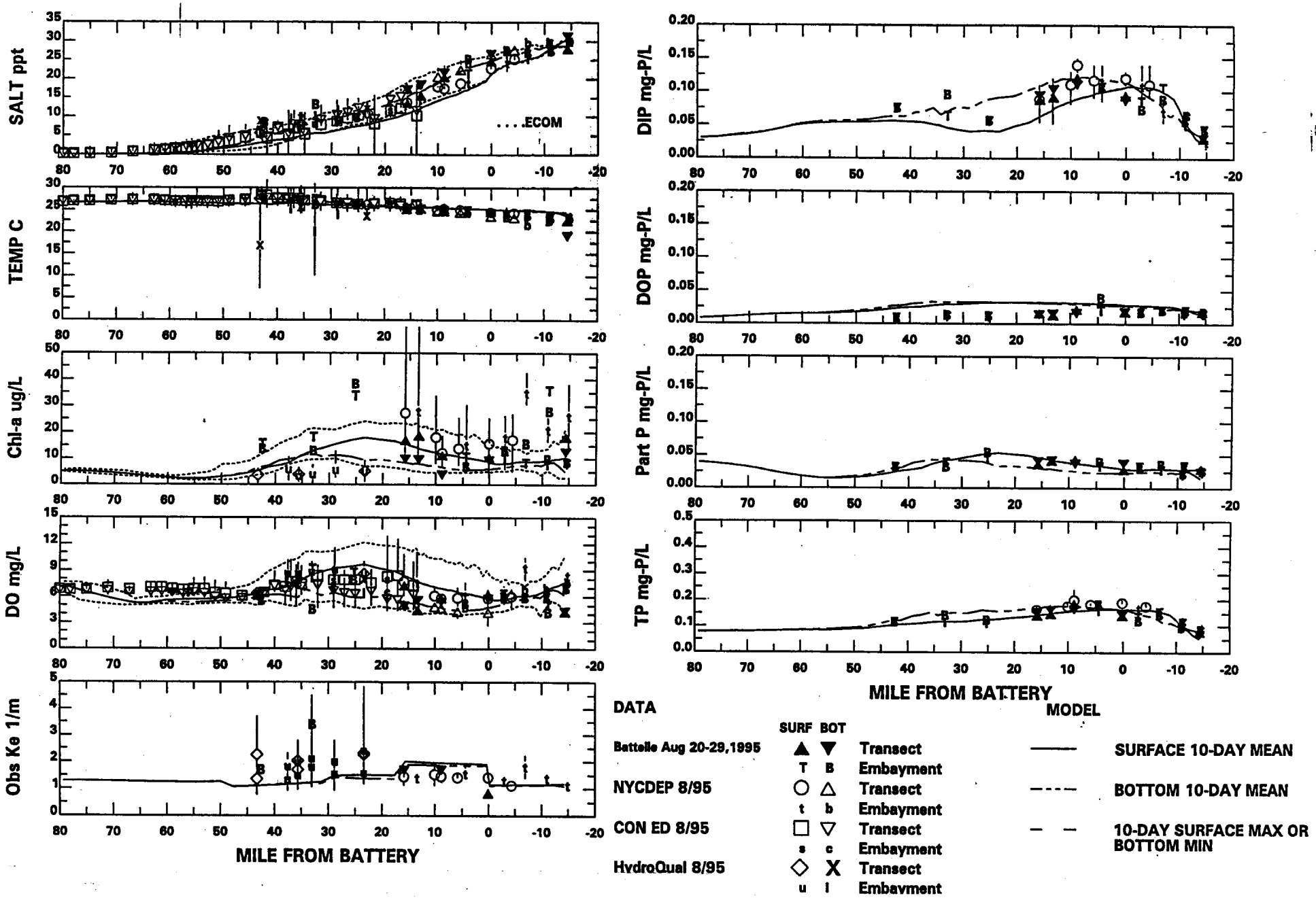

Figure 3-12b. 1994-95 SWEM Calibration, August, Hudson River, Upper and Lower Bay, Ocean Spatial Comparison

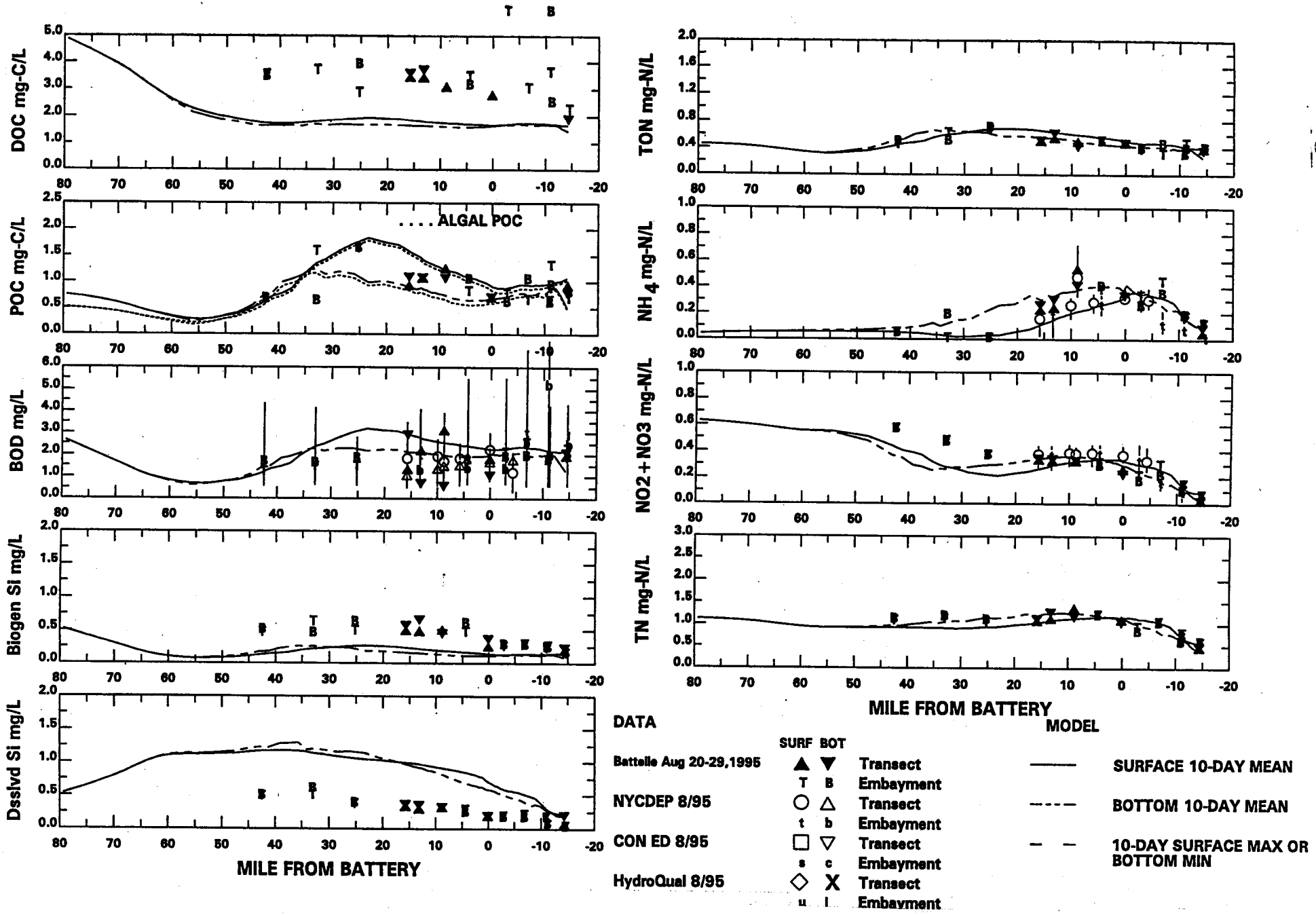

Figure 3-12b. 1994-95 SWEM Calibration, August, Hudson River, Upper and Lower Bay, Ocean Spatial Comparison (Continued)

peak concentrations near milepoint 25 (Haverstraw Bay) and the general dissolved oxygen profile throughout the Hudson River, Upper Bay, and Lower Bay.

3.3.1.3 Growth Limitation Analysis

This section provides a series of temporal plots meant to provide additional insight into the factors limiting primary productivity in different areas of the system. Temperature, light, and nutrients act simultaneously to limit algal growth. As discussed above in Section 2, it is appropriate to model the simultaneous effects of temperature, light, and nutrients on algal growth with a multiplicative formulation.

Figure 3-13 presents the factors affecting the growth of the winter algal group at six positions throughout the system. Notice at each of the six locations, temperature is the factor which suppresses the growth of the winter diatoms during the fall and summer months. System-wide algal growth during winter months is generally controlled by light as opposed to nutrients as shown on Figure 3-13. A specific exception to this generalization is shown on Figure 3-13 in panel 6. At the New York Bight Apex during late February, nutrient availability is the dominant factor controlling algal growth. The overall growth limiting factor at this point is 0.12, that is potential growth is equal to 1.7 per day and net growth after limitation is 0.2 per day. The overall growth limiting factor of 0.12 has two multiplicative components, a nutrient limitation factor of 0.17 and a light limitation factor of 0.69. Since 0.17 is much smaller than 0.69, nutrient limitation is the controlling factor.

Figure 3-14 presents the factors affecting the growth of the summer algal group at six positions throughout the system. Notice at each of the six locations, temperature is the factor which suppresses the growth of the summer algal group during the winter months. System-wide algal growth during summer months is generally controlled by light as opposed to nutrients in many areas of the system as shown on Figure 3-14. A specific exception to this generalization is shown on Figure 3-14 in panels 4 and 6. For much of the summer it is nutrients, and not light, which control algal growth in western Long Island Sound and at the NY Bight Apex.

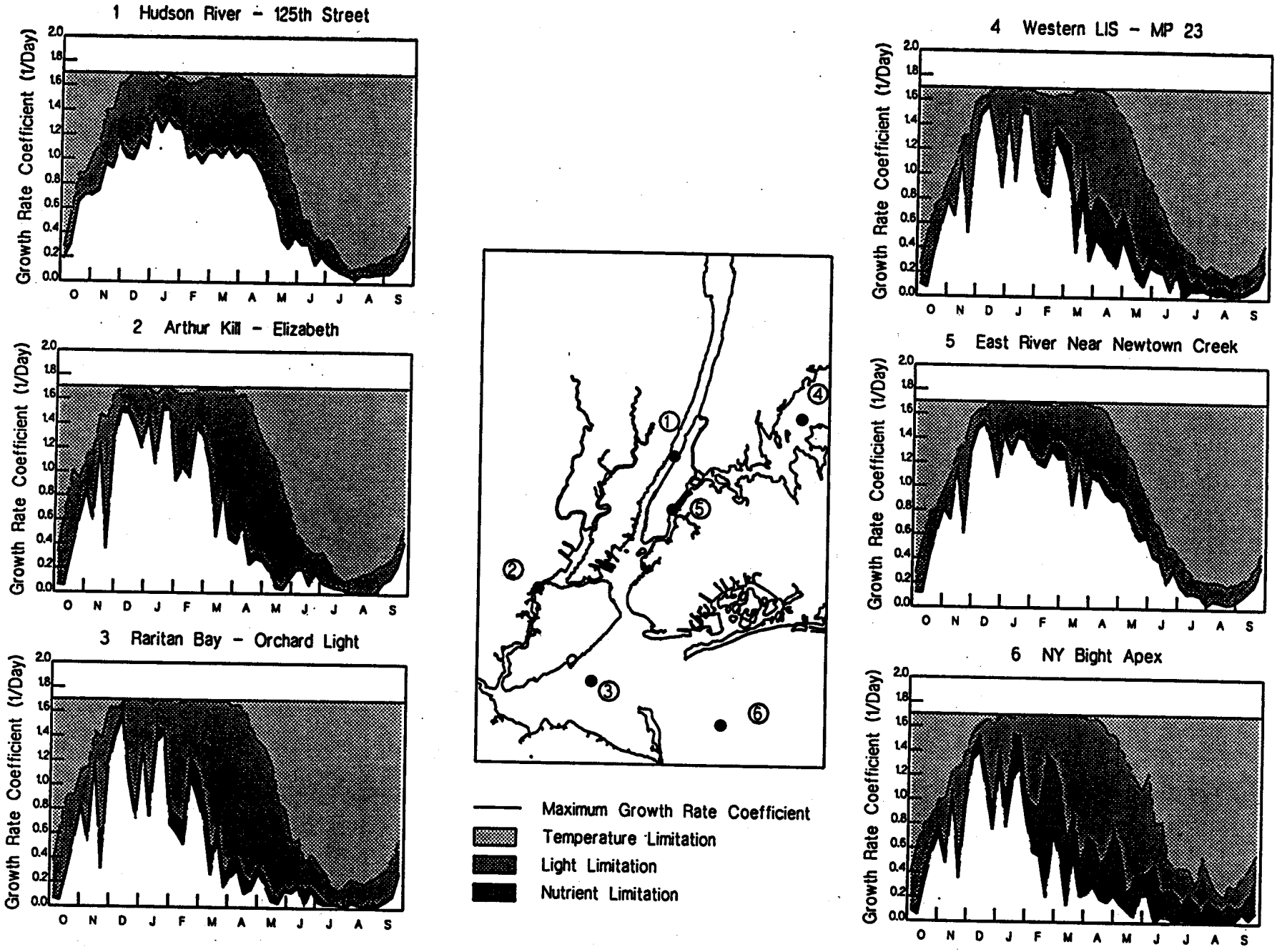

Figure 3-13. Factors Affecting Winter Algal Group Growth Rate Coefficient SWEM 1994-95

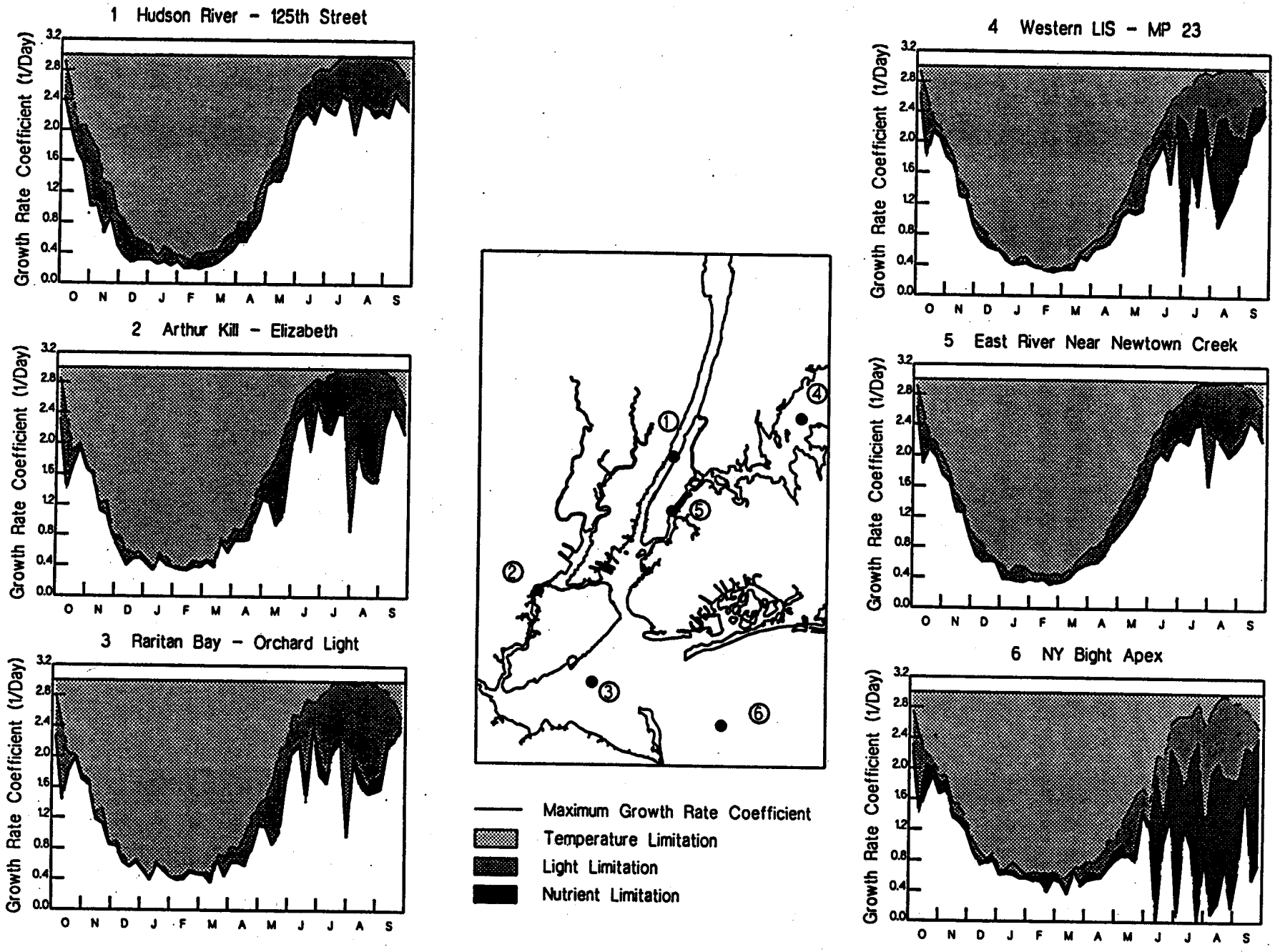

Figure 3-14. Factors Affecting Summer Algal Group Growth Rate Coefficient SWEM 1994-95

3.3.1.4 Primary Productivity and Respiration Comparison

To provide additional insight into the factors accounting for the loss of primary productivity in different areas of the system, a series of temporal plots is presented. Analogous to Figures 3-13 and 3-14 presented above in Section 3.3.1.3 which show the factors controlling algal growth, Figures 3-15 and 3-16 show respiration and other components of algal loss. Figures 3-15 and 3-16 show that over the annual cycle, respiration is the major mechanism of algal loss throughout much of the system. At certain times of the year, loss due to zooplankton grazing is also significant in many areas of the system. In certain locations, such as the lower East River, the dominant algal loss mechanism is benthic filtration as evidenced by results presented in panel 5 of Figures 3-15 and 3-16.

3.3.2 Sediment Model Results

Sediment fluxes of oxygen and nutrients were measured as part of the field program in support of SWEM. Figures 3-17 through 3-18 present a series of comparisons between model estimates and measured fluxes for SOD and ammonium (JNH_4). Comparisons between model estimates and measured fluxes of nitrate (JNO_3), inorganic phosphorus (JPO_4), and silica (Jsi) as well as comparisons between model estimates and observed porewater and bulk sediment constituent concentrations are included in more detailed figures presented in Appendix B.

Each of the flux observations shown on Figures 3-17 and 3-18 represents the mean and standard deviation of a replicated core. The model computations, which are reported every 3.5 days, are presented as solid lines. Figures 3-17 and 3-18 show that the model is able to pick up both spatial (between panels) and temporal (across a panel) patterns in SOD and ammonium flux throughout the system.

Figure 3-19 is an example of the detailed comparisons between sediment model results and measurements presented in Appendix B. Figure 3-19 includes 3 pages and 27 panels descriptive of sediment dynamics in the Hudson River near Mount St Vincent. Page 1 of Figure 3-19 presents nitrogen results. Panel 2 of page 1 of Figure 3-19 shows the model data comparison for pore water ammonium nitrogen. Measured values should represent layer 2 model results. In this case, the model over estimates the observed pore water ammonium during the winter and compares more favorably in the summer. Panel 3 of page 1 of Figure 3-19 shows pore water nitrate nitrogen.

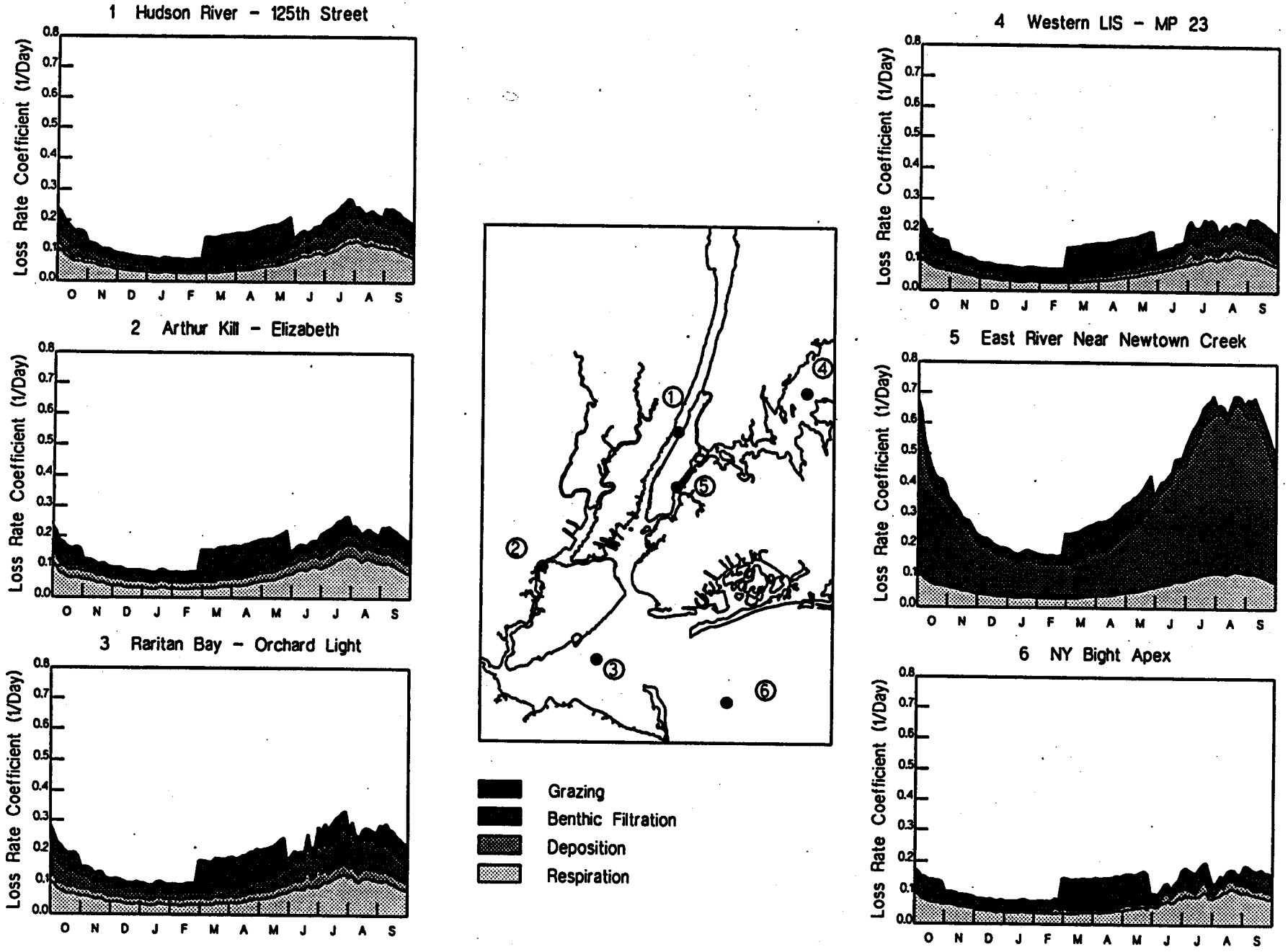

Figure 3-15. Factors Affecting Winter Algal Group Loss Rate Coefficient (Temperature Corrected) SWEM 1994-95

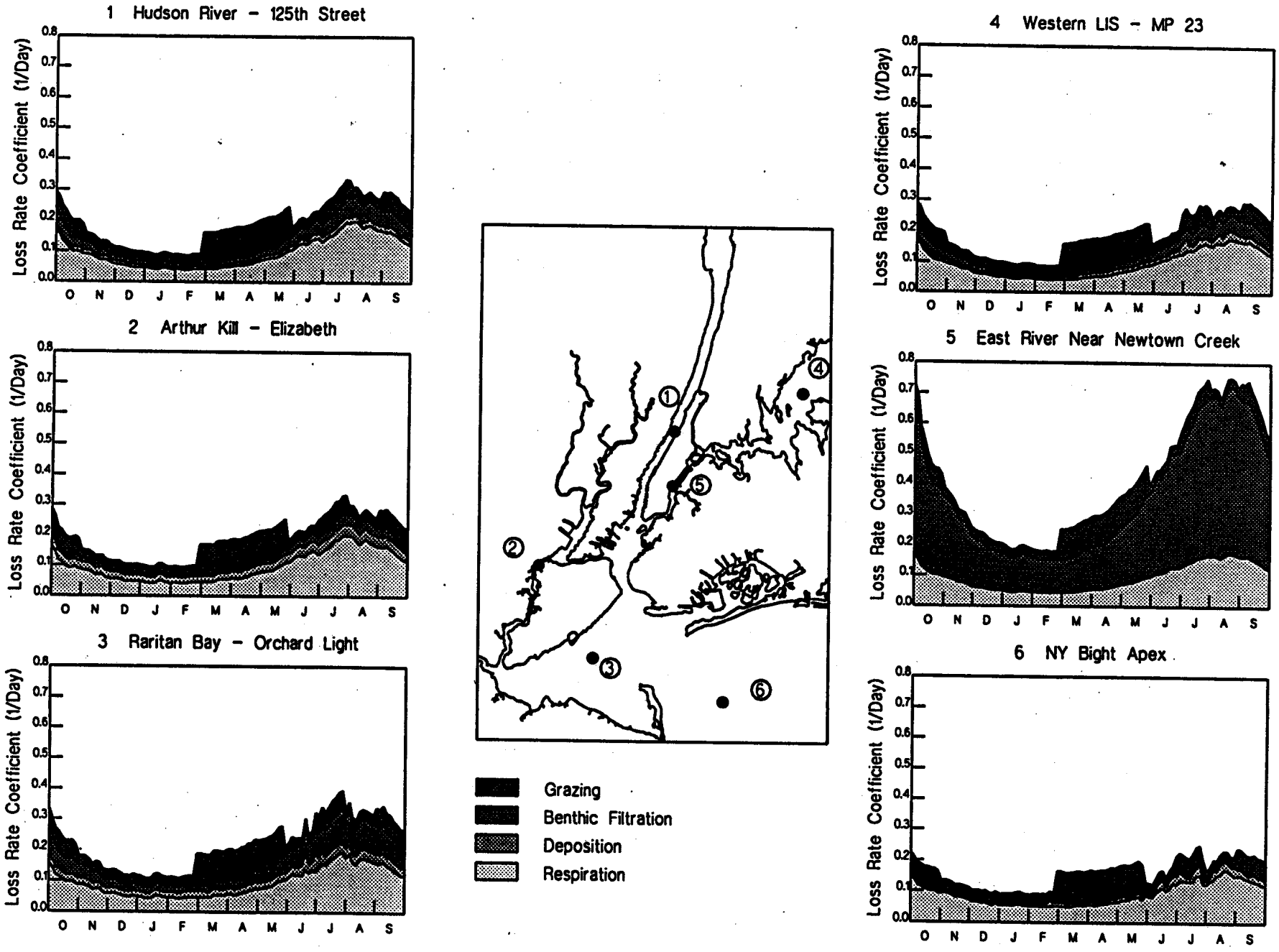

Figure 3-16. Factors Affecting Summer Algal Group Loss Rate Coefficient (Temperature Corrected) SWEM 1994-95

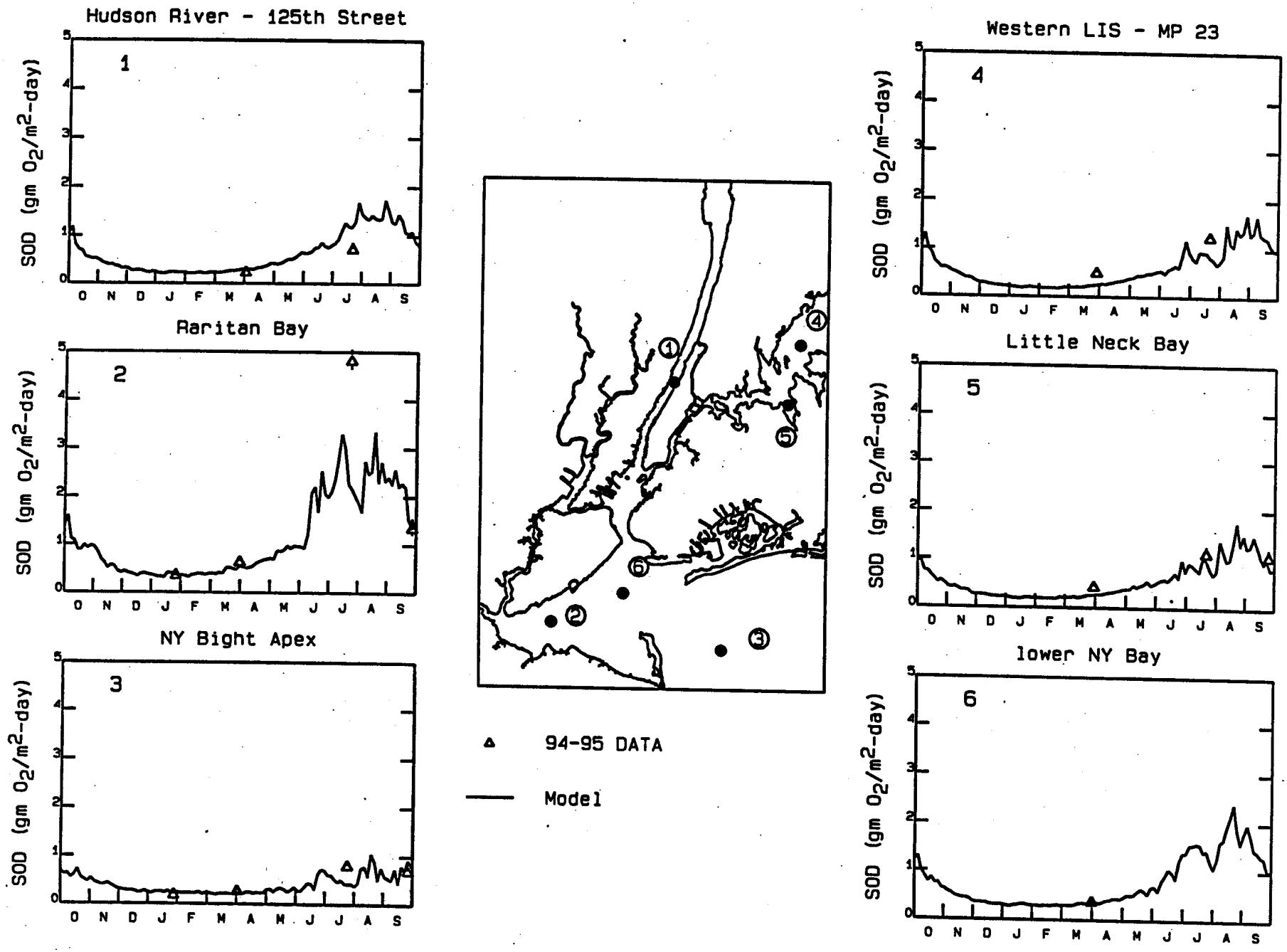

Figure 3-17. 1994-95 SWEM Calibration
Sediment Oxygen Demand

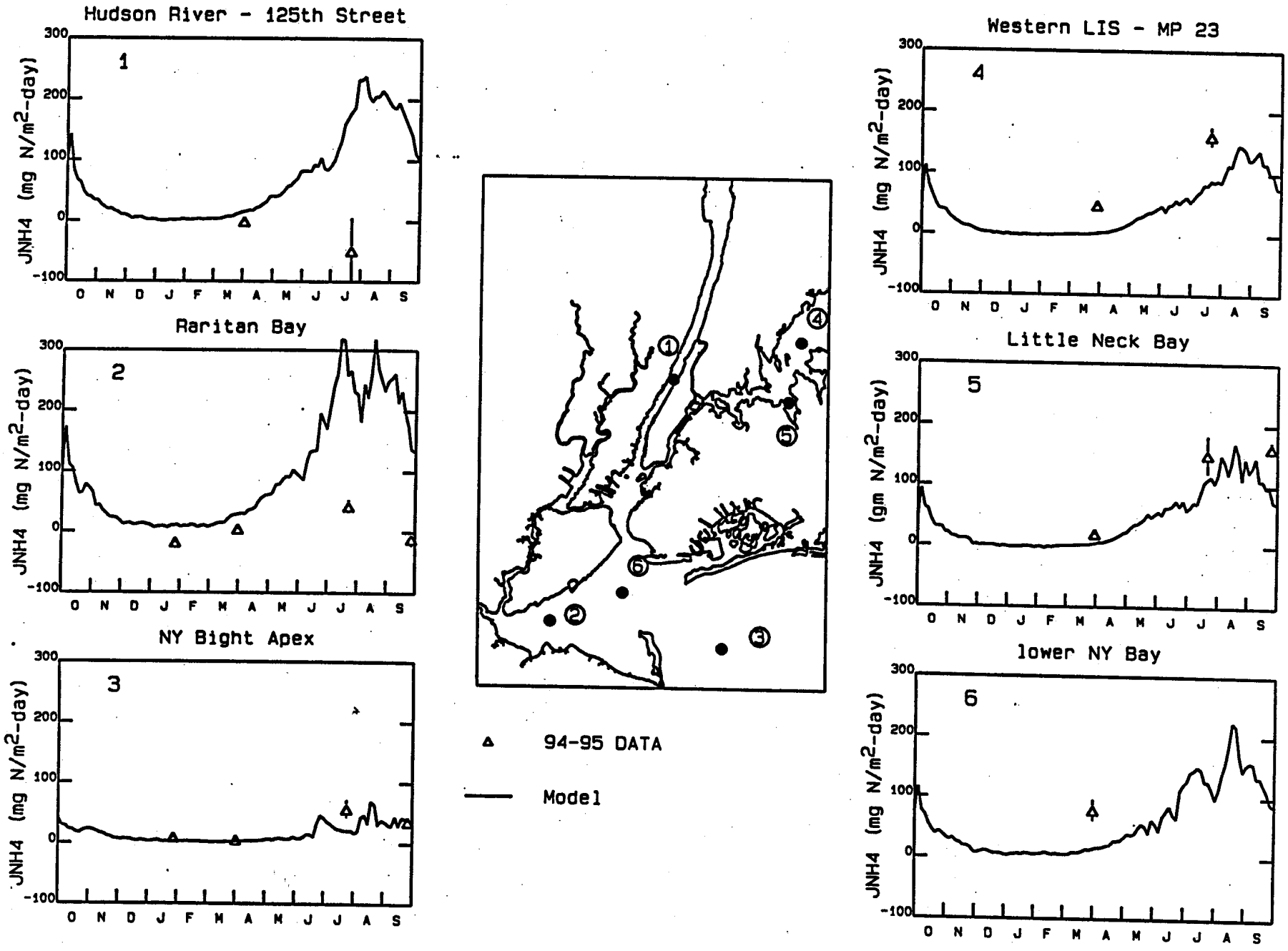

Figure 3-18. 1994-95 SWEM Calibration
Sediment Ammonia Fluxes

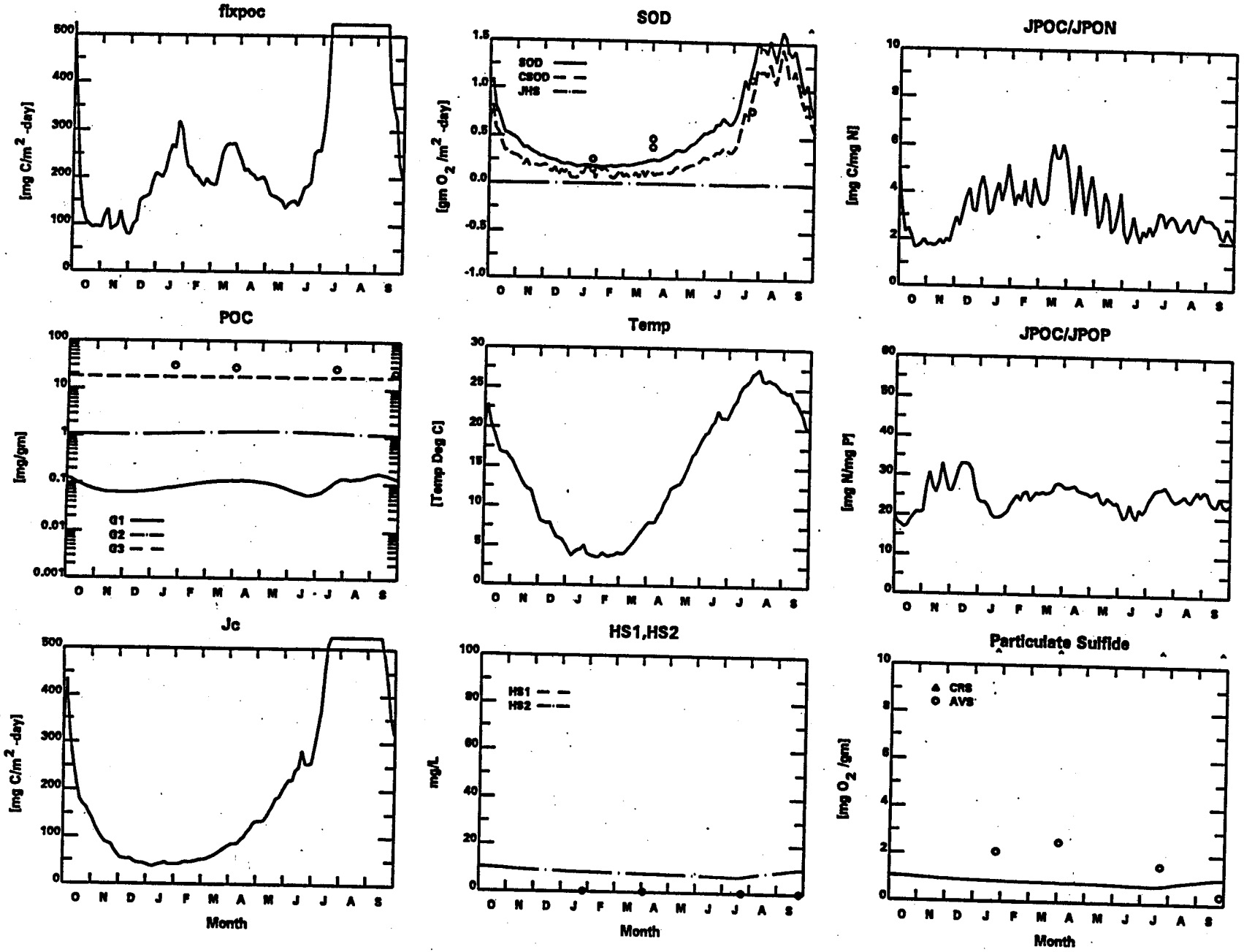

Figure 3-19. 1994-1995 Calibration Results for Segment (19/70)
Station 130 - Hudson River Mt. St. Vincent

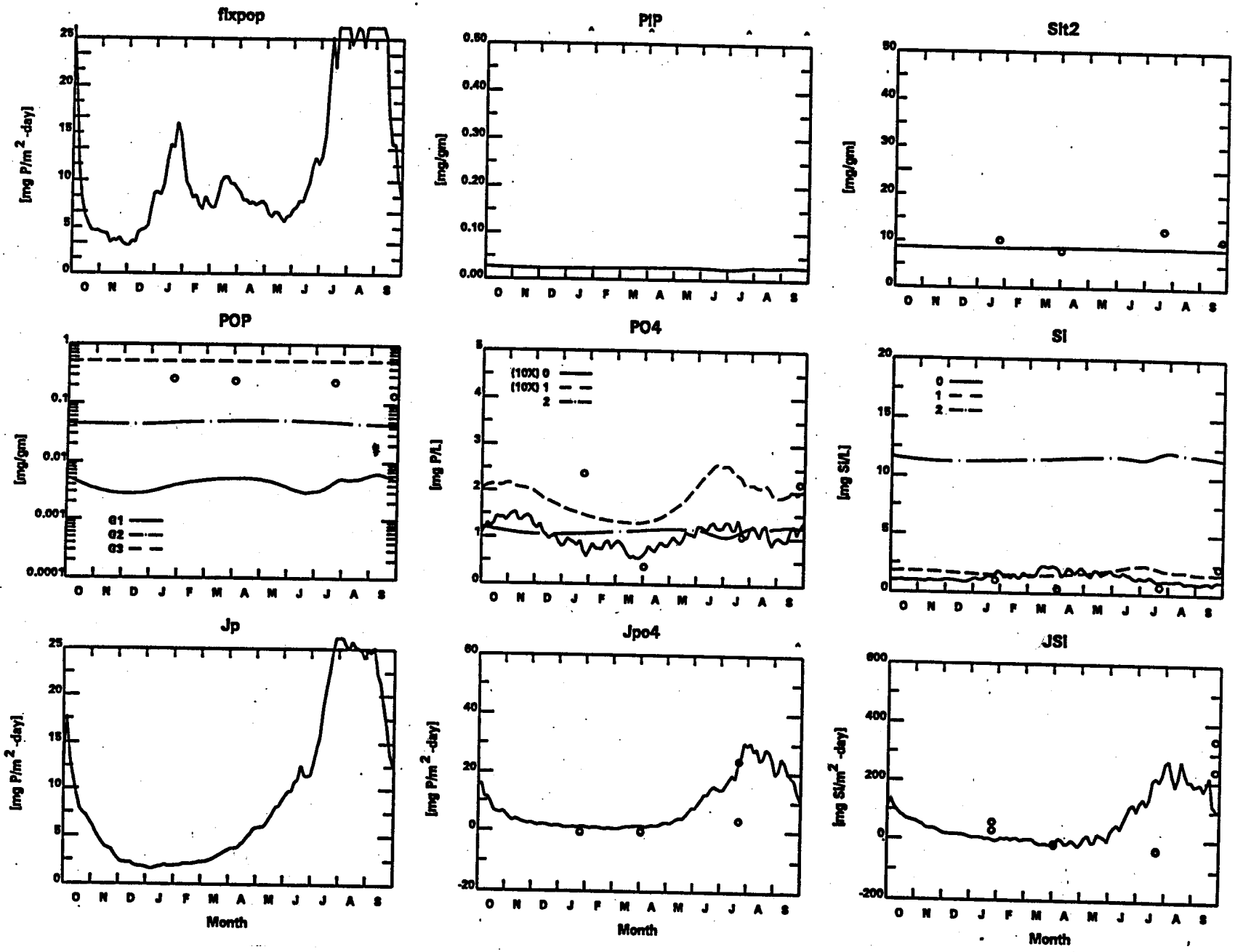

Figure 3-19. 1994-1995 Calibration Results for Segment (19/70)
Station 130 - Hudson River Mt. St. Vincent
(Continued)

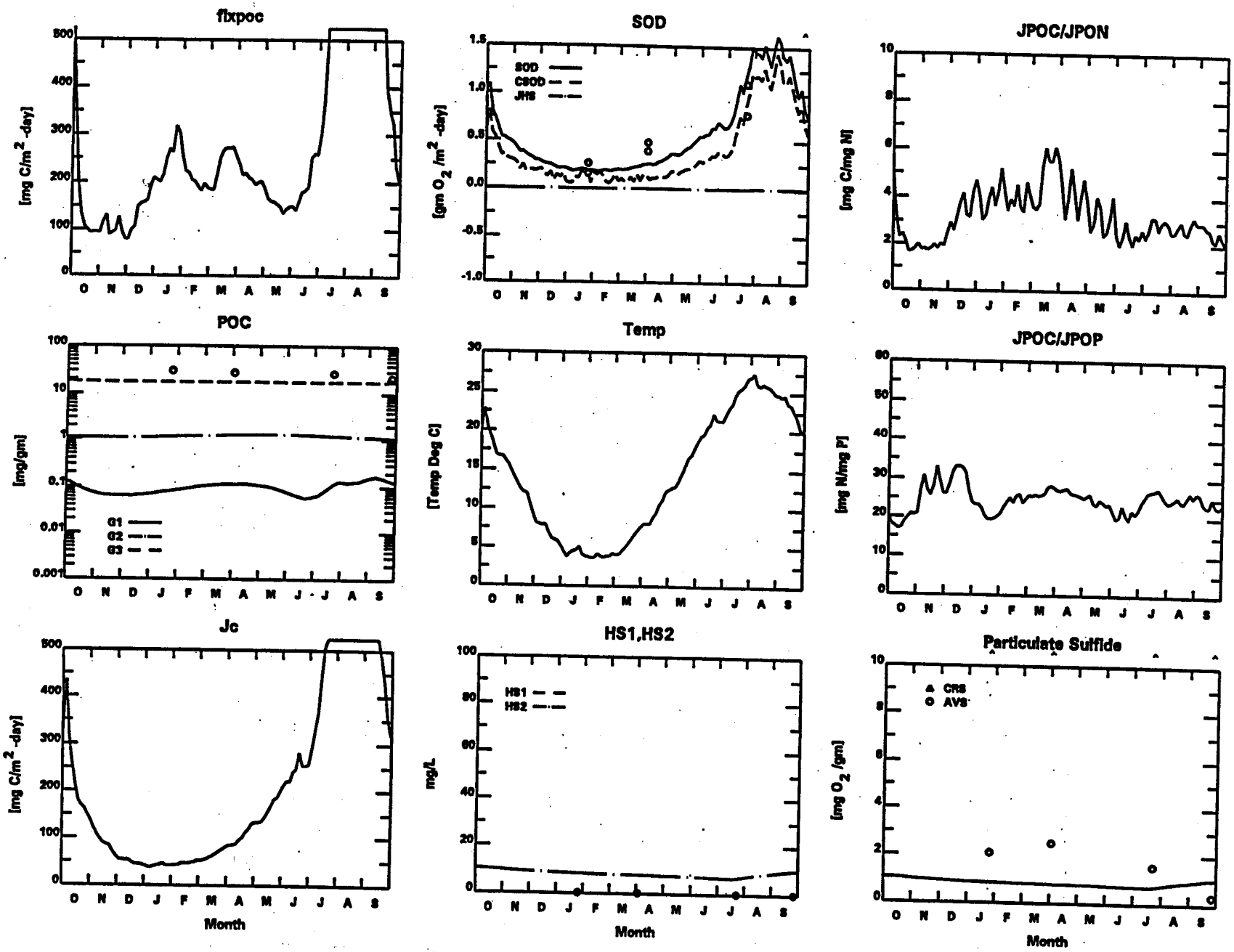

Figure 3-19. 1994-1995 Calibration Results for Segment (19/70)
Station 130 - Hudson River Mt. St. Vincent
(Continued)

Agreement between the model calculation for sediment layer 2 and observations is acceptable. Panel 4 of page 1 of Figure 3-19 shows excellent agreement between calculated G3 (least reactive) PON and measured PON. Calculated G1 and G2 PON are also shown for illustrative purposes. Panel 5 of page1 of Figure 3-19 shows that the model reproduces the measured ammonium flux almost exactly. Panel 6 of page 1 of Figure 3-19 shows that the modeled nitrate nitrogen flux agrees better with measurements under winter conditions than summer conditions. Panel 8 of page 1 of Figure 3-19 illustrates the ability of the model to reproduce measured SOD. For reference, the calculated fraction of SOD attributed to sediment ammonium, nitrification, is shown with a dashed line. The calculated dissolved oxygen concentrations in the overlying water column are provided in panel 9 since they can help to explain some of the spatial variation observed in the sediment flux rates.

Page 2 of Figure 3-19 presents phosphorus and silica results. Panels 3, 6, and 9 of page 2 illustrate that in the Hudson River near Mount St Vincent, SWEM is well calibrated to solid phase sediment silica (panel 3) and silica flux (panel 9), but SWEM overestimates pore water silica in the anaerobic layer (panel 6). Panels 1, 2, 4, 5, 7, and 8 of page 2 of Figure 3-19 show examples of SWEM and data comparisons for sediment phosphorus. Panels 4, 5, and 8 show reasonable agreement between model and data for G3 POP, pore water PO4-P, and flux of PO4-P between sediment and water column. Panel 2 shows an extreme disagreement between calculated and observed PIP.

Page 3 of Figure 3-19 presents organic carbon and sulfide results. Panel 4 shows good agreement between observed POC and computed G3 POC. Panel 8 shows that in the Hudson River near Mount St Vincent, SWEM slightly overestimates dissolved sulfide in the anaerobic layer. Figure 9 shows the model data comparisons for particulate sulfide. Particulate sulfide computed by SWEM should fall between observations of AVS and CRS. It appears that at this position SWEM somewhat underestimates the observed particulate sulfide.

SECTION 4

MODEL VALIDATION

4.1 INTRODUCTION

The overall objective of water quality model validation is to demonstrate the robustness of the calibration. In model validation, a hydrodynamic and loading condition different from that of the calibration is selected. As discussed in the preceding sections of this report, the SWEM calibration period is October 1994 through September 1995. Summer 1995 was relatively dry. The period October 1988 through September 1989 was selected for SWEM validation because summer 1989 was a wet summer, the 1988-89 period is coincident with the Long Island Sound Study , and 1988-89 is a period for which there are substantial water quality data.

The model validation procedure consists of the application of the set of model coefficients and parameters that were developed during model calibration to the hydrodynamic and loading condition selected for model validation. The model validation results are compared to observed data and field studies from the validation period. This section provides the details of the validation effort and presents model versus data comparisons for the validation run.

4.2 MODEL INPUTS

A number of exogenous variables incorporated in the SWEM modeling framework, such as freshwater flow and solar radiation, are specific to the period of interest, either calibration or validation. Exogenous variables in SWEM were specified for model validation by step functions developed from data collected during the validation period. Differences in inputs between SWEM calibration and validation are discussed below.

As discussed in Section 3.0, the water circulation patterns are imported from the hydrodynamic submodel which is discussed in separate reports under Sub-tasks 10.3 and 10.6. Loadings to the 1988-89 validation are primarily based on historical DMR data and the 1994 Interstate Sanitation Commission monitoring. Load developments is discussed in detail in the Sub-task 10.2 report

4.2.1 Model Grid

The three-dimensional hydrodynamic submodel for SWEM, which operates independently of the water quality model, and was developed under Sub-task 10.3 was run for the 1988-89 validation period. The model domain is comprised of the same 41,160 wet and dry grid cells used for model calibration. Quantities computed by the hydrodynamic submodel include surface elevation, three-dimensional velocities and diffusivities, temperature and salinity. Details of the hydrodynamic validation results are presented in the report for Sub-task 10.3. The model grid information, tidal stage, velocities and diffusivities, were outputted as one-hour averages and were stored for subsequent use by the water quality submodel. The model grid is presented in Figure 3-1.

4.2.2 Boundary Conditions

Flow entering or leaving Long Island Sound or the New York Bight along the boundaries of SWEM carries with it phytoplankton, nutrients, organic carbon and dissolved oxygen. These mass fluxes may be a substantial source or sink of material to the system. This is an important consideration in terms of the total controllable load. Therefore, considerable attention was focused on the specification of the boundary concentrations. Attempts were made to correlate the concentrations of the various water quality state- variables to time of the year. Data collected during the monitoring program in support of SWEM in 1994 and 1995 were used as data near the boundaries of SWEM were not available for the 1988-89 period. Figures 3-2 and 3-3 show the monitoring program stations which cover the southern and eastern reaches of the SWEM open boundary. Boundary concentrations of the water quality constituents are shown on the validation diagrams (Section 4.3 and Appendix C).

4.2.3 Extinction Coefficients

Water column transparency and, therefore, extinction coefficient plays an important role in primary productivity. Phytoplankton primary productivity is greater in areas of high light penetration than in light-limited areas, given the same nutrient availability. There is considerable variability in water column transparency over the domain of SWEM. Generally, the inner Harbor has higher extinction coefficients than outer areas, due to suspended solids loadings from municipal treatment plants and CSO inputs. Monthly-averaged estimates of extinction coefficients were made

phytoplankton chl-a, using Equation 2-22. Computed and observed extinction coefficients are shown on the validation diagrams (Section 4.3 and Appendix C).

4.2.4 Reaeration Coefficients

Reaeration coefficients are determined internally in the water quality model, by providing estimates of K_L, the surface transfer coefficient for oxygen, and then using Equations 2-15a and 2-15b. Figure 3-4 presents the time-invariant but spatially-variable estimates of K_L used for both the 1994-95 calibration and the 1988-89 validation. The spatial variability reflects the high tidal velocities in the East River, leading to higher values for K_L by comparison to the segments located in the Narrows, and the effects of winds and tides in the eastern portion of the Sound.

4.2.5 Water Temperature

The temperature regime of the Harbor/Bight/Sound system is an important exogenous variable because it acts as a key driving force for the behavior of phytoplankton and for temperature-mediated bacterial decomposition and recycle kinetics. Temperature is also used together with salinity data to calibrate the transport structure. As such, considerable effort was made to define the annual cycle of water column temperature during the validation of the hydrodynamic submodel of SWEM as detailed in the report for Sub-task 10.3.

4.2.6 Solar Radiation

Daily incident solar radiation for the 1988-89 validation of SWEM was picked up from LIS3.0. Incident solar radiation used in LIS3.0 was estimated using daily estimates of percent cloud cover from LaGuardia Airport and a methodology developed which relates time of year, latitude, and percent cloud cover to incident solar radiation. Table 4-1 presents the incident solar radiation as a function of time for the 12 month validation period.

4.2.7 Fraction of Daylight

The growth rate formulation for phytoplankton, as described in Section 2, depends on the length, or fraction, of daylight, since photosynthesis takes place only in the presence of sunlight. Fraction of daylight for use in SWEM validation was picked up from LIS3.0. Daily fractions of

daylight were calculated for LIS3.0 calibration from basic trigonometry assuming that the earth is a perfect sphere. Using a methodology developed by Duffie and Beckman (1974), monthly-averaged fractions of daylight were generated. The Duffie and Beckman methodology depends on latitude and the declination of the sun as a function of time of year. Table 4-1 presents the fraction of daylight used in SWEM as a function of time for the 12 month validation period.

Table 4-1 - Incident Solar Radiation and Fraction of Daylight for Validation Period

Date	Incident Solar Radiation (ly/day)	Fraction of Daylight
October 1988	242	0.471
November 1988	156	0.412
December 1988	145	0.389
January 1989	158	0.400
February 1989	172	0.437
March 1989	360	0.487
April 1989	518	0.541
May 1989	558	0.587
June1989	591	0.609
July 1989	567	0.609
August 1989	483	0.576
September 1989	419	0.525

4.2.8 Particulate Organic Deposition Rates and Sedimentation Rates

An important parameter required by the sediment model is the net deposition rate of POM from the water column to the sediment. Estimates of net deposition were guided by estimates of bottom layer net non-tidal velocities as arrived at from the calibration to salinity and temperature. It is assumed that little or no net deposition would occur in regions of the system where net bottom velocities are high, due to scour and resuspension. Net deposition is also the mechanism by which

the effects of benthic filtration are simulated in SWEM. As in the calibration, rates of net deposition in the validation were adjusted on a spatially varying basis to reflect the water column filtration of POM by benthic bivalves.

The sedimentation velocity is the rate at which material is buried in the sediment due to the deposition of fresh organic and inorganic material. No direct measurements are available for estimating sedimentation velocities for the sediment model. However, for coastal estuaries these rates are usually low, on the order of 0.1 to several cm/year. Lacking better estimates, a spatially uniform sedimentation rate of 0.25 cm/year was used in this study. The model is fairly insensitive to this rate, since at 1 cm/year and for a 10 cm thick surface sediment layer and a 100 cm thick bottom sediment layer, little or no POM is lost via burial. This is because it all decomposes, within the 110 year period required for a particle to traverse the depth of the sediment layer.

Both deposition and sedimentation rates are consistent between SWEM calibration and validation.

4.2.9 Variable Stoichiometry

As explained in Section 3.2.9, the ability of phytoplankton to adjust their internal stoichiometry as a nutrient becomes limiting is accounted for in SWEM kinetics. Accordingly, while the behavior of the carbon to nutrient ratios is identical in SWEM calibration and validation, actual nutrient to carbon ratios in the calibration and validation differ as dissolved inorganic nutrient concentrations differ between calibration and validation.

4.3 MODEL RESULTS

The primary goal of the SWEM validation effort is to demonstrate that although SWEM was developed and calibrated for 1994-95 conditions, it is useful under other conditions, such as those of 1988-89, without having to undergo extensive recalibration. To be useful under the 1988-89 validation conditions, SWEM must adequately represent the eutrophication and hypoxia processes of the Harbor/Bight/Sound system for 1988-89. The method for demonstrating the adequacy of SWEM for capturing the dynamics of 1988-89 is to compare SWEM validation calculations to 1988-89 observed data. It should be noted that the available hydrodynamic and water quality data

descriptive of 1988-89 conditions, while superior to what is available for other years, are far less comprehensive than the 1994-95 data.

4.3.1 Water Column Results

Model validation results are presented as a series of computer-generated plots which compare model computations versus observed data. These plots are presented in two fashions for the water column: as a sequence of spatial plots and as a sequence of temporal plots. The plots present surface and bottom computations of the concentrations of various water quality state variables, using solid lines (surface) and dashed lines (bottom) to represent the model output. Observed data are presented as discrete points, representing the average and the range of the data. In these plots, the observed data are grouped into surface and bottom layers based on the sampling locations and the bathymetric depths of their corresponding model cells. All data sampled at depths within 50 percent of the bathymetric depths below the water surface or above the bottom, are included in the surface and the bottom layers, respectively. In addition, only those data stations lying along or within one box of the model spatial transect are included in the spatial comparisons.

The temporal plots present model computations averaged over 3.5-day periods at 36 locations. Spatial plots represent 30-day averaged model output with the exception that real minimum and maximum values of chlorophyll-a and dissolved oxygen are displayed. The spatial plots include 2 spatial transects which cover the East River and Long Island Sound as well as the Hudson River and Upper and Lower New York Bay.

Rather than present all the time-series and monthly-averaged spatial plots at this point (456 spatial profiles and 648 temporal profiles), examples will be presented in the main body of this report. The complete set of validation figures is presented in Appendix C.

4.3.1.1 Temporal Comparisons

An example of temporal comparisons between model output and observed data for validation is presented in Figure 4-1a for Western Long Island Sound and Figure 4-1b for the Hudson River at 125th Street. There are two pages associated with each position showing 18 water quality variables. The first page presents comparisons (left to right) for chl-a, POC, dissolved oxygen, DIN, DIP, dissolved inorganic silica (Diss Si), salinity (SAL), temperature (TEMP), and light extinction

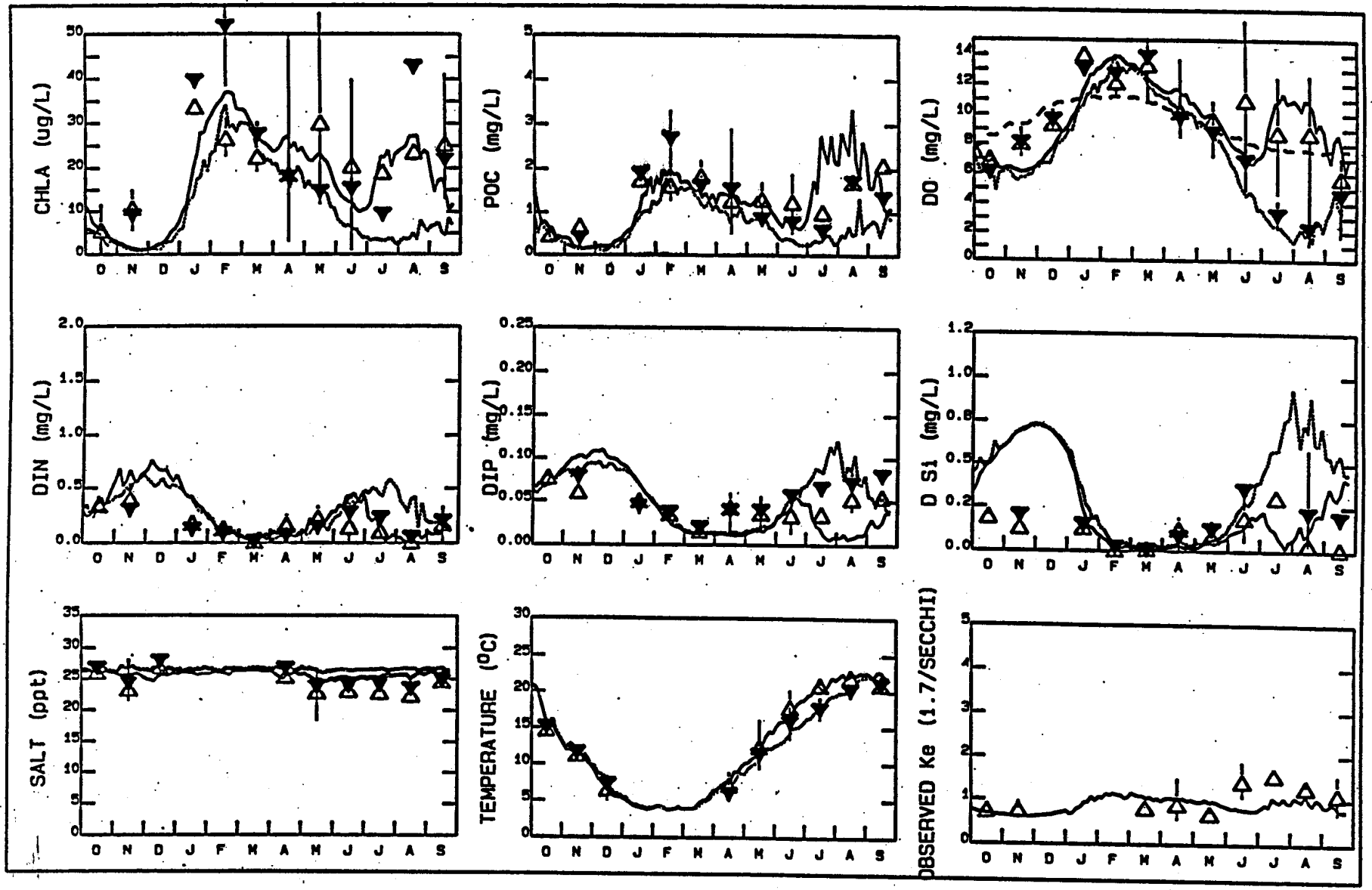

Figure 4-1a. 1988-89 SWEM Validation, Temporal Comparisons for Western Long Island Sound - MP 23

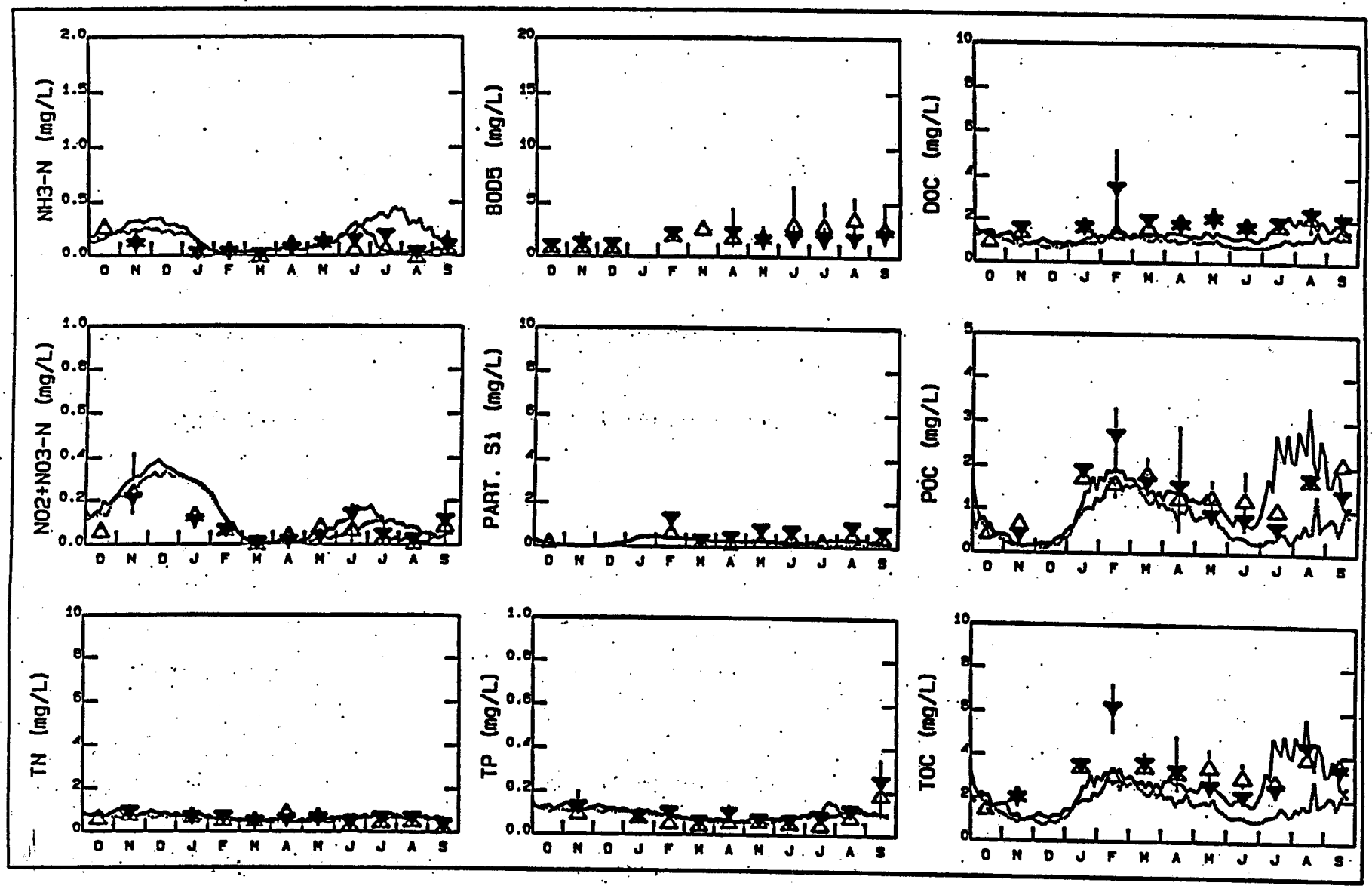

Figure 4-1a. 1988-89 SWEM Validation, Temporal Comparisons for Western Long Island Sound - MP 23 (Continued)

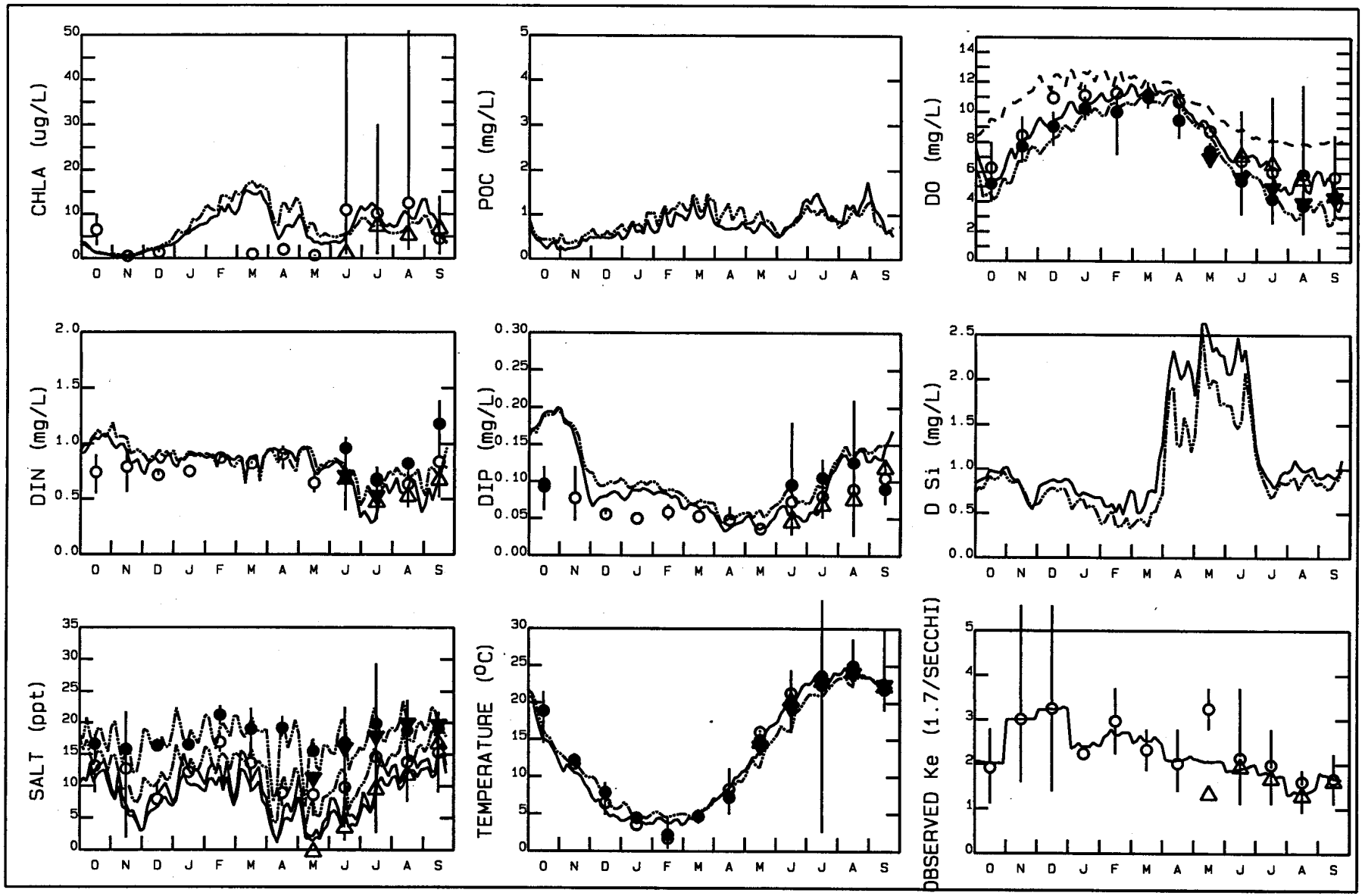

Figure 4-1b. 1988-89 SWEM Validation, Temporal Comparisons for the Hudson River, 125th Street

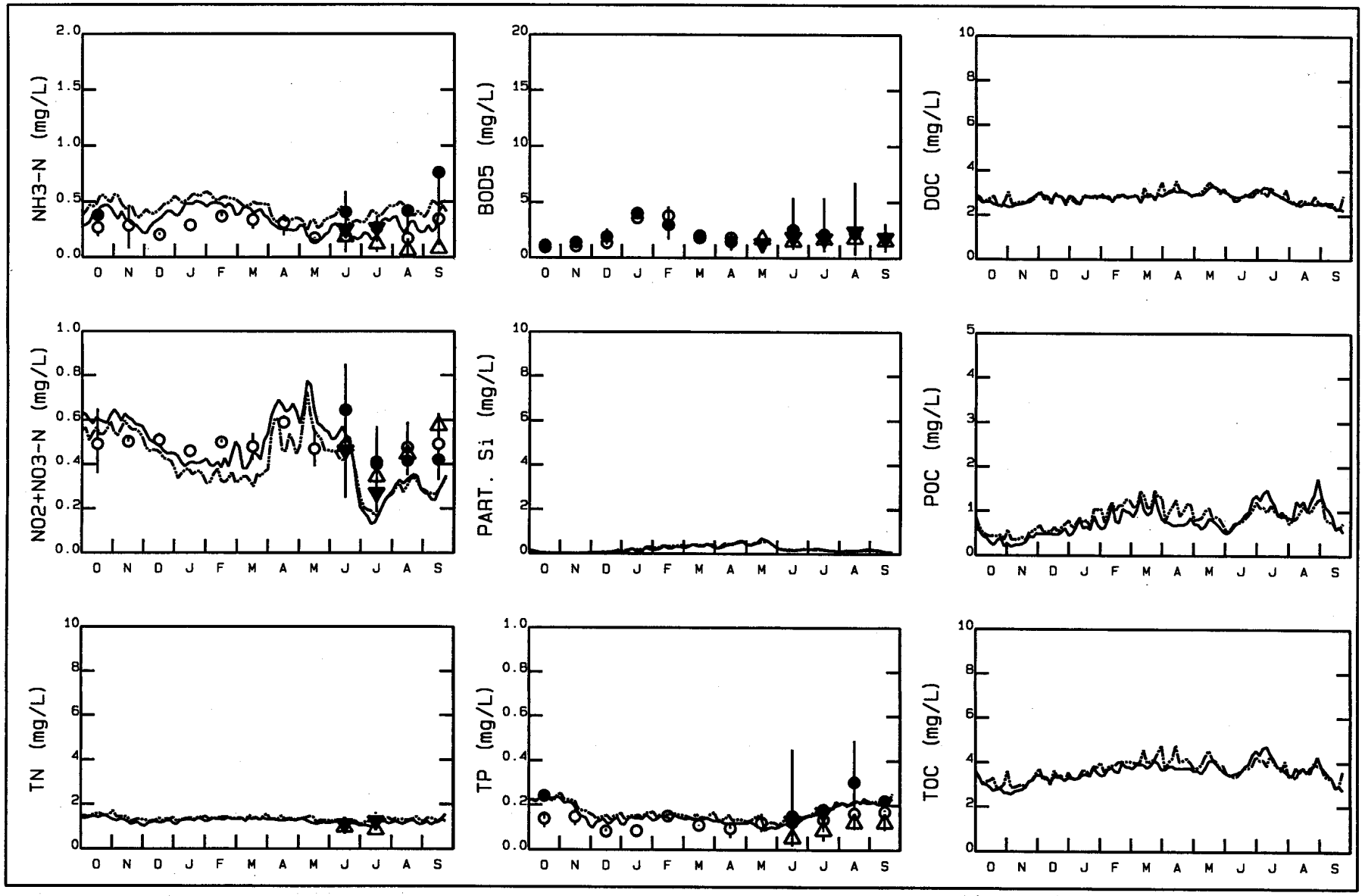

Figure 4-1b. 1988-89 SWEM Validation, Temporal Comparisons for the Hudson River, 125th Street (Continued)

(Ke). The second page presents comparisons (top to bottom) of ammonia nitrogen (NH_4-N), nitrite plus nitrate nitrogen (NO_2+NO_3), TN, BOD-5, particulate biogenic silica (Part silica), TP, DOC, POC, and TOC.

Figures 4-1a and 4-1b present results for both surface and bottom layer segments versus surface and bottom layer data. The model computation for the surface is represented by a solid line; bottom layer computations are represented by a dashed line. The surface observed data are presented as an open upward pointing triangle; bottom observed data are shown using a filled downward pointing triangle. In the dissolved oxygen panel, the saturation concentration of the surface layer is shown as a coarsely dashed line. The Figures show that the model validation reproduces the annual cycle of phytoplankton biomass, as evidenced by the POC, chlorophyll, and dissolved oxygen data comparisons.

In the Sound both computed and observed POC and chlorophyll-a show a winter algal bloom occurring in January and persisting through the late spring as well as the development of a summer bloom in August. Model and data agreement for both POC and chlorophyll-a are excellent during January through May and are acceptable June through September. Dissolved oxygen concentrations are computed and observed to be above saturation for the winter and early spring. The model reproduces the 4 to 6 mg/L deficit observed for bottom waters in July and August as well as the observed 7 mg/L stratification in dissolved oxygen between surface and bottom waters.

Also, in the Sound, nutrient limitations are observed. During March, both Si and DIN observations approach limiting levels. In August, a depletion of DIN is observed. The model computations of inorganic nutrients shown on Figure 4-1a reasonably reproduce the observed values and capture the limitations.

For reference, the salinity and temperature validations from the hydrodynamic submodel are shown. Also shown on Figure 4-1 is the model and data comparisons for Ke, the light extinction coefficient. The second page of Figure 4-1 shows that the comparisons for total nitrogen and total phosphorus are very good. The comparisons for particulate biogenic silica (Figure 4-1a) are also good. For additional comparisons, the components of calculated and observed DIN, ammonia and nitrate plus nitrate are shown.

Figure 4-1a demonstrates the ability of the model to reproduce pre-bloom conditions, the development of the spring bloom, its subsequent limitation by silica and zooplankton predation; the onset of hypoxia beginning in July and the limitation of the summer bloom by inorganic nitrogen depletion for 1988-89, the validation condition. Recall a similar demonstration of the ability of SWEM to reproduce the key features of eutrophication for 1994-95, the calibration condition, in Figure 3-7.

4.3.1.2 Spatial Comparisons

The purpose of this section is to examine the model calibration along 2 longitudinal axes covering key portions of the system. As with the temporal plots presented earlier, both surface and bottom model results and data are presented. Model calculations are shown by a solid line for surface results and a dashed line for the bottom, with dotted lines for the maxima and minima of the model computations of dissolved oxygen and phytoplankton biomass during a 30-day period. Two sets of lines are included on the POC panel to show the algal fraction of the POC. Data are shown by upward pointing open triangles and downward pointing solid triangles for the surface and bottom. On the dissolved oxygen panel, probe data are shown by open (surface) and solid (bottom) circles. Five pages each containing 4 profiles are presented for each of 12 months for each of 2 transects. In order to reduce the number of plots presented here, all spatial profiles are included in Appendix C.

The major sources of data for model-data comparisons are the NYCDEP Harbor Survey and the Long Island Sound Study. For comparison purposes, computed 30-day average concentrations are used for model results.

Figure 4-2a which presents model validation results for August 1989 in the East River and Long Island Sound is an example spatial profile. As can be seen from the plots of salinity and temperature the hydrodynamic submodel reproduces favorably the observed salinity and temperature. The model (dotted lines) is able to capture the sharp salinity gradient observed between milepoints 0 and 20, and the relatively flat spatial profile observed between milepoints 20 and 80.

As shown on Figure 4-2a, the model 30-average approximately reproduces the spatial profile of chl-a, with peak concentrations in the Western Narrows, between milepoints 15 to 30. The model maxima, however, slightly underestimate the absolute peak chl-a near milepoint 20, by 5 ug/L. The

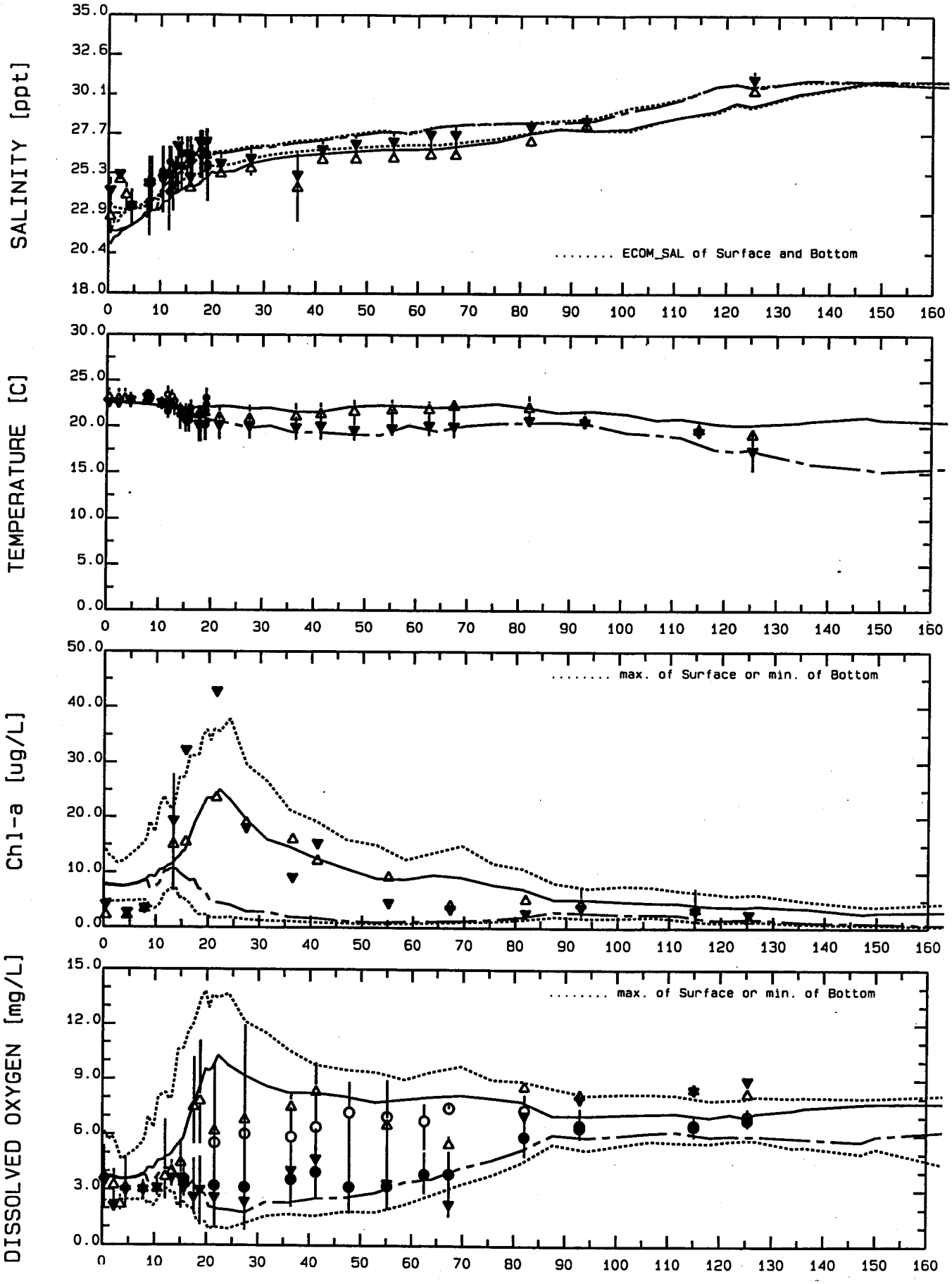

Figure 4-2a. SWEM 1988-89 Validation, August, East River and Long Island Sound Spatial Profile

——— SURFACE MODEL
– – – BOTTOM MODEL

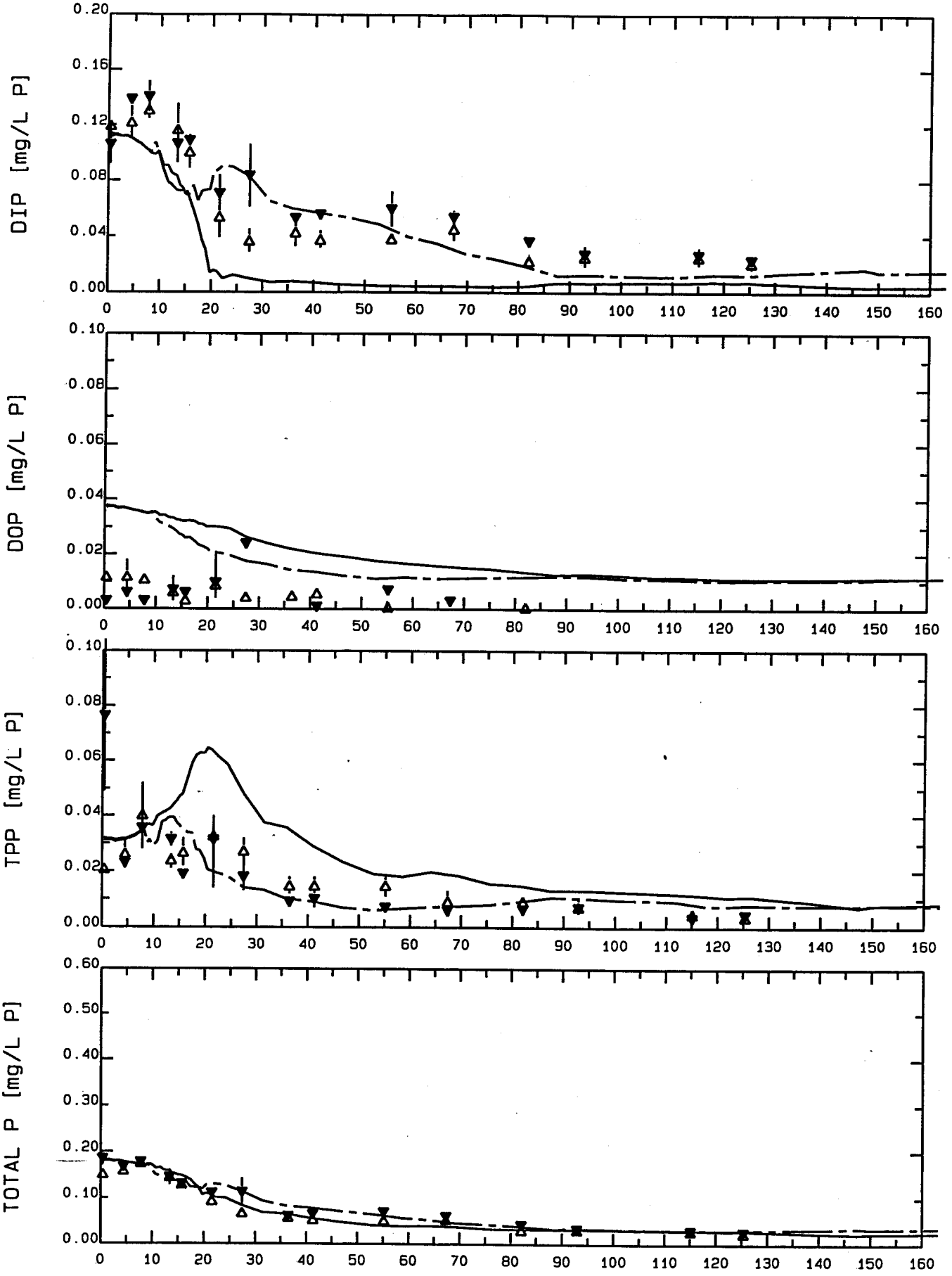

Figure 4-2a. SWEM 1988-89 Validation, August, East River and Long Island Sound Spatial Profile (Continued)

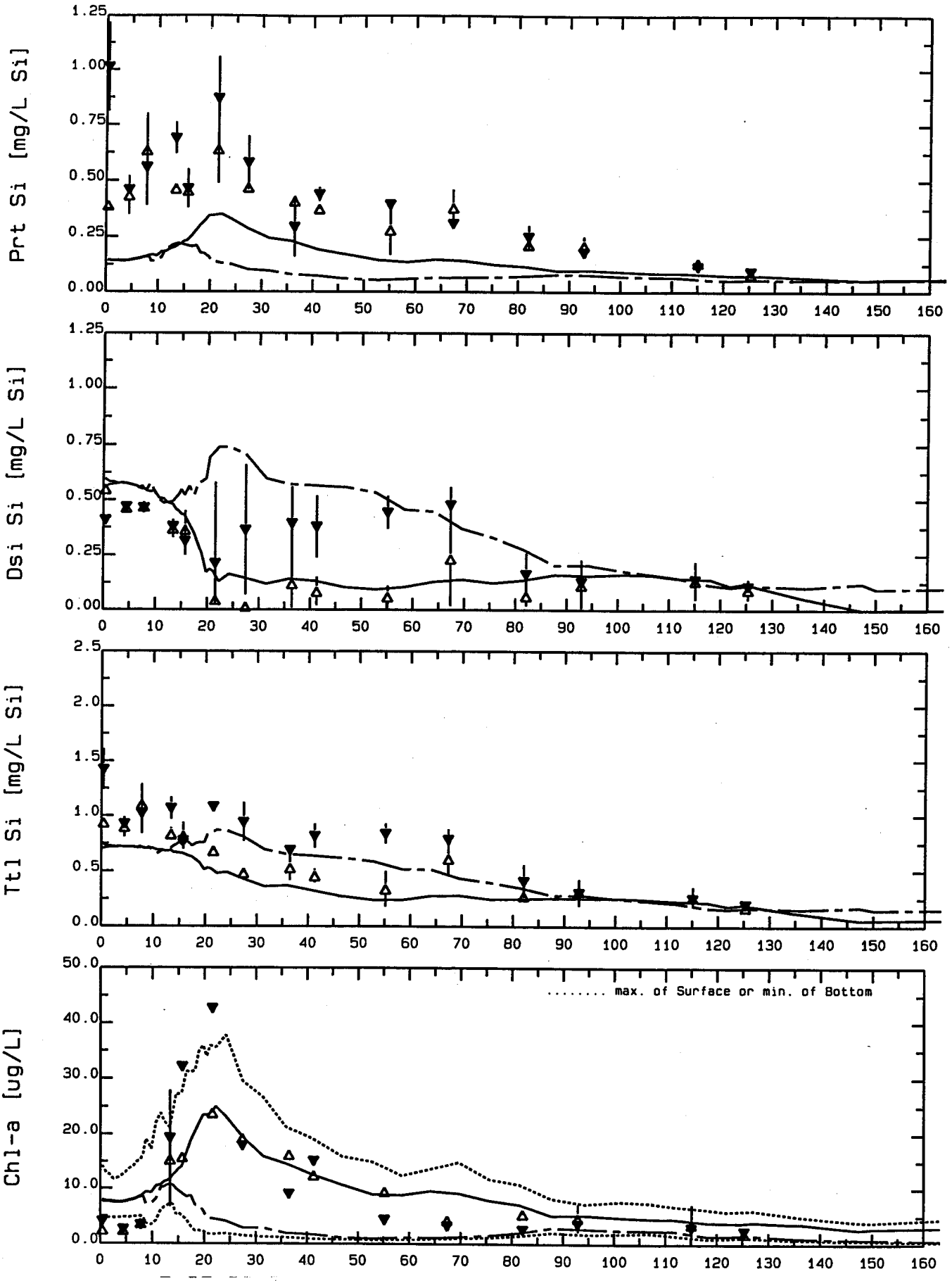

Figure 4-2a. SWEM 1988-89 Validation, August, East River and Long Island Sound Spatial Profile (Continued)

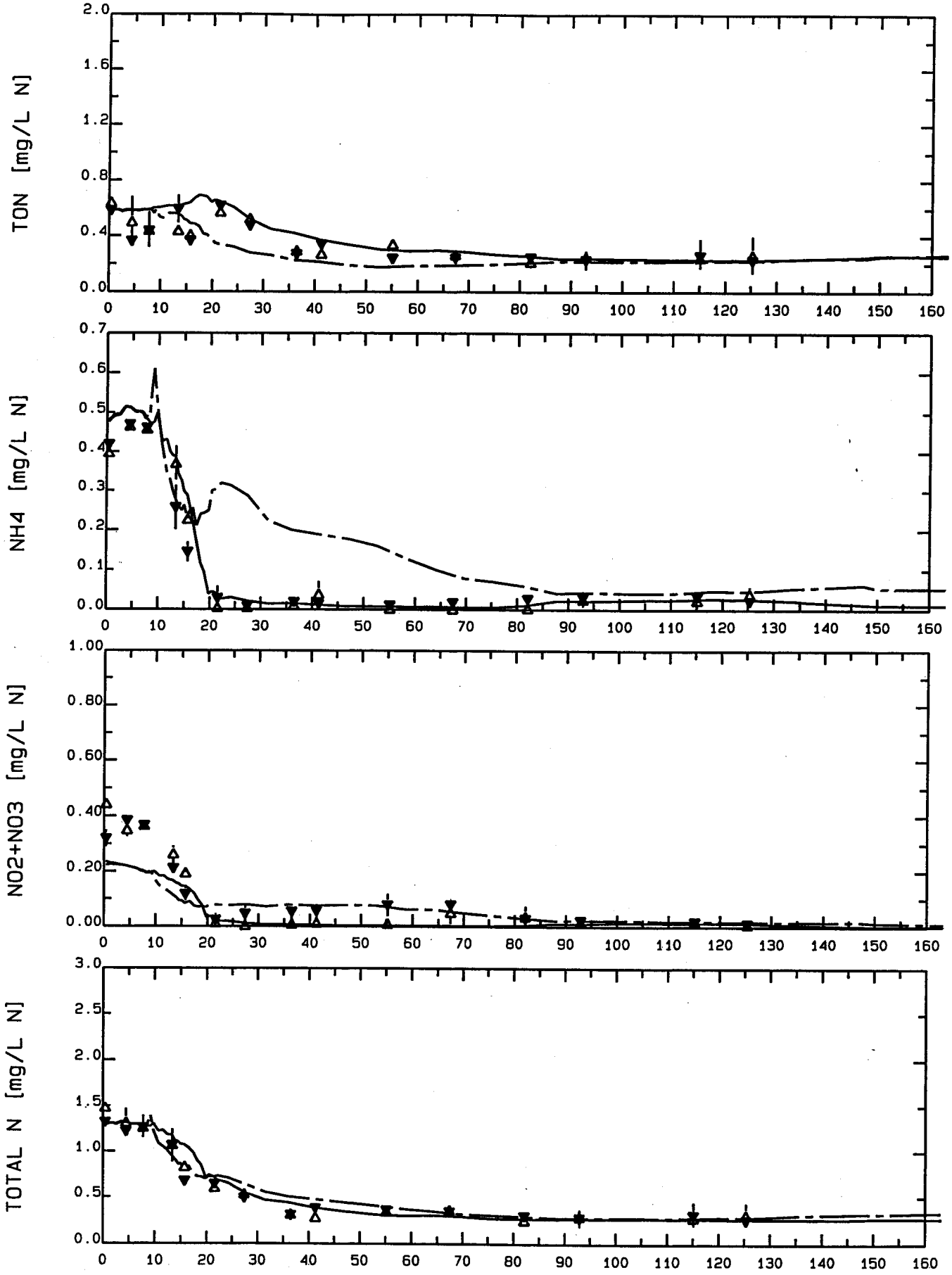

Figure 4-2a. SWEM 1988-89 Validation, August, East River and Long Island Sound Spatial Profile (Continued)

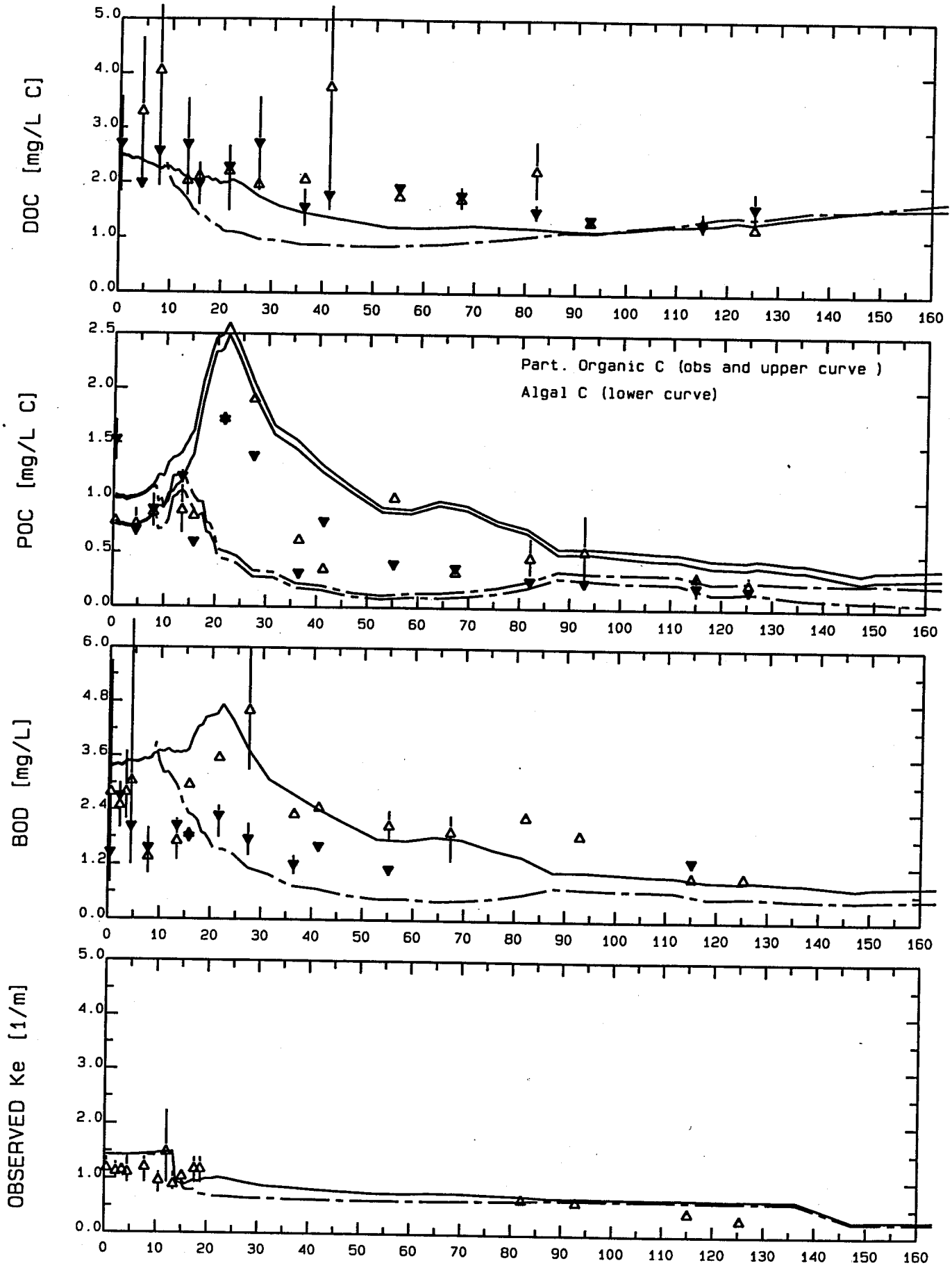

Figure 4-2a. SWEM 1988-89 Validation, August, East River and Long Island Sound Spatial Profile (Continued)

model-data comparison of dissolved oxygen is favorable for most of the Sound. The model captures the peak of super-saturated concentration around milepoint 25 and the low concentrations between milepoints 20 and 30.

Figure 4-2a page 4 presents the model validation for total organic nitrogen (TON), NH_4, NO_2+NO_3 and TN. In general, the validation results are satisfactory. The model underestimates NO_2+NO_3 from milepoints 0 to 10, but captures a significant portion of the observed spatial gradient between milepoints 10 and 20. The NH4 validation picks up the observed sharp gradient between milepoints 10 and 20 extremely well. The overall spatial fit to TN is reproduced by the model very well. Of key importance is the ability of the validation to approach limiting levels of DIN (NH4 and NO2+NO3) in the surface layer beyond milepoint 20 consistent with the observed data.

Validation results for dissolved inorganic silica (Dis Si) and particulate biogenic silica (Prt Si) are presented on page 3 of Figure 4-2a. While the model and data comparison is favorable for dissolved inorganic silica, overall the particulate biogenic silica results do not compare well with the observed data. It would appear that a source of biogenic silica has been underestimated or missed. This is also evident in the total silica (Ttl Si) model and data comparison.

Figure 4-2b shows the model-data comparison for August 1995 in the Hudson River. Overall the model-data comparisons are very favorable. In particular, the model captures the POC peak concentrations near milepoint 25 (Haverstraw Bay) and the general dissolved oxygen profile throughout the Hudson River, Upper Bay, and Lower Bay.

In summary, the ten pages of Figure 4-2 demonstrate the ability of the model to reproduce spatial gradients in nutrients, spatially varying development of algal biomass, and the associated impacts on dissolved oxygen for 1988-89. This demonstration is indicative of not only proper specification of eutrophication kinetics in the model, but of proper specification of transport and the light field. Recall a similar demonstration of the ability of SWEM to simultaneously reproduce physics and kinetics for 1994-95, the calibration condition, in Figure 3-12.

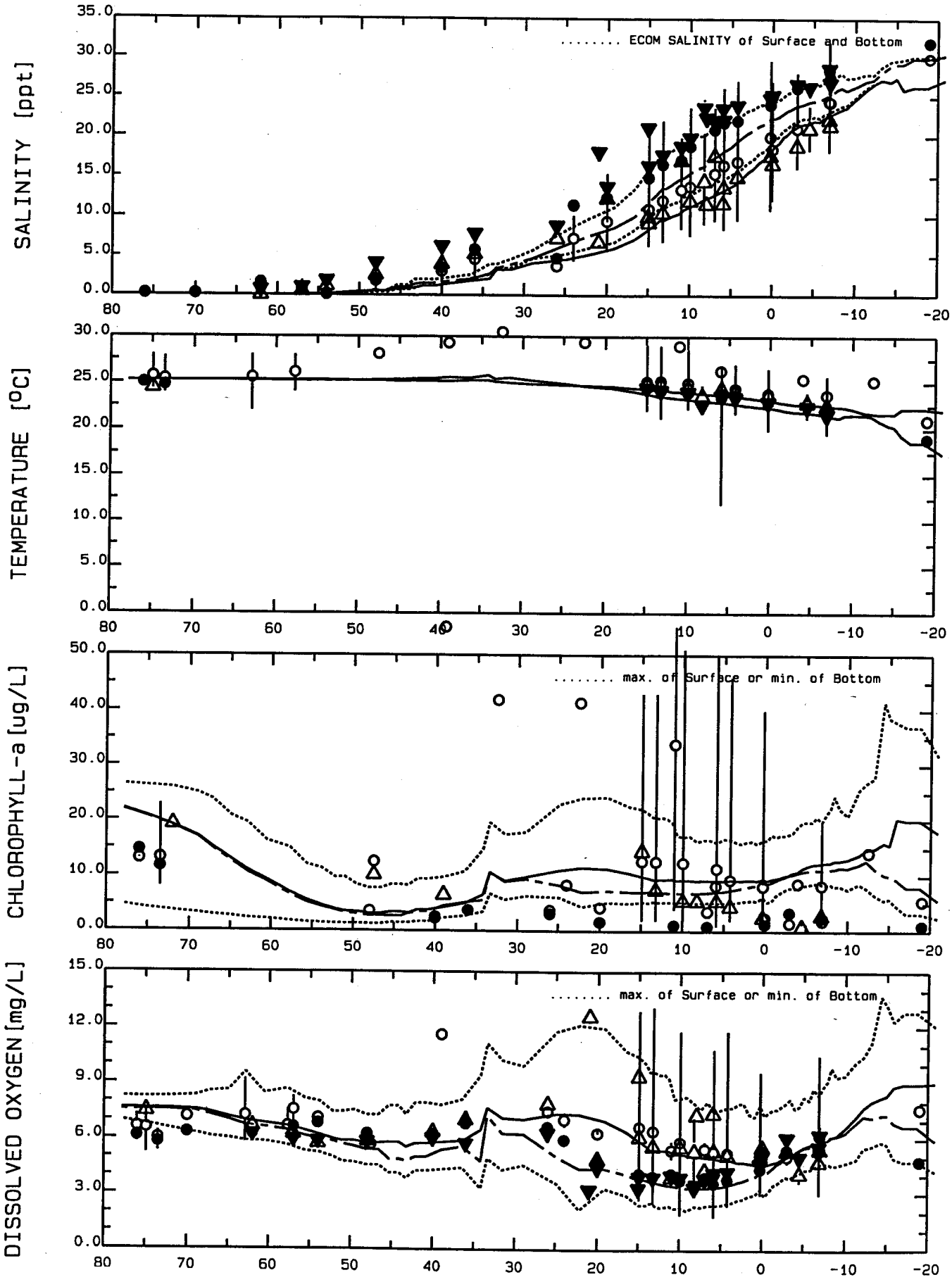

Figure 4-2b. SWEM 1988-1989 Validation August, Hudson River, Upper and Lower Bay, and Ocean Spatial Profile

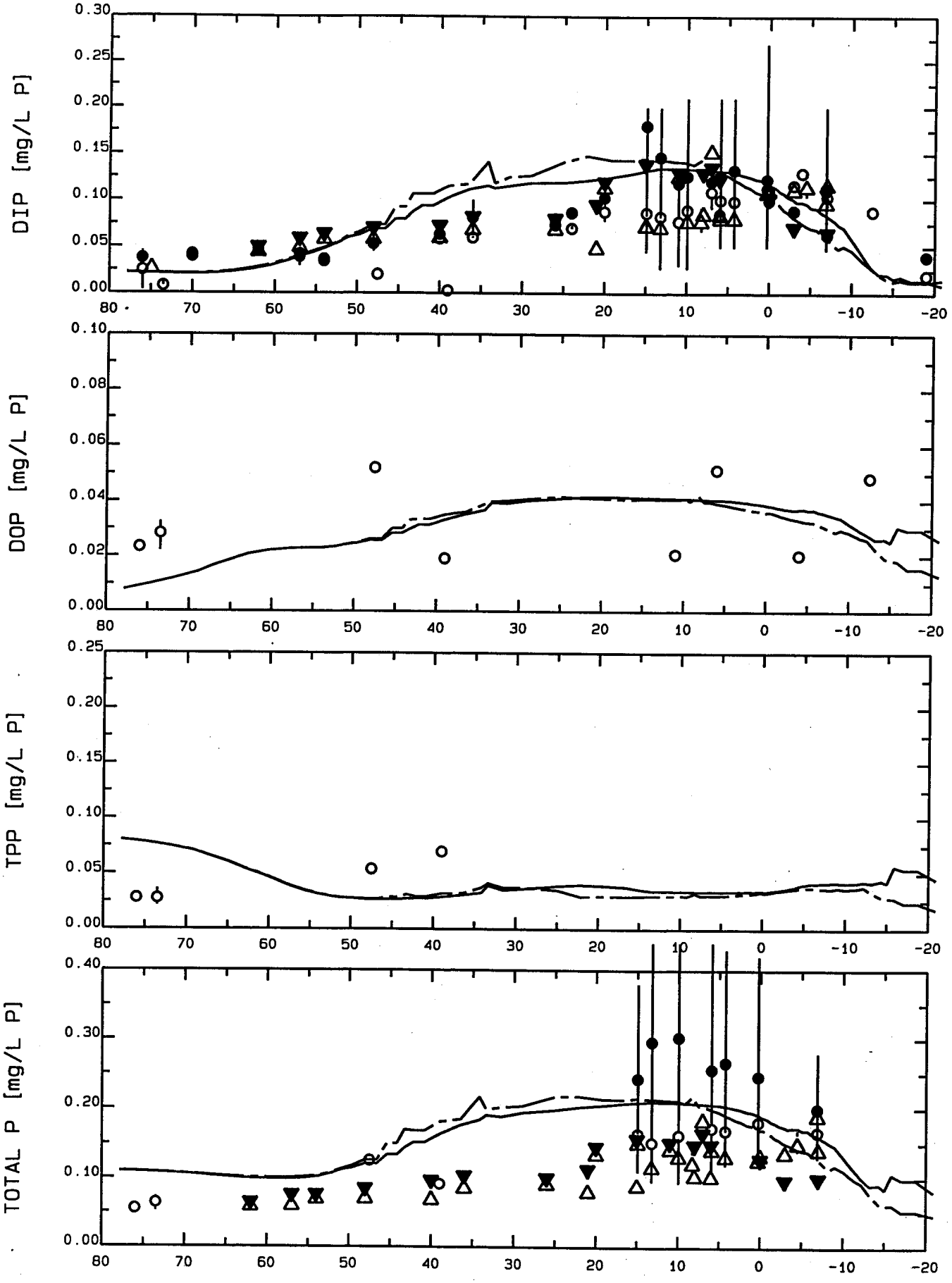

Figure 4-2b. SWEM 1988-1989 Validation August, Hudson River, Upper and Lower Bay, and Ocean Spatial Profile (Continued)

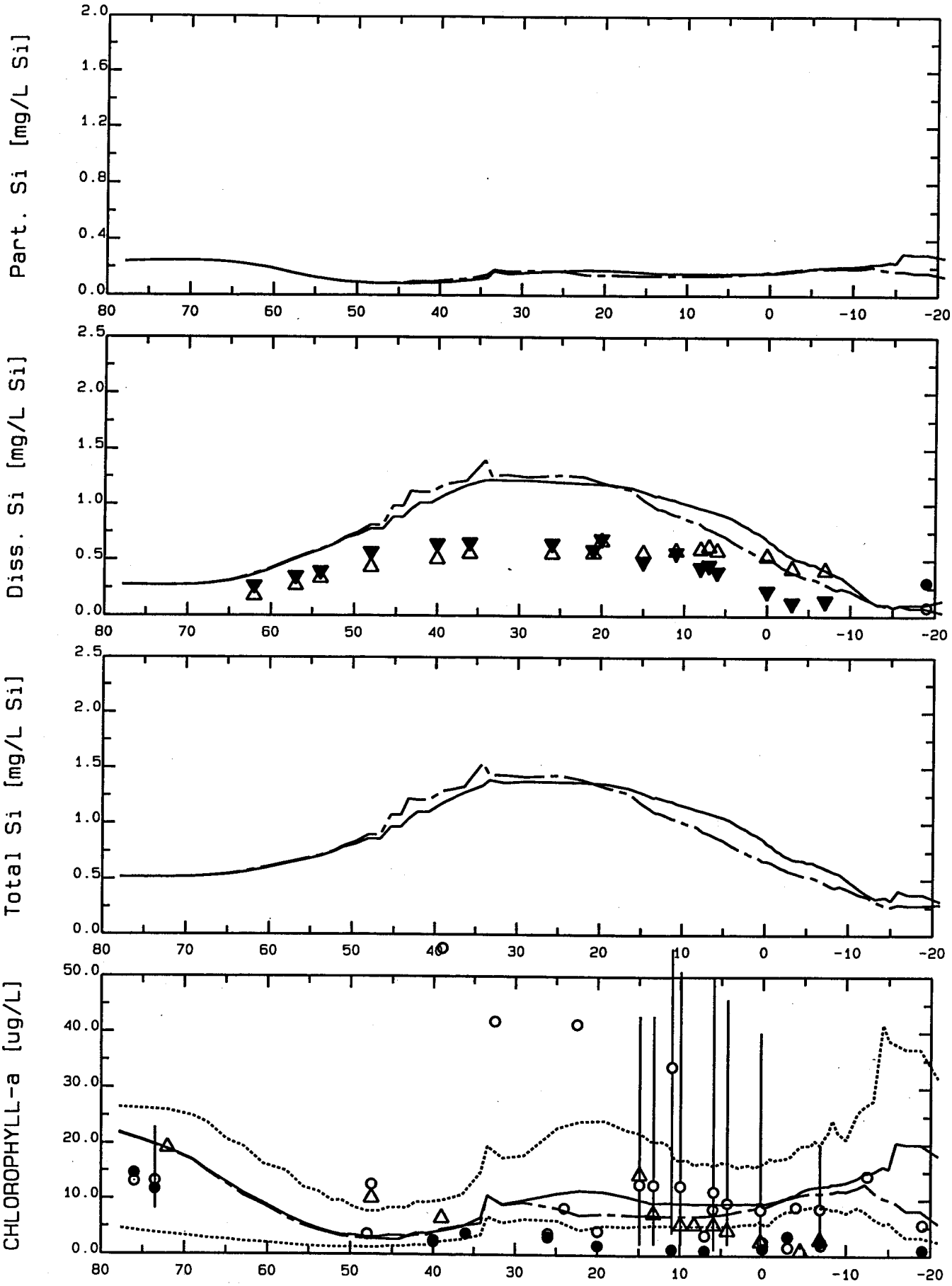

Figure 4-2b. SWEM 1988-1989 Validation August, Hudson River, Upper and Lower Bay, and Ocean Spatial Profile (Continued)

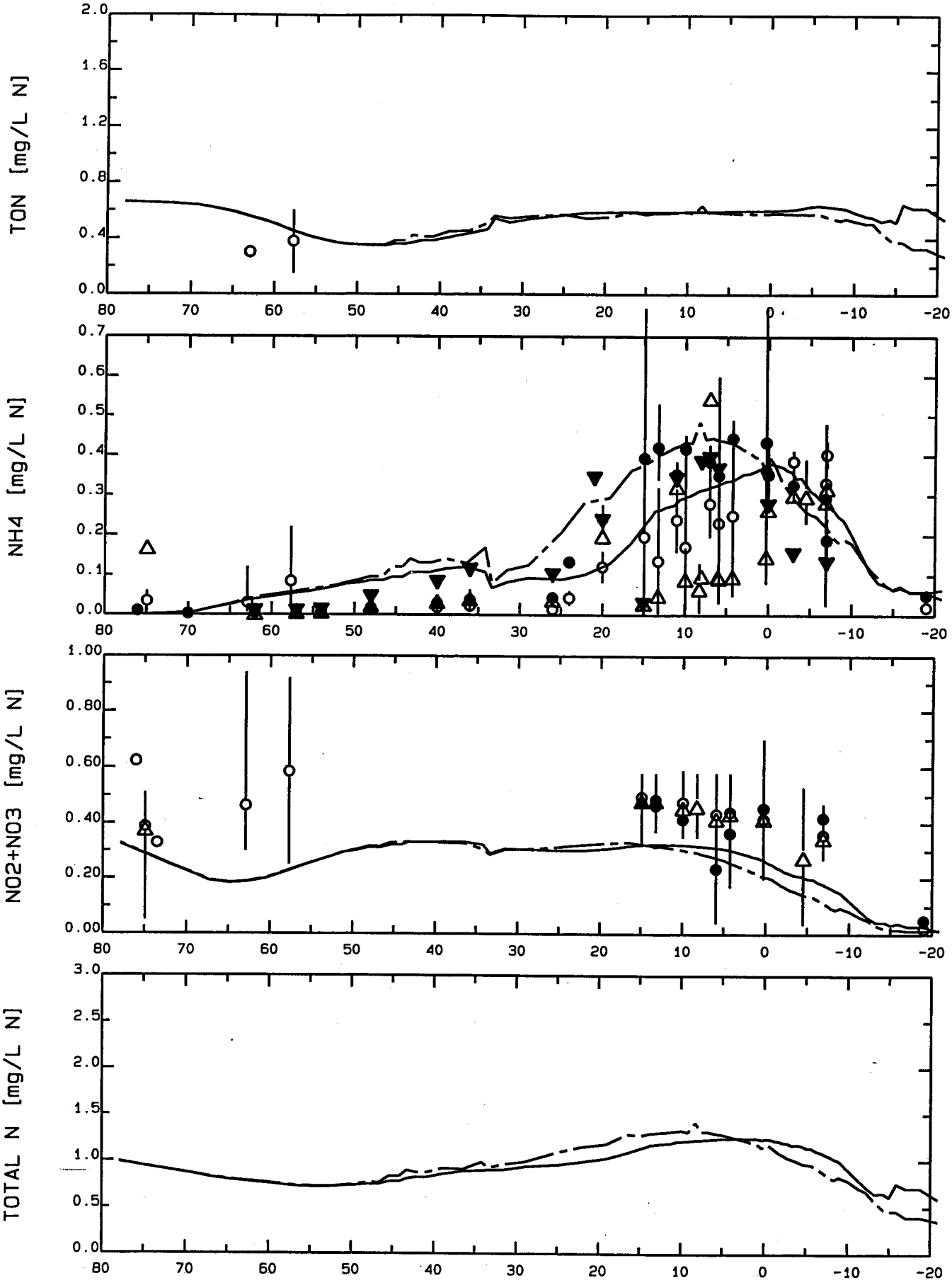

Figure 4-2b. SWEM 1988-1989 Validation August, Hudson River, Upper and Lower Bay, and Ocean Spatial Profile (Continued)

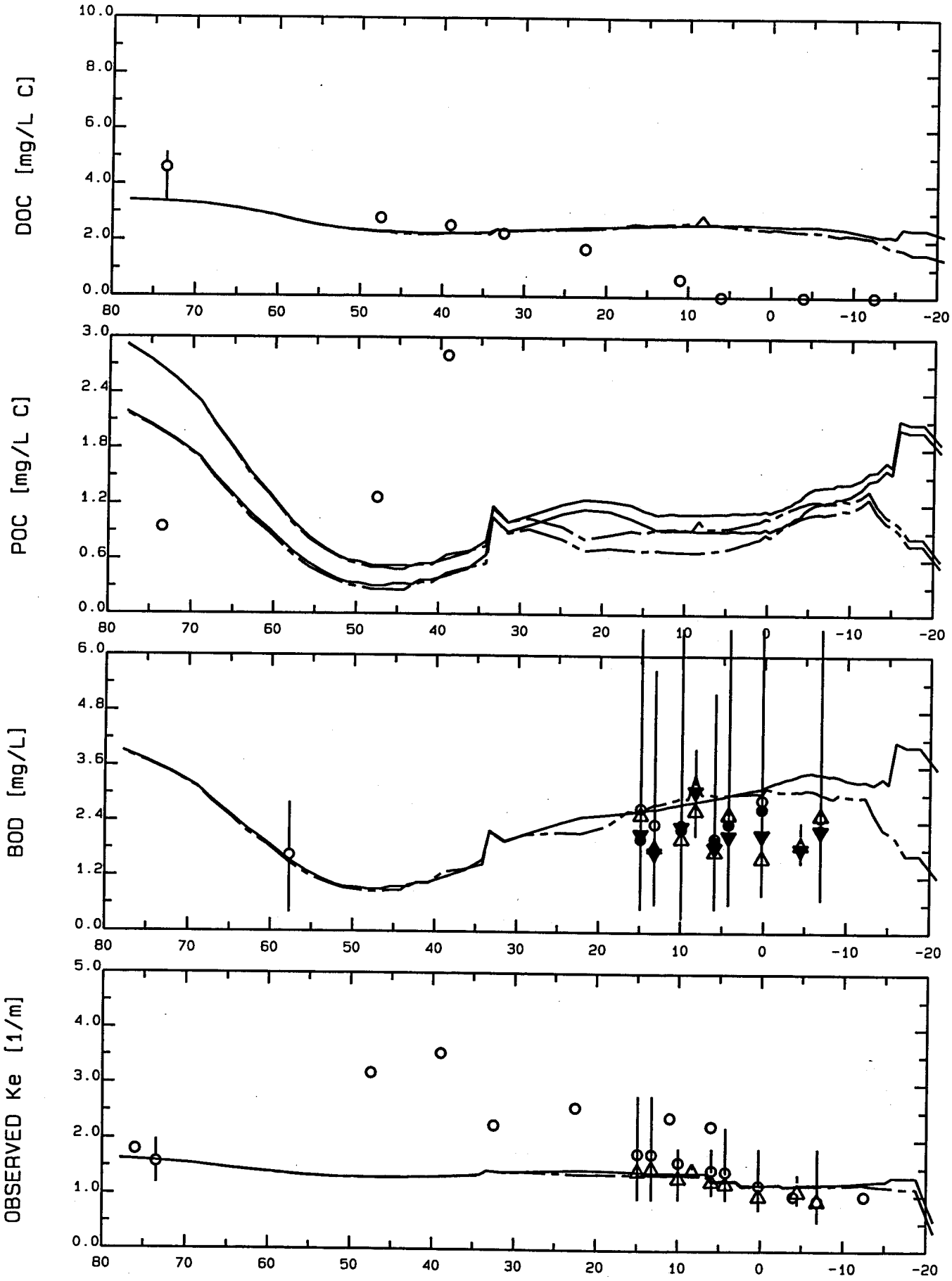

Figure 4-2b. SWEM 1988-1989 Validation August, Hudson River, Upper and Lower Bay, and Ocean Spatial Profile (Continued)

SECTION 5

REFERENCES

Berner, R.A., 1964. "An Idealized Model of Dissolved Sulfate Distribution in Recent Sediments," Geochim. Cosmochim., Acta 28: 1497-1503.

Berner, R.A., 1974. "Kinetic Models for the Early Diagenesis of Nitrogen, Sulfur, Phosphorus and Silicon in Anoxic Marine Sediments," in E.D. Goldberg (Ed.), The Sea, V.5. Wiley, pp. 427-450.

Berner, R.A., 1980: Early Diagenesis. A Theoretical Approach. Princeton Univ. Press, Princeton, NJ.

Bienfang, P.K., P.J. Harrison and L.M. Quarmby, 1982. "Sinking Rate Response to Depletion of Nitrate, Phosphate and Silicate in Four Marine Diatoms," Marine Biology, 67, 295-302.

Blumberg, A.F. and G.L. Mellor, 1987. "A Description of a Three-Dimensional Coastal Ocean Circulation Model," In: Three-Dimensional Coastal Ocean Models, Coastal and Estuarine Sciences, 4, N.S. Heaps, Editor, AGU, Washington, D.C., 1-16.

Cerco, C.F. and T. Cole, 1993. "Application of the 3-D Eutrophication Model CD-QUAL-ICM to Chesapeake Bay," Draft Report to the U.S. EPA Chesapeake Bay Program. Prepared by U.S. Army Corps of Engineers, WES, Vicksburg, Mississippi.

Culver, M.E. and W.O. Smith, Jr., 1989. "Effects of Environmental Variation on Sinking Rates of Marine Phytoplankton," J. Phycol. 25, 262-270.

Di Toro, D.M. and J.J. Fitzpatrick, 1993. "Chesapeake Bay Sediment Flux Model," Contract Report EL-93-2, U.S. Army Engineer Waterways Experiment Station, Vicksburg, MS; 200 pp, June 1993.

Di Toro, D.M. and W.F. Matystick, 1980. "'Mathematical Models of Water Quality in Large Lakes, Part 1: Lake Huron and Saginaw Bay," EPA/600/3-80/056, 28-30.

Di Toro, D.M. J.A. Mueller and M.J. Small, 1978. "Rainfall - Runoff and Statistical Receiving Water Models"; NYC 208 Task Report 225 prepared by Hydroscience, Inc., for Hazen and Sawyer Engineers and New York City DWR, 271 pp., March 1978.

Duffie, J.A. and W.A. Bechman, 1974. "Solar Radiation Thermal Processes," John Wiley and Sons, New York, New York.

Fogg, G.E., 1965. "Algal Cultures and Phytoplankton Ecology," University of Wisconsin Press, Madison, Wis., p. 20.

Hendry, G.S., 1977. "Relationships Between Bacterial Levels and Other Characteristics of Recreational Lakes in the District of Muskoka," Interim Microbiology Report, Laboratory Service Branch, Ontario Ministry of the Environment.

Henrici, A.T., 1938. "Seasonal Fluctuation of Lake Bacteria in Relation to Plankton Production," J. Bacteriol., 35, 129-139.

Hutchinson, G.E., 1967. "A Treatise on Limnology," In Introduction to Lake Biology and Limnoplankton, Vol. II, Wiley, New York, 306-354.

HydroQual, Inc, 1987. "Evaluation of the Effectiveness of Tertiary Treatment Processes in Removing Toxics and Conventional Pollutants," EPA Contract #68-01-6986.

HydroQual, Inc, 1989. "Development and Calibration of a Coupled Hydrodynamic/Water Quality/Sediment Model of Chesapeake Bay," prepared for the USEPA Chesapeake Bay Program, Mahwah, New Jersey.

Hyer, P.V., C.S. Fang, E.P. Ruzecki and W.J. Hargis, 1971. "Hydrography and Hydrodynamics of Virginia Estuaries, Studies of the Distribution of Salinity and Dissolved Oxygen in the Upper York System," Virginia Institute of Marine Science.

Jewell, W.J. and P.L. McCarty, 1971. "Aerobic Decomposition of Algae." Environ. Sci. Technol., 5(10), 1023.

Lowe, W.E., 1976. Personal Communication. Canada Centre for Inland Waters, Burlington, Canada.

Lund, J.W.G., 1965. "The Ecology of the Freshwater Phytoplankton," Biol. Rev., 40, 231-293.

Matisoff, Gerald, 1978. "Early Diagenesis of Chesapeake Bay Sediments: A Time Series Study of Temperature, Chloride and Silica," Ph.D. Dissertation, The Johns Hopkins University, Baltimore, Maryland.

Menon, A.S., W.A. Gloschenko and N.M. Burns, 1972. "Bacteria-Phytoplankton Relationships in Lake Erie," Proc. 15th Conf. Great Lakes Res., 94, Inter. Assoc. Great Lakes Res., 101.

Miller, D.R., N.P. Nikolaidis, L.H. Yang, M.A. Geigert, I Heitert and H.S. Chen, 1993. "Technical Report on the Long Island Sound Atmospheric Deposition Project;" University of Connecticut, for Connecticut Dept. of Environ. Prot. July 1, 1993.

Morel, F.M., 1983. Principles of Aquatic Chemistry, John Wiley and Sons, New York, New York.

NOAA, 1986. "The National Coastal Pollutant Discharge Inventory-Estimates for Long Island Sound," prepared by the Strategic Assessment Branch, Ocean Assessments Division, Office of Oceanography and Marine Assessment, National Oceanographic and Atmospheric Administration.

Rao, S.S., 1976. "Observations on Bacteriological Conditions in the Upper Great Lakes 1968-1974," Scientific Series, No. 64, Inland Waters Directorate CCIW Branch, Burlington, Canada.

Raymont, J.E.G., 1963. Plankton and Productivity in the Oceans, Pergamon, New York, 93-466.

Rhee, G.Y, 1973. "A Continuous Culture Study of Phosphate Uptake, Growth Rate and Polyphosphates in Secendemus sp," J. Phycol, 9, 495-506.

Riley, G.A., H. Stommel and d.F. Bumpus, 1949. "Quantitative Ecology of the Plankton of the Western North Atlantic," Bull. Bingham Oceanogr. Coll., 12(3), 1-169.

Smaltz, R.A., 1994. "Application and Documentation of the Long Island Sound Three-Dimensional Circulation Model"; Summary Report, Volume 1, Long Island Sound Oceanography Report; NOAA Technical Report NOS OES 003; 77 pp, Jan. 1994.

Smaltz, R.A., M.F. Devine and P.H. Richardson, 1994a. "Residual Circulation and Thermohaline Structure"; Summary Report, Volume 2, Long Island Sound Oceanography Report; NOAA Technical Report NOS OES 003; 199 pp +3 App, Jan. 1994.

Smaltz, R.A., L.C. Sun and E.J. Wei, 1994b. "Scientific Publications"; Summary Report, Volume 3, Long Island Sound Oceanography Report; NOAA Technical Report NOS OES 003; 78 pp, Jan. 1994.

Stacey, Paul, 1990. Private Communication, Connecticut Department of Environmental Protection.

Steele, J.H., 1962. "Environmental Control of Photosynthesis in the Sea," Limnol. Oceanogr., 7, 137-150.

Strickland, J.D.H., 1965. Chemical Oceanography, Production of Organic Matter in the Primary Stages of the Marine Food Chain, Vol. 1., J.P. Riley and G. Skivow, Eds., Academic Press, New York, 503pp.

Thomann, R.V., 1972. "Systems Analysis and Water Quality Management, McGraw-Hill, New York, 286 pp. (Reprint: J. Williams Book Co., Oklahoma City, OK.)

City of New York
Department of Environmental Protection
New York, New York

NEWTOWN CREEK WATER POLLUTION CONTROL PROJECT EAST RIVER WATER QUALITY PLAN

TASK 10.0 SYSTEM-WIDE EUTROPHICATION MODEL (SWEM)

SUBTASK 10.4 CALIBRATE SWEM WATER QUALITY

SUBTASK 10.6 VALIDATE SWEM WATER QUALITY

Prepared under subcontract to:
Greeley and Hansen
115 Broadway, Suite 13B
New York, NY 10006-1604

April 2001
Project No: GRHN0020/209